POLITECNICO DI MILANO

FACOLTÁ DI INGEGNERIA INDUSTRIALE E DELL'INFORMAZIONE

Corso di Laurea in Ingegneria Nucleare

CHANGING THE DISTRIBUTION OF THE ENERGY AND PARTICLE FLUXES INTO SCRAPE-OFF LAYER VIA ION ORBIT LOSS

Advisor: Dr. MATTEO PASSONI
Co-advisor: Dr.WESTON M. STACEY

Thesis by :
RAFFAELE TATALI
Matr. 817196

Anno Accademico 2015 - 2016

"When we look up at night and view the stars, everything we see is shinning because of distant nuclear fusion." (C.E. Sagan)

ACKNOWLEDGEMENTS

Non sarebbe stato possibile giungere fino a questo punto senza l'aiuto di tutte le persone che mi sono state accanto durante questo lungo cammino. Mia Madre e mio Padre per non avermi mai fatto mancare niente. Per essere stati i primi sostenitori, avermi dato la libertá di scegliere chi essere e cosa fare anche quando le idee erano confuse. Mia sorella per essere sempre presente con un sorriso anche nei momenti di difficoltá. Dr. Matteo Passoni per avermi mostrato e trasmesso la passione per la scienza e la ricerca. I miei nonni per il loro silenzioso ed enorme sostegno. Zio Fulvio per avermi insegnato ad affrontare anche i momenti piú duri in modo razionale con l'ironia e la forza di volontá. Tutti i miei zii e i miei cugini lontani e vicini per avermi aiutato,supportato e sopportato in ogni situazione. Maria per avermi sostenuto e aiutato a crescere durante questo percorso. Luca per non avermi mai abbandonato nonostante la moltitudine di impegni e per non avere mai smesso di dubitare nelle mie capacitá. Luca L. perché nonostante fossimo sempre in luoghi diversi riuscito comunque a spronarmi. Michele, Pasquale, Luigi perché nonostante tutto sono gli amici su cui ho potuto e potró sempre contare. Federica per essere stata una compagna audace e paziente avendomi sostenuto e sopportato nonostante le sfide a cui la vita l'ha sottoposta. Furthermore I want to thank you : Dr. Stacey for giving me this huge opportunity to be one of his student and supervise my research. The Georgia Institute of Technology to make me feel home. The guys of Fusion Research Lab: Max, Andrew, Theresa, Nick and Jonathan for giving me all the help I needed. Richard, John and William for being like a little family during my stay in the US. Jane for being a precious friend supporting me no matter what.

TABLE OF CONTENTS

LIST OF TABLES

LIST OF FIGURES

LIST OF SYMBOLS

$\mathbf{a}$	Minor radius of the plasma, p. 50.
$\mathbf{B}$	Magnetic induction, p. 27.
$B_{\phi 0}$	toroidal magnetic field at intial location, p. 44.
B_0	total magnetic field at launch location, p. 44.
$B_{\theta 0}$	poloidal magnetic field at launch location, p. 44.
$B_{\phi S}$	toroidal magnetic field on LCSF, p. 44.
B_S	total magnetic field on LCSF, p. 44.
$B_{\theta S}$	poloidal magnetic field on LCSF, p. 44.
ϵ_0	inverse aspect ratio for the launch location, p. 49.
ϵ_{min}	reduced energy, p. 56.
ϵ_S	inverse aspect ratio on the separatrix, p. 49.
$f_{\phi 0}$	magnetic field ratio at initial location, p. 44.
$f_{\phi S}$	magnetic field ratio on LCSF, p. 44.
Γ_i	radial particle flux, p. 42.
$\Gamma(n)$	gamma function of order n, p. 57.
$\Gamma(n, \epsilon_{min})$	incomplete gamma function of order n, p. 57.
$\hat{\Gamma}_i(r)$	effective radial particle fluxes, p. 68.
$\hat{Q}_i(r)$	effective radial energy fluxes, p. 68.
$\mathbf{I}$	plasma current, p. 22.
$\mathbf{j}$	density current, p. 27.
$\langle \sigma \upsilon \rangle_{ion}$	neutral reactivity, p. 42.
n_i	particle density, p. 42.
ϕ_0	electric potential at launch location, p. 44.
ϕ_S	electric potential on LCSF, p. 44.
ψ_0	flux surface at launch location, p. 44.

ψ_S	flux surface on LCSF, p. 44.
Q_i	ion total energy fluxes, p. 42.
q_{ie}	ion to electron collisional energy transfer, p. 42.
q_{nb}	neutral beam heating, p. 42.
$\mathbf{R}$	Major radius of the plasma, p. 22.
R_0	major radius at launch location, p. 44.
R_S	major radius of LCSF, p. 44.
$\sigma_f(E)$	Fusion cross section, p. 4.
S_{nb}	neutral beam source, p. 42.
θ_0	launch location, p. viii.
θ_S	angular exit location, p. ix.
T_m	Temperature of material, p. 27.
$v_{\|0}$	parallel velocity at initial location, p. 44.
v_0	total velocity at launch location, p. 47.
$v_{\perp 0}$	perpendicular velocity at initial location, p. 47.
$v_{\|S}$	parallel velocity on LCSF, p. 47.
$v_{\perp S}$	perpendicular velocity on LCSF, p. 47.
v_{ri}	second velocity momentum, p. 42.
ζ_0	directional cosine, p. viii.

SUMMARY

Research in magnetic confinement thermonuclear fusion explores the possibility of producing carbon-free electric power by using fusion reaction in deuterium-tritium plasmas heated to temperatures of up to $10^7 - 10^8$ K and confined by magnetic field in toroidal shape machines known as Tokamaks. The world roadmap foresees fusion technology to contribute at the energy mix around 2050. This remains a long-term prospect but the power production using fusion remains an ambitious physical and engineering challenge that requires a long and sustained research effort. Aiming to show the feasibility and competitiveness of fusion technology several research reactors are running a massive experimental campaigns and DIII-D is one of them. Such an effort is put in order to characterize the operation of biggest world fusion experiment: ITER.

It is well-known in the fusion community how critical the problem of power exhausted in a fusion reactor is. While the high energy neutrons are able to overcome the first wall and stopped in the blanket, other fusion products like α-particle or impurities have a lower range and quite high energy. Hence they need to be worked off in a region called scrape-off layer (SOL), placed between the plasma edge and the first wall and . In the SOL charged particles follow the open magnetic field line and are forced to hit the target plate called divertor. This device is necessary to unburden the heat load on the first wall, extend the lifetime of reactor components and consequentially improving its performance.

The Ion orbit loss theory (IOL) has shown that the ion energy and particle fluxes crossing the last closed flux surface are strongly peaked about the outboard midplane

(centering the coordinate system in the middle of the Tokamak) . This is due to the toroidal geometry that give rise to an asymmetric magnetic field which causes inhomogeneous losses on poloidal exit locations with a likely critical consequence for the whole reactor.

The purpose of the thesis is to success a possible way to make more uniform the distribution of exit particles and the heat load on the divertor target plates. In doing so, two cases are investigated: one related to the change of magnetic field by adding an extra set of toroidal field coils and the second related to the change of electrostatic potential in the scrape off layer. The latter case is not an easy task to accomplish, but we assumed it could be achieved.

SOMMARIO

La produzione di energia elettrica per mezzo della fusione termonucleare resta una sfida ambiziosa sia dal punto vista scientifico sia dal punto di vista tecnologico e richiede una continua ed intensa attività di ricerca. Le recenti previsioni indicano che questa tecnologia potrà dare un contributo sostanziale al fabbisogno energetico mondiale a partire dal 2050.

Per consentire alla reazione di fusione di aver lugo è necessario riscaldare il combustibile nucleare fino a temperature dell'ordine dei $10^7 - 10^8$ K. La materia in questo stato è chiamata plasma. I plasmi possono essere confinati da campi magnetici attraverso appositi reattori dalla forma toroidale conosciuti conosciuti come Tokamak. Molti impianti sperimentali sono attivi attualmente in tutto il mondo e perseguono un' attività di ricerca volta a dimostrare la fattibilità e la competitività di questa fonte alternativa di energia. Ne è un esempio il reattore DIII-D di proprietá della General Atomics, da cui sono stati presi i valori dei parametri di interesse e i dati sperimentali di questa tesi. Uno dei rami su cui si focalizza la ricerca scientifica sui reattori a fusione riguarda il problema del *power exhausted*. Questo è uno dei aspetti più critici soprattutto per quanto concerne l'attività svolta e in generale ai fini del portare a termine il più importante progetto internazionale nell'ambito dei reattori a fusione: ITER.

Esso é progettato per produrre 500 MW di potenza attraverso la reazione nucleare di fusione tra i nuclei di dueterio e trizio e, tenendo in conto anche i circa 50 MW di potenza esterna da fornire al plasma per riscaldarlo inizialmente, si arriva ad avere una potenza complessiva nel reattore di 550MW.

Se in un reattore di potenza si vuole operare a regime stazionario, la potenza

stessa deve essere asportata dal sistema al tasso con cui viene immessa e tutto questo senza procurare un danneggiamento alle PFCs (*plasma facing components*) che rappresentano la prima barriera fisica progettata appositamente per sostenere il flusso di plasma.

La maggior parte di questa potenza è trasportata dai neutroni emessi durante il processo di fusione, quindi depositata nel blanket e infine asportata mediante un fluido termovettore. I restanti 150MW sono formati dai 50MW della potenza esterna e dai 100MW trasportati dalle particelle α, prodotte dalla reazione di fusione, ed è proprio per questi ultimi che si ricerca una modalità finalizzata allo smaltimento. Circa 50MW vengono smaltiti attraverso i processi di interazione delle particelle con la materia nel *first wall*. Senza le dovute precauzioni, l'energia delle particelle α si deposita su delle superfici target producendo una densità di potenza dell'ordine di $100MW/m^2$ che è dello stesso ordine di grandezza di quella presente sulla superficie solare. Le superfici target formano quello che è chiamato divertore, ossia una camera separata dal plasma che ha evidenziato vantaggi nel processamento della potenza da smaltire. Con riferimento alla figura 1, si visualizzano le aree che saranno di interesse nelle analisi susccessive. La topologia delle linee di campo magnetico in geometria toroidale porta naturalmente a definire una configurazione che evidenzia ed individua diverse regioni.

L' *X-point* è definito come il punto dello spazio in cui il campo magnetico poloidale si annulla. La superficie di flusso magnetico che si interseca con il punto X è chiamata *Separatrix* e tutte le superfici di flusso esterno ad essa sono aperte, quindi non confinate. Per questo motivo la *Separatrix* definisce l'ultima superficie di flusso chiusa (LCFS). Precedentemente le LCFS erano determinate inserendo un'interfaccia materiale denominata *Limiter*.

Le più recenti tecnologie disponibili per il divertore e più in generale per PFCs, indipendetemente dal fatto che siano fatte di CFC o di W, sono in grado di gestire

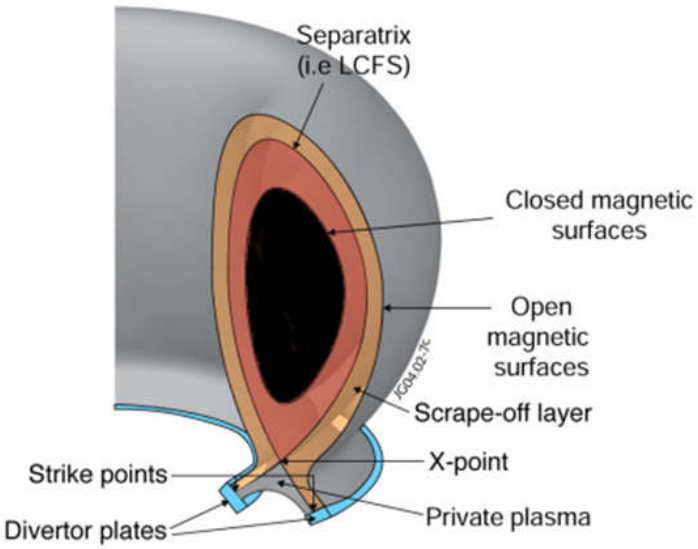

Figure 1: Schema del bordo del plasma investigato

in regime stazionario delle densità di potenza dell'ordine dei $10MW/m^2$. Perciò l'approccio principale per le operazioni di funzionamento del divertore di ITER è basato sulla rimozione di questa potenza in un apposito canale prima che essa arrivi a contatto con la superficie del divertore stesso. Bisogna tener presente che l' ottimizzazione del funzionamento di tale componente e la previsione del flusso di potenza che grava sulla prima parete risultano compiti ardui, non essendo completamente chiari tutti i processi in gioco e le loro interazioni. In questa situazione infatti la potenza termica risulta influenzata da diversi fattori quali sono l' interazione di processi di trasporto nel plasma, le perdite nella parete, i complessi processi atomici e le interazioni molecolari. Le proprietà della potenza smaltita sono determinate in larga parte dalla SOL(*scrape-off layer*), definita come la regione che possiede linee di campo magnetico aperto al di là dell'ultima superficie chiusa di flusso. Il trasporto in direzione perpendicolare alle linee di forza del campo rappresenta uno dei parametri più importanti per capire l'ordine di grandezza della potenza che attraversa lo SOL e che depositata sul vessel. Questo trasporto è in larga parte regolato da fenomeni di tipo turbolento di modo che lo spessore dello SOL dipende dal rapporto tra la potenza trasportata parallelamente e quella trasportata perpendicolarmente.

È proprio nell' ambito dei fenomeni che avvengono al bordo del plasma che si colloca la teoria dell'*Ion Orbit Loss*(IOL). Tale effetto è stato spesso considerato come secondario ma i recenti sviluppi hanno dimostrato che è in grado di spiegare fenomeni di cui si possedeva solo un'evidenza sperimentale quale ad esempio la rotazione intriseca misurata a seguito di una perdita di corrente attraverso il bordo.

L'IOL può avvenire secondo due diversi meccanismi, entrambi i quali comportano la fuoriscita di particelle attraverso il bordo del plasma. Il primo, nonchè quello più conosciuto e quello su cui si focalizza questa tesi, considera il caso di quegli ioni che, muovendosi lungo sezione poloidale seguendo un'orbita passante o un'orbita a banana, possono lasciare il plasma subendo delle derive che li portano ad attraversare

il *Separatrix*. Questo primo meccanismo prende il nome di *standard Ion Orbit Loss*. Esso è valido sia per gli ioni termalizzati del plasma che per quelli più energetici che vengono o emessi dalla reazione di fusione o iniettati attraverso NBI, *Neutral Beam Injection*. Gli NBIs sono dispositivi che permettono il riscaldamento di un plasma, per iniziare una reazione di fusione nucleare sostenuta. In un plasma di isotopi di idrogeno confinato magneticamente, un fascio di particelle neutre ad alta energia è in grado di trasferire la propria energia cinetica al plasma, aumentandone così la temperatura.

Il secondo meccanismo di *Ion Orbit loss* è un processo associato all'esistenza dell' *X-point*. Quando uno ione si trova su un orbita che passa nell'intorno *X-point*, esso subisce un spostamento poloidale dal momento che in questa area il campo magnetico poloidale è molto piccolo. Esso perciò risulta intrappollato nell'intorno dell'*X-point* ed è soggeto alla forze di drift dovute sia alla curvatura verticale della linea di campo magnetico e sia al gradiente del campo magnetico, che danno la possibilità allo ione di attraversare la LCFS e finire nella zona del divertore. La velocità degli elettroni è tale che non subiscano l'intrappolamento e quindi non sono affetti da questo meccanismo. Perciò esiste una corrente netta ionica che flusice in senso radiale, dall' *X-point* verso l'esterno, generando un campo elettrico radiale. Quest'ultimo interagisce con il campo magnetico toroidale per produre quello che è chiamato $E \times B$-*drfit*, che nel caso specifico è in direzione poloidale. Questo drift fornisce agli ioni una via per evadere dalla zona dell'*X-point* e proseguire il moto poloidale. Perciò l'effetto complessivo, cioè il tasso degli ioni persi, è dovuto ad un bilancio tra la forze generate dalla curvatura delle linee di campo e dal gradiente B rispetto a quelle indotte dal $E \times B$-*drfit* che ne consente la fuga. Questa tipologia di *Ion Orbit Loss* viene indicata come *X-loss*.

Per ricavere l'equazione fondamentale dell' *Ion Orbit Loss* si utilizzano tre equazioni di bilancio: conservazione del momento angolare toroidale, conservazione dell'energia

e conservazione del momento di dipolo magnetico ricavato dalla la teoria degli invarianti adiabatici. Combinado le ultime due queste equazioni è possibile ricavare una formula che lega la velocità iniziale alla componente parallela (rispetto alle linee di campo della velocità) ed quindi possibile individuare una condizione quando questa componente si annulla. Questa non è altro che la condizione minima per cui la particella possa compiere un'orbita a forma di banana. Sostituendo il valore della componente parallela ricavata dal conservazione del momento angolare toroidale, si riesce ad ottenere un'equazione quadratica la cui incognita è il modulo della velocità iniziale. Da questa è possibile ottenere un'equazione equivalente per l'energia.

Si noti che nel ricavare questa espressione, non si è fatto riferimento ad una particolare geometria che potrà per tanto essere specificata a seconda dei casi di interesse. In quelli qui presi in considerazione, si utlilizzato un modello a geometria circolare per descrivere una sezione poloidale del plasma, rinunciando alla pi realistica forma a "D". Fissando una posizione iniziale contraddistinta dal pedice "0", per uno ione che abbia un coseno direttore inizale ζ_0, e specificando una posizione finale caratterizata adal pedice "S" sulla LCFS ψ, è possibile risolvere l'equazione ricavando la velocità minima che uno ione deve avere per entrare nello SOL ed essere così fondamentalmente perso.

Risolvendo l'equazione si notano due aspetti fondamentali. Il primo è che l'energia minima affinchè uno ione finisca nel SOL risulta maggiore per gli ioni che viaggiano nello stesso verso con cui gira la corrente di plasma rispetto a quelli che si muovono in verso opposto. fig 2.

Dall'equazione quadratica è possibile ricavare le frazioni perse sia di energia che di particelle nello SOL utilizzando opportunamente la teoria fluida e assumendo che la particelle possiedano una funzione di distribuzione di tipo maxwelliano. Da qui si evidenza il secondo aspetto fondamentale, ossia il fatto che l'emissione di particelle e quindi di energia non è uniformemente distributa lungo la sezione poloidale. fig3.

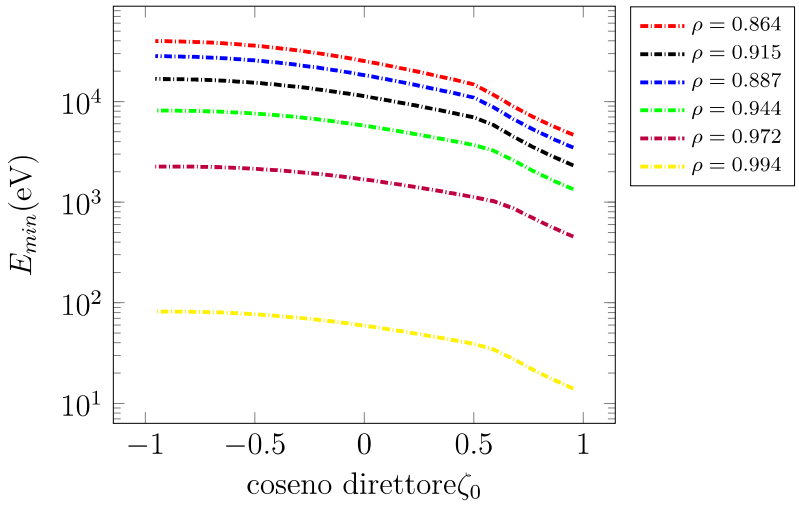

Figure 2: Valore di $E_{min}(\zeta_0, \rho_0)$ per ogni punto di partenza definito da θ_0 sulle diverse superfici di flusso

Questa disuniformità rappresenta il punto di partenza stesso della tesi. Infatti è noto che i materiali utilizzati nel *first wall* forniscano le condizioni al contorno per le quantità termodinamiche del plasma quali densità, temperatura e pressione. La loro efficienza determina il massimo guadagno raggiungiubile e quindi le prestazioni globali del Tokamak. Avere una distribuzione di energia persa così sbilanciata da un lato piuttosto che dall'altro fa si che esistano delle zone in cui i limiti strutturali vengono ampiamente superati compromettendo il funzionamento di tutto l'impianto. Cercare una via per rendere la distribuzione più uniforme e quindi rilocare le perdite risulta di fondamentale importanza per la vita delle componenti strutturali. La figura 4 aiuta a visualizzare i piani su cui le perdite sono maggiori, l' *outboard midplane* e quelli su cui sono minori. l'*inboard midplane* utlizzando lo schema di una sezione poloidale nell'ipotesi di superfici di flusso circolari. Nella stessa figura è evidenziata anche la discretizzazione che verrà utilizzata nel codice di calcolo.

In realtà è la struttura stessa della stessa geometria toroidale a dare luogo a perdite differenti sui due lati del divertore. Il campo magnetico toroidale è inversamente proporzionale al raggio avente come origine l' asse centrale del Tokamak. Questo crea

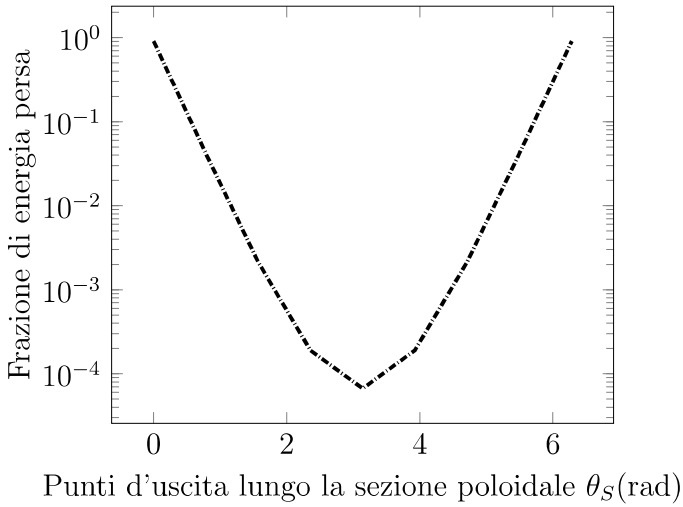

Figure 3: Frazione di energia persa lungo LCFS

un campo magnetico molto più intenso all'interno che all'esterno peggiorandone il confinamento.

L'obiettivo principale della tesi è stato quello di cercare di rendere più unifrome questa distribuzione, partendo dall'equazione quadratica e analizzando quali siano i termini che influenzino maggioramente il valore della velocità minima. I termini sono stati individuati nel campo magnetico toroidale e nel potenziale elettrostastico di ciascuna superficie chiusa.

Per modificare il campo magnetico toroidale si è pensato di aggiungere un'extra set di magneti chimati *shim coils*, in modo da aumentare il valore del campo magnetico sull' *outboard midplane*. Così facendo si sono analizzato tre casi: il primo dove il campo magnetico toroidale è stato aumentato del 10%, il secondo offre un aumento del 30% e infine il terzo presenta un valore doppio rispetto al caso iniziale. L'ultimo caso è stato considerato solo come un studio, dal momento che rappresenta un caso irrealistico. Infatti se fosse possibile cambiare così tanto il valore del campo magnetico il sistema non sarebbe neanche più da considerarsi un Tokamak.

Il software utilizzato per risolvere quest' equazione è GTEDGE. Questo è un codice sviluppato alla Georgia Tech dal Dr. Stacey che descrive il bordo del plasma

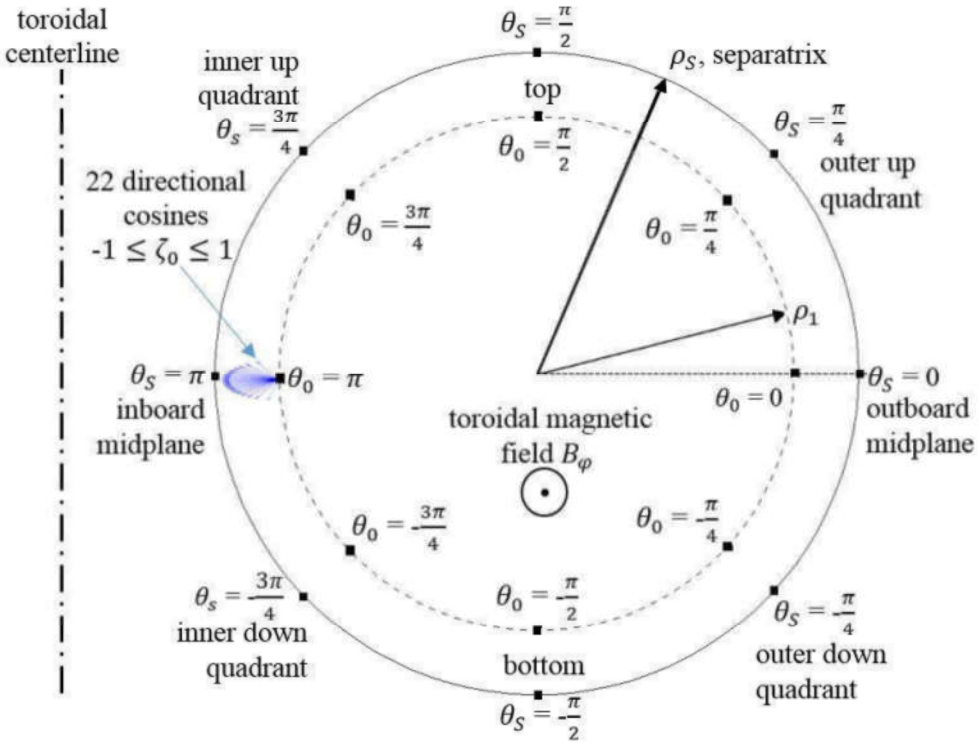

Figure 4: Illustrazione sulla sezione poloidale dei punti di partenza θ_0, sulla prima superficie di flusso ρ_1 e dei punti d'uscita con campionamento dei coseni direttori ζ_0 rispetto a B_ϕ.

tenendo conto delle equazioni di bilancio della teoria fludia e assumendo un modello 2D per *neutral recycling* includendo delle correzioni cinetiche. Esso è utilizzato sia per interpretare dei dati osservati sperimentalmente provenienti dal reattore DIII-D ed utile anche con uno scopo predittivo. Bisogna considerare il fatto che, quando si risolve l'equazione quadratica e si calcolano le varie frazioni di energia e di particelle perse, non si ha nessuna indicazione riguardo la posizione in cui le particelle sono state perse. Per questo motivo uno degli ultimi aggiornamenti al codice stato quello di scrivere un'apposita sezione per l'allocazione delle particelle. L'allocazione viene fatta lungo sia lungo la LCFS, sia per ciascuna delle superficie chiuse di partenza. In questo ultimo si tiene conto delle particelle che abbandonano il plasma sulla superficie precedente attraverso l'ultilizzo di una funzione Maxwelliana troncata a valori di energia sempre crescenti.

Le simulazioni riguardanti la modifica del campo magnetico sono state condotte anche raffinando il codice, aumentando il numero di punti in cui variava il campo magnetico e inserendo incrementi proporzionali alla distanza del punto considerato dallo *shim coil*. Nonostante fossero più accurati, i risultati non hanno stravolto l'andamento rispetto al caso originale e questo è possibile osservarlo dalla figura **??** in cui si ritiene realizzabile l'incremento del 30% del campo magnetico iniziale. Si tiene ben presente che ciò comporterebbe una crescita della corrente che scorre nei *coil* e tutta una serie di difficoltà alla tecnologia dei superconduttori, oltre al fatto che il costo dell'impianto aumenterebbe sensibilmente. In modo equivalente gli stessi aumenti vengono applicati al potenziale elettrostatico. Per ottenere questa modifica bisognerebbe modificare la corrente che scorre nei piatti del divertore, ci porterebbe a considerare ulteriori relazione che tengono in conto anche la presenza delle impurtà. Anche in questo caso i risultati ottenuti non sono stati quelli sperati, si veda la figura 6.

Perciò si cercato di effettuare un'analisi di sensitività sui tre coefficienti dell'equazione

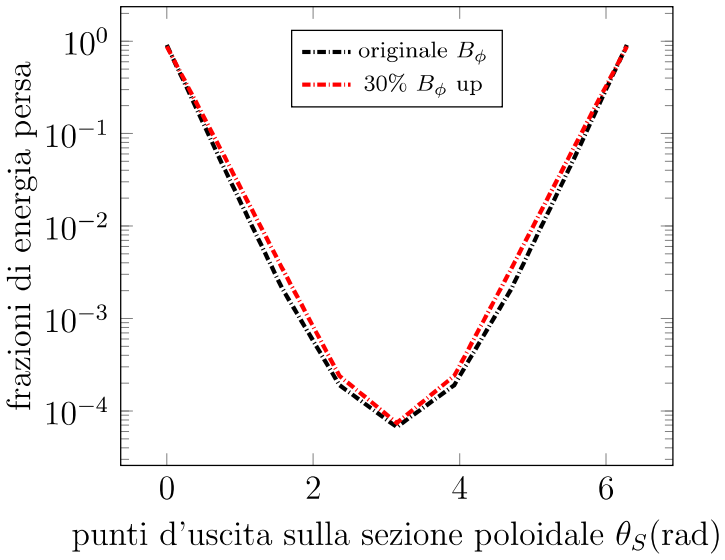

Figure 5: Frazione di energia persa lungo LCFS

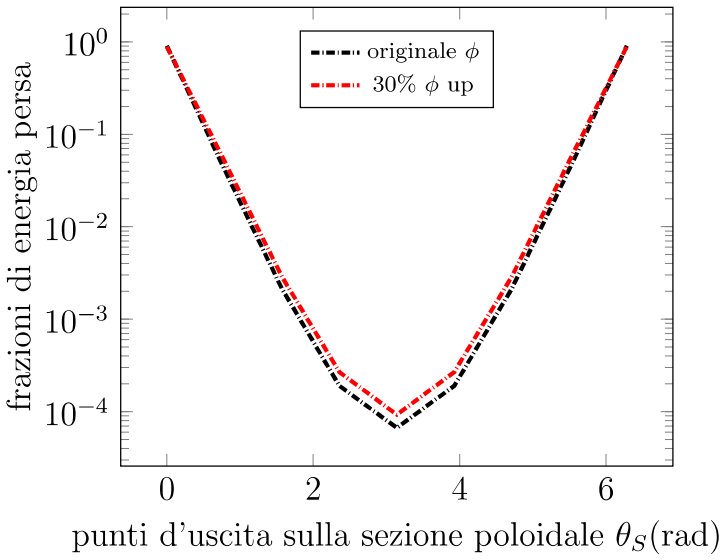

Figure 6: Frazione di energia persa lungo LCFS

quadratica:

$$a = \left[\left(\frac{R_0}{R_s} \frac{f_{\varphi 0}}{f_{\varphi S}} \zeta_0 \right)^2 - 1 + (1 - \zeta_0^2) \frac{B_S}{B_0} \right]$$
$$b = \left[\frac{2e(\psi_0 - \psi)}{R_S m f_{\varphi S}} \left(\frac{R_0}{R_S} \frac{f_{\varphi 0}}{f_{\varphi S}} \zeta_0 \right) \right]$$
$$c = \left[\left(\frac{e(\psi_0 - \psi_S)}{R_S m f_{\varphi s}} \right)^2 - \frac{2e(\phi_0 - \phi_S)}{m} \right]$$

Con a coefficente del termine quadratico, b del termine lineare e c è il termine noto. Il coefficiente del termine quadratico è l'unico che contiene il campo magnetico toroidale in una forma diversa da quella di un rapporto. Si osserva che questo termine molto piccolo rispetto agli altri due e questo spiegherebbe i non eseltanti risultati legati agli incrementi del campo magnetico. Il termine noto invece contiene tutta la dipendenza del potenziale elettrostatico, ma come è nota nella formula risolutiva di un'equazione di secondo grado esso è sempre moltiplicato per il coefficente del termine quadratico, facendo si che i valori vengono sensibilmente ridotti.

Per concludere bisogna tenere presente che tutta una serie di ipotesi sono state fatte a tale riguardo. Ad esempio nel caso analizzato si stanno ignorando i possibili effetti legati allo scattering, che possono in qualche modo far si che la particella ritorni nel plasma. Sono stati ignorati tutti gli effetti e i fenomeni dovuti alle impurità. Un'altra ipotesi importante è quella per cui si trascura il trasporto perpendicolare alle linee di campo che coinvolge fenomeni di turbolenza. Assumere un' unica distribuzione Maxwelliana e troncarla man mano che ci sposta verso il bordo del plasma potrebbe essere un'assunzione limitante dal momento che quando ci si sposta verso il bordo del plasma cambia la temperatura e di conseguenza la maxwelliana dovrebbe essere diversa su ogni superficie di flusso chiusa. Si sono omessi gli effetti dovuti allo *Shafranov-shift* che cambierebbero le espressioni delle superfici di flusso assunte circolari. Infine quando si è cambiato il valore campo magnetico e del potenziale elettrostatico sono stati trascurti gli effetti di interazione tra il campo magnetico e quello elettrico. Queste assunzioni che a prima vista sembrano rendere la trattazione del

problema molto ideale in realtà conduce a dei risultati molto vicini alle osservazioni sperimentali. A valle dei risultati ottenuti si può affermare che con tutta probabilità le azioni intraprese non sono sufficienti per uniformare la distribuzione di potenza lungo la sezione poloidale e bisognerà ricercare altre vie.

CHAPTER I

THERMONUCLEAR FUSION

It has been well known for many years that standard of living is directly proportional to energy consumption[1]. Energy is used for producing everything a modern human being need. Recent studies acknowledge that by the year 2100 world energy demand could at very least be double present world usage. Nowadays the importance of having an alternative to the fossil fuels is at center of world debate. Governs of all the world have called to make a choice and they have to deal with economical and environmental aspects. Different power source has been studying right after the second world war. Besides the coal, oil and natural gas the the relative new energy sources are nuclear fuels and renewable sources,especially hydroelectric. It is not a secret that the fossil fuels will not last forever and the renewable technology has some issue as well.Therefore the nuclear power seems to be a competitive choice for the future both on economical and environmental side. Since the nuclear power plants were born, there were undeniable advantages. In the first place the astonishing advantage of the nuclear power is due to the fact that when a chemical bond is formed the energy released is on the order of electronvolt instead when we a nuclear bond is broken or formed the energy released is on the order of mega-eletctronvolt(MeV). This huge difference is reflected on the usage of the fuel that will be a small amount compared to the the one used from fossil fuels. This feature has got a crucial importance on the cost of producing electricity. Indeed this cost is largely related to the cost of fuel and the amount consumed. In a carbon power plant to reduce the cost it is necessary to raise up the the efficiency of the plant (the power produced through the turbine over the thermal power introduced by the reactor). This requirement is useless when it

comes to a nuclear power plant, since the energy released by small amount of nuclear fuel is way greater than the one released by the same amount of carbon fuel. Proliferation has always been a critical factor and it needs to be taken carefully into account in every nuclear project Fusion is a form of nuclear energy. Its main application is the production of electricity in large base load plants. Today the wide diffused nuclear power plant are based on the fission reaction (splitting of an heavy nucleus) and they already represent a large percent of electricity production for countries like France and Japan. Nuclear fusion refers to the nuclear reaction that merges two hydrogen isotope (and in general two light nucleus) into a heavier nucleus,producing neutrons, α-particle or ions. Nuclear safety is by far the most speculated feature, but with no doubt is primarily important. One of the main issue of fission reactor is to avoid the meltdown of core, to prevent accident as Three Mile Island. The physic law governing fusion reaction make this impossible. Specifically, in a fission reactor the entire energy content corresponding to several years of power production is stored within the reactor core at any instant of time (decay heat). This huge energy makes a meltdown possible. A fusion reactor does not depend on maintaining a chain reaction in a large sitting mass fuel. Instead, fuel must be constantly fed into the reactor at a rate allowing it to be consumed as needed. The end result is that at any instant of time the mass of fuel in a fusion reactor is very small, this makes a meltdown impossible in a fusion reaction.

However fusion has disadvantages too. Firstly the scientific and engineering challenges inherent the building of fusion power plant. After overcome this issues, the last step will be to integrate all the solution into an economically competitive power plant that would allow fusion to become a valuable option for energy production. To begin with, we are going to discuss briefly the basic concept of magnetic confinement fusion reactor and the reactor components involved into the thesis, which are first and second chapter respectively. The third and fourth chapter will explain the basic

of Ion orbit loss theory and the tool that we used for our calculation. In doing so we are going to figure out what are the terms of the IOL equation that rule the equation. In the last chapter the results will be discussed.

1.1 Fusion reaction

The mass of atomic nucleus is not the sum of the masses m_p of the Z-proton and masses m_n of the $A - Z$ neutrons of which it is composted.The stable nuclides have a mass defect $\Delta = [Zm_p + (A - Z)m_n] - Am_z$. This mass defect is equivalent to an energy ,according to Einstein's formula ($\Delta E = (\Delta m) \times c^2$), at the time that the nucleus was formed, putting it into a stable state. The amount of externally supplied energy that would have to be converted to mass in disassembling a nucleus is known as the "binding energy" of the nucleus $BE = \Delta c^2$.The plot of binding energy per nucleon (BE/A)is shown in (7). Thus any process which results in nuclides being

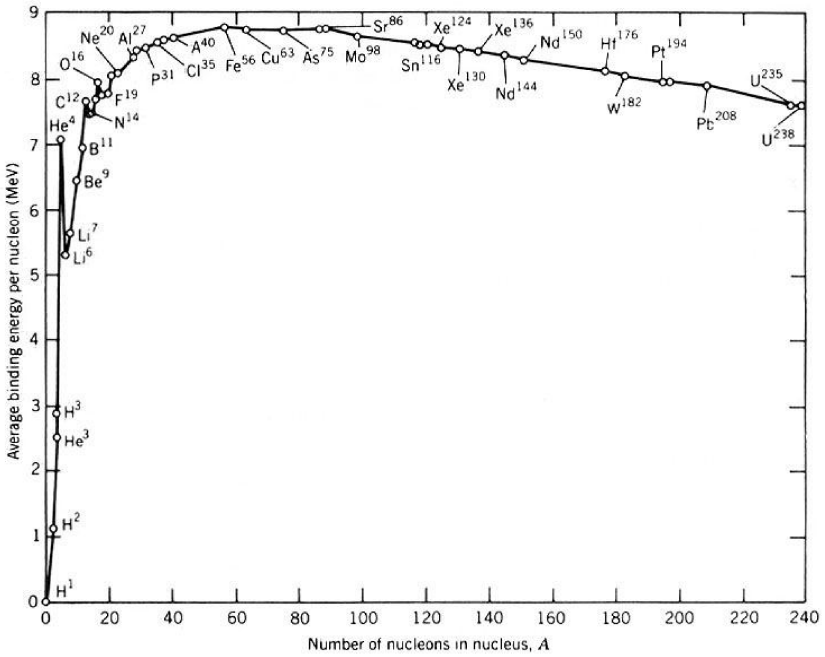

Figure 7: Binding energy per nucleon

converted to the other nuclides with an increasing of binding energy per nucleon will result in the conversion of mass into energy. [2] The binding energy is almost

a constant around the 8MeV value, excpet for the light nucleus. The figure shows that if a nuclide with $A > 60$ is split in two or more lighter nuclides or with $A < 60$ are combined together, the binding energy raise up. This means that after these two processes the nuclides are more bonded, more stable and since the binding energy is enhanced there is a release of nuclear energy.The first process is called nuclear fission and the second nuclear fusion. $A = 60$ is the condition where there is the highest bond,corresponding to a metal like Fe. In order for the fusion reaction to take place the two nuclei must overcome the long-range Coulomb repulsion force and approach sufficiently close that that the short-range nuclear attraction force can lead to the formation of a compound nucleus. For fusion to occur as a result of random encounters between atomic nuclei, the nuclei must be made sufficiently energetic to overcome the Coulomb repulsive force. The probability of the reaction, when two nuclei are colliding, depends on their relative kinetic energy and is provided by the cross section, $\sigma_f(E)$. This is usually measured in "barns"(b), equivalent to $10^{-24}cm^2$. The figure (8) shows that the energy required are of the order of 10keV to 100 keV which corresponds to temperatures of 10^8keV to 10^9keV ($1eV$ is about 10^5K). These temperatures are comparable to those in the center of the sun, therefore at these temperature the light atoms are fully ionized. This macroscopically neutral gas of positive charged nuclei and electrons is called thermonuclear plasma. Its behavior is dominated by long range electromagnetic collective effects rather then interaction of single close particles. It is an excellent electricity conductor, shielding both DC and AC electric fields, and exhibits local quasi-neutrality property: the electron density is locally equal to the ion density. Hence no static electric fields are present due to charge imbalance. The fusion reactions of primary interest are shown in table 1 At the temperatures below the threshold value the reaction rates are negligible (9). The deuterium-tritium (D-T) reaction produces more energy than a pure deuterium reactions. Moreover D-T reactions occur at a faster rate, therefore it makes easier

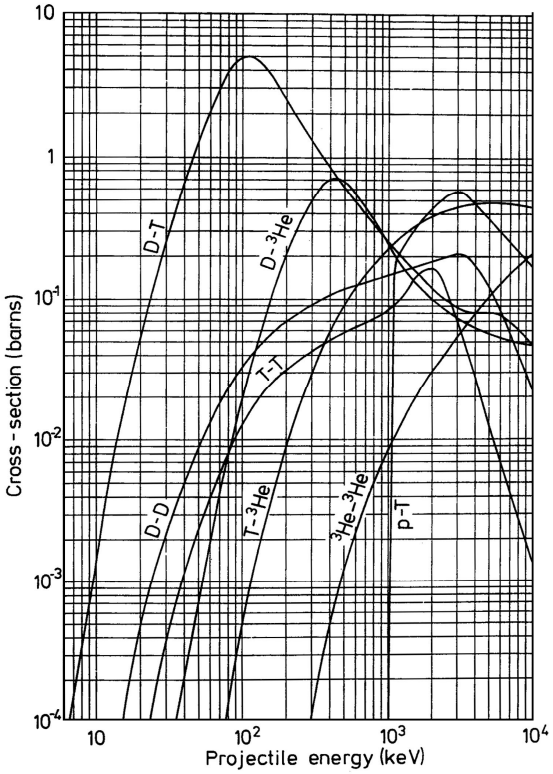

Figure 8: Cross section fusion reaction

Elemento	Thermonuclear energy release(MeV)	Threshold energy K	KeV
$D + T \rightarrow {}^4He + n(14.1MeV)$	17. 6	4.5×10^7	4
D+D$\rightarrow$ $\begin{cases} T + p \\ {}^3He + n(2.5MeV) \end{cases}$	4.0 3.25	4.0×10^8	35
$D + {}^3He \rightarrow {}^4He + p$	18.2	3.5×10^8	30

Table 1: Fusion reaction of primary interest

built such a reactor, even though tritium is not a natural isotope and it must be artificially produced. The table(1) points out the most probable reaction at lower kinetic energy is the deuterium-tritium reaction, it gives rise to a α particle and neutrons. The Q-value (energy released for each reaction) is 17.6 MeV. In macroscopic terms, just 1kg of this fuel would release 10^8kWh of energy and would provide the requirements of a 1 GW (electrical) power station for a day. [3] Four over five of this

energy leave the plasma by the neutrons and the leftover energy is in the form of α particles.The alpha particle is confined within the plasma and its energy is distributed via collisions among the plasma ion and electrons and eventually is incident upon the wall of the reaction chamber as a surface heat flux. The neutrons leaves the plasma immediately and gives up its energy to the surrounding material via elastic and inelastic collisions with lattice atoms, producing a volume heat source and, in the process, radiation damage to the material due to atomic displacements. The fusion neutron is ultimately captured or leaks from the system.[4] The deuterium is an isotope of hydrogen and it is provided naturally in the ocean water. There is atom of deuterium for every 6700 atoms of hydrogen. The tritium is a radioactive isotope with a half life of only about 12 years and there is no natural tritium to be found on earth. Thus we need to produce it artificially by breeding with the lithium isotope. The production reaction are:

$$n + {}^{6}Li \rightarrow T + {}^{4}He$$

$$n + {}^{7}Li \rightarrow T + {}^{4}He + n'$$

The first reaction has a large cross section for thermal neutrons, while the second reaction is more probable with the fast neutrons.

It is not necessary the all the plasma particles are at high energy for producing a significant amount of energy. In fact ions inside the plasma have a different kinetic energy characterized by a distribution function. If a certain amount of particles, even in the tail of the distribution function overcome the threshold, there exists a probability to undergo a fusion reaction. The reaction rate can be evaluated as a function of particles velocity for the distribution function $\langle \sigma v \rangle$. This is the important parameter to address when we are interested to a sustained fusion reaction inside the

plasma. The fusion reaction rate per unit volume can be written

$$R\left(\frac{fusions}{m^3}\right) = n_1 n_2 \langle \sigma \upsilon \rangle$$

where n_1 and n_2 are the densities of species 1 and 2 and

$$\langle \sigma \upsilon \rangle_{12} = \int\int d^3\upsilon_1 d^3\upsilon_2 f_1(\boldsymbol{\upsilon}_1) f_2(\boldsymbol{\upsilon}_2) \mid \boldsymbol{\upsilon}_1 - \boldsymbol{\upsilon}_2 \mid \sigma_f(\mid \boldsymbol{\upsilon}_1 - \boldsymbol{\upsilon}_2 \mid)$$

is the fusion reactivity. Here υ is the velocity, f is the velocity distribution function and $\sigma_f(E)$ is the fusion cross section. It is usually adequate to use a Maxwellian distribution:

$$f_{Max} = \left(\frac{m}{2\pi\kappa T}\right)^{\frac{3}{2}} \exp\left(-\frac{m\upsilon^2}{2\kappa T}\right)$$

to evaluate the fusion reactivity, in which case the value of the integral depends only upon the temperature T of the plasma. The fusion reactivity is shown in figure (9).

1.2 Tokamaks

Since the plasma is ionized the presence of a magnetic field constrains the particles to move in a spiral around the magnetic field lines, as a consequence of Lorentz force, $F = q\boldsymbol{\upsilon} \times \boldsymbol{B}$ where q is the particle charge, $\boldsymbol{\upsilon}$ is its velocity and $\boldsymbol{B}$ is the magnetic field. One of the possible strategy to confine the plasma is therefore to use appropriate magnetic field,resulting in the usually called "magnetic confined fusion". The Tokomak is a toroidal plasma confinement system, the plasma being confined by a magnetic field. This device is the most studied in the last 50 years and up to now has demonstrated to be the most promising solution for building a fusion power plant in the future. Tokamak were invented in the 1950s by USRR scientist Igor Tamm and Andrei Sakharov, inspired by an original idea of Oleg Lavrentiev.Tokamak is a Russian word "toroidal'naya kamera s magnitnymi katushkami" that stand for toroidal chamber with magnetic coils. The principal magnetic field is the toroidal

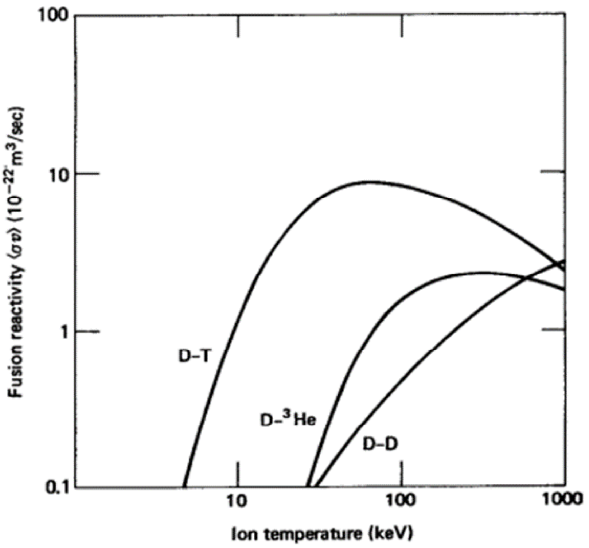

Figure 9: Reaction rate

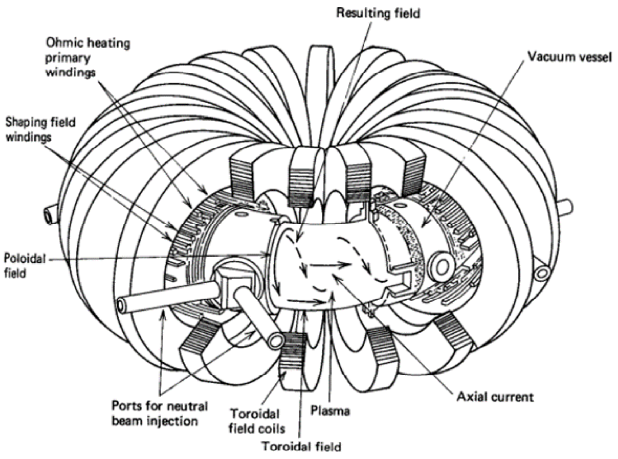

Figure 10: Tokamak schematic

field (B_ϕ). However, this field alone does not allow confinement of the plasma. The curvature and non uniformity of the toroidal field line produce forces which act upon the charged particle to produce drift motions that are radially outward. In order to have an equilibrium in which the plasma pressure is balanced by the magnetic forces it is necessary also to have a poloidal magnetic field (B_θ). In a Tokamak this field is produced mainly by the current in the plasma itself, this current flowing in the toroidal direction. The combination of B_ϕ and B_θ give rise to magnetic field lines which have a helical trajectory around the torus. The toroidal magnetic field is produced by currents in coils linking the plasma.The normal coils have several issues that make their usage limited. Superconducting coils are considered for building up the magnetic field around the plasma. Moreover the plasma is surrounded by a blanket which has three roles. Firstly , it absorbs neutron at 14 MeV, transforming their energy into heat which is then carried away by a suitable coolant to provide most of the reactor power output. Secondly, in absorbing neutrons the blanket shields the superconducting coils and other outer components. Thirdly, the blanket allows the necessary breeding of tritium to fuel the reactor as discussed in the past section. A fusion plasma cannot be maintained at thermonuclear temperatures it is allowed to come in contact with the walls of confinement chamber, because the material eroded from the walls would quickly cool the plasma. The direct contact between the plasma and the first wall is avoided by means of either a material limiter or by a divertor which leads the magnetic field line away from the plasma to a dump plate. [3]

1.3 Power balance

Heating a plasma to thermonuclear temperature and then confining it sufficiently well that a net positive energy balance can be achieved are two premier issues which will determine the scientific feasibility of fusion. In D-T plasma the thermonuclear power per unit volume in a D-T plasma is $p_{Tn} = n_d n_t \langle \sigma v \rangle \varepsilon$ where n_d and n_t are the

deuterium and tritium densities, $\langle\sigma v\rangle$ is the rate given in figure(9) and ε is the energy released per reaction. The total ion density is $n_d + n_t = n$. For a given density this power is maximized by $n_d = 1/2n$, therefore for this optimum mixture the thermonuclear power density is $p_{Tn} = 1/4n^2\langle\sigma v\rangle\varepsilon$. In a Tokamak there is a continuous loss of energy from the plasma which has to be replenished by plasma heating. The average energy of plasma particle at a temperature T is $3/2T$ Since there is an equal number of electrons and ions the plasma energy per unit of volume is $3nT$. The total energy in the plasma is therefore $W = \int 3nTd^3x = 3\overline{nT}V$ where V is the plasma volume. The rate of energy loss P_L is characterized by an energy confinement time τ_E defined by the definition $P_L = W/\tau_E$. In present Tokamaks the thermonuclear power is usually small and in steady state the energy loss is balanced by externally supplied heating. Thus if the power supplied is P_H, it means $P_L = P_H$. Inverting the expression of P_L , it can provide a means of determining τ_E from experimentally known quantities. The thermonuclear power consist in two parts: $4/5$ of the reaction energy is carried by the neutrons and the remainder, ε_α, is carried by the $\alpha-$particle. The neutrons leave the plasma without interaction, but $\alpha-$particles,being charged, are confined by the magnetic field. The $\alpha-$particles then transfer their $3.5MeV$ energy to the plasma through collisions. Thus the $\alpha-$particle heating per unit volume is $p_\alpha = 1/4n^2\langle\sigma v\rangle\varepsilon_\alpha$ and the total $\alpha-$particles heating is $P_\alpha = \int p_\alpha d^3x = 1/4\overline{n^2\langle\sigma v\rangle}\varepsilon_\alpha V$. On the whole power balance the power loss is balanced by the externally suppied power plus $\alpha-$particles: $P_H + 1/4\overline{n^2\langle\sigma v\rangle}\varepsilon_\alpha V = 3(\overline{nT})/\tau_E V$. As a D-T plasma is heated to thermonuclear conditions the $\alpha-$particles heating provides an increasing fraction of total heating. When adequate confinement conditions are provided, a point is reached where the plasma temperature can be maintained against the energy losses solely by $\alpha-$particles. The applied heating can then be removed and plasma temperature is sutained by internal heating. By analogy with the burning of fossil fuels this event it is called ignition.[3] From the last equation, setting $P_H = 0$we get a criteria for the plasma burn to be

self-sustaining being: $nT\tau_E \geq \frac{12}{\langle\sigma v\rangle}\frac{T^2}{\varepsilon_\alpha} \equiv (nT\tau_E)_{Lawson}$. This is the Lawson criterition for ignition. The plasma power amplification factor:$Q_p = 1/4n^2\langle\sigma v\rangle\varepsilon V/P_H$ is a conventional measure of scientific feasibility. $Q_p > 1$ will constitute the minimum require on the plasma energy balance. That means that the power produced by the fusion reaction in the plasma is larger than the power provided by an external source. This condition of $Q_p = \infty$ corresponds to the ignition. However, no matter what how good the confinement, future fusion reactors will operate with some external power for control purposes, so the practical definition of scientific feasibility is Q_p large enough that net electrical power can be economically produced, which is probably $Q_p > 10$ [4]. The product nT is equal to plasma pressure p as well. The magnitude of plasma pressure that can be achieved is related to the magnitude of plasma pressure that can be achieved is related to the magnitude of the confining magnetic field pressure magnetohydrodynamic (MHD) instability limits which can be characterized in terms of limiting values of $\beta \equiv \frac{plasmapressure}{magneticpressure} = \frac{nKT}{B^2/\mu_0}$. So the triple product $nT\tau_e$ indicating that the achievement of power balance at high Q_p requires achieving high plasma pressure(high β) and long plasma energy confinement time.

1.4 ITER & DIII-D

In 1979 USA, USSR, Europe and Japan came together under the auspices of International Atomic Energy Agency(IAEA) in a series of Tokamak Reactor (INTOR) Workshop.The main aim were to move forward to a burning plasma, or experimental reactor ,phase,to identify the physical characteristics and required R&D for such a device and to perform supporting feasibility and conceptual design analyses.The positive result of that workshop led to a proposal of an INTOR device, that subsequentely led to the International Thermonuclear experimental Reactor(ITER). This project has included more parties during the years. ITER is a latin word that it means the way. The site selected for assembling all the part is Cadarache in France.

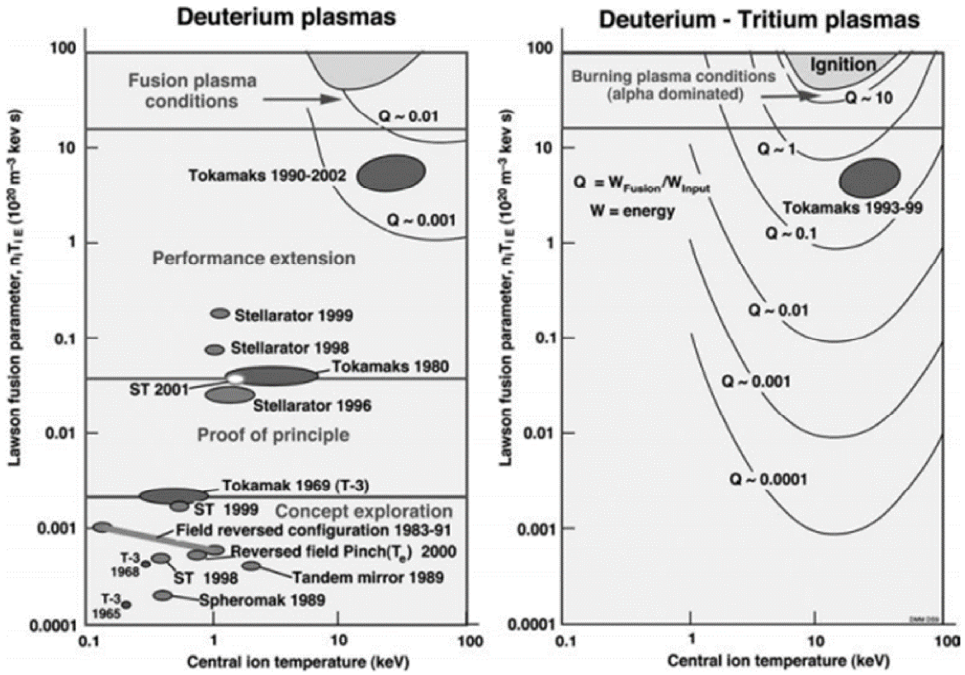

Figure 11: Progress towards scientific feasibility as measured by the Lawson criterion

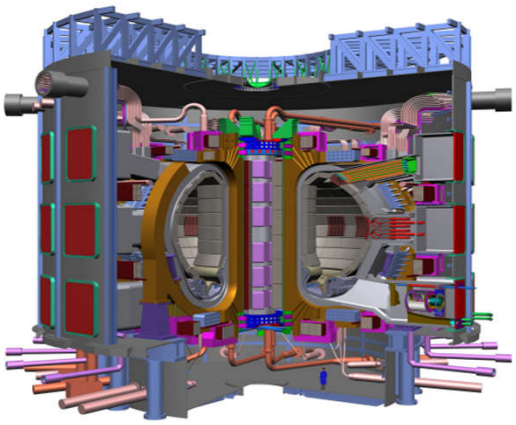

Figure 12: ITER

The world record for fusion power is held by the European tokamak JET. In 1997, JET produced 16 MW of fusion power from a total input power of 24 MW (Q=0.67). ITER is designed to produce a ten-fold return on energy (Q=10), or 500 MW of fusion power from 50 MW of input power. ITER will not capture the energy it produces as electricity, butas first of all fusion experiments in history to produce net energy gainit will prepare the way for the machine that can. Demonstrate the integrated operation of technologies for a fusion power plant ITER will bridge the gap between today's smaller-scale experimental fusion devices and the demonstration fusion power plants of the future. Scientists will be able to study plasmas under conditions similar to those expected in a future power plant and test technologies such as heating, control, diagnostics, cryogenics and remote maintenance. Achieve a deuterium-tritium plasma in which the reaction is sustained through internal heating. Fusion research today is at the threshold of exploring a "burning plasma"one in which the heat from the fusion reaction is confined within the plasma efficiently enough for the reaction to be sustained for a long duration. Scientists are confident that the plasmas in ITER will not only produce much more fusion energy, but will remain stable for longer periods of time. One of the missions for the later stages of ITER operation is to demonstrate the feasibility of producing tritium within the vacuum vessel. The world supply of tritium (used with deuterium to fuel the fusion reaction) is not sufficient to cover the needs of future power plants. ITER will provide a unique opportunity to test mockup in-vessel tritium breeding blankets in a real fusion environment. Demonstrate the safety characteristics of a fusion device ITER achieved an important landmark in fusion history when, in 2012, the ITER Organization was licensed as a nuclear operator in France based on the rigorous and impartial examination of its safety files. One of the primary goals of ITER operation is to demonstrate the control of the plasma and the fusion reactions with negligible consequences to the environment. The ITER magnets are superconducting with Nb_3Sn conductor for the toroidal fields coils and

central solenoid and with NbTi conductor for the poloidal ring coils. the vacuum vessel/first wall is water cooled copper, coated on the plasma side with beryllium, bonded onto an austenitic stainless steel structure. The divertor target plate has a similar configuration, but with tungsten coating, except near the peak heating locations where a carbon fibre composite is used.The most important uncertainties that could affect ITER performance are the achievable energy confinement and plasma density.[4]. General Atomics DIII-D was developed from Doublet III tokamak, which

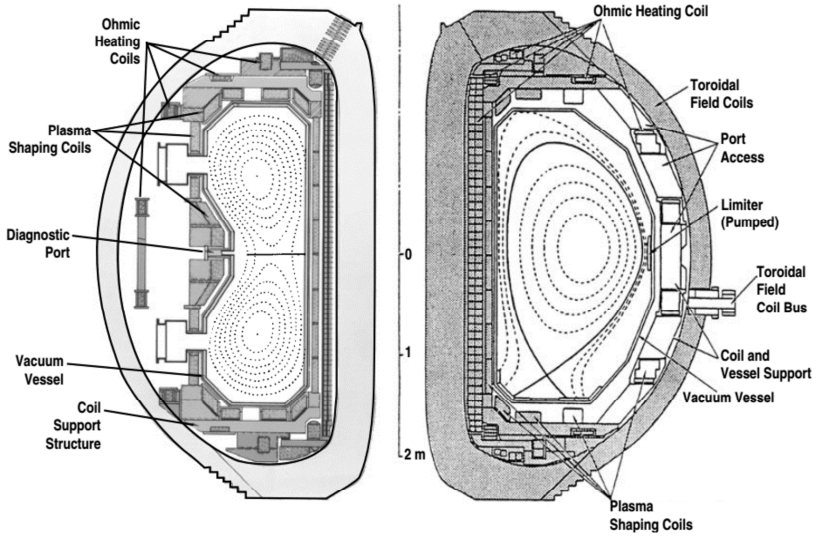

Figure 13: Left hand side, cross-section of Doublet III with a doublet shaped MHD equilibrium superposed. Right hand side, cross-section of DIII-D (1986) with a diverted equilibrium superposed; the shaded components were retained from Doublet III.

had been designed to investigate the properties of doublet shaped plasmas, in which a waist is created in the midplane of an elongated equilibrium. The Doublet III experimental was more successful when operated with a conventional plasma geometry having an ' expanded boundary ' divertor, that is with an internal magnetic separatrix but without a divertor chamber. It was, therefore decided to rebuilt the tokamak within the existing toroidal field coil set so as to maximize the volume available for

the configuration at the same time increasing the shaping capability. Compared to ITER, DIII-D is a D-D plasma instead of D-T. Different kind of studies are run as confinement H-mode (transition L-H and H-L), ELMs studies, enhanced confinement, MHD equilibrium and stability, current drive system and divertor performance.

[5]

Over the past fifteen years, the DIII-D tokamak has been a key tool in advancing the science of high temperature plasmas. The DIII-D tokamak evolved from the earlier Doublet I, Doublet II and Doublet III tokamaks.(figure(13)) A doublet is a two lobed toroidally symmetric plasma configuration with a cross section containing a separatrix in the shape of a figure 8 usually with the lobes shifted radially outwards. Doublet I (major radius $R = 17.5cm$, minor halfwidth $a = 3.75cm$) was a small device that demonstrated that a highly non-circular plasma could be stably confined using a solid copper field Doublet II (1972) extended this concept to a larger plasma ($R = 0.6m$, $a = 0.1m$) still using a copper shell. Doublet IIA (1976) demonstrated that the plasma ($R = 0.66m, a = 0.15m$) could be stably shaping shell, confined and the pulse length extended using copper coils and power supplies in place of the copper shell . Doublet III was considerably larger ($BT = 2.6TatR = 1.43m, a = 0.44m$) and designed with a copper coil configuration specialized for shaping doublet plasmas. It was also used to shape D shaped plasmas in the upper half of the chamber. Doublet III first went into operation in 1978, and operations were stopped in 1984 for the upgrade to DIII-D. An excellent summary of the history of the Doublet programme can be found in [6]. The DIII-D device was first proposed in the late 1970s, with construction being completed and the device commissioned in 1986. The name Doublet III was shortened to DIII and -D was added to indicate the new shape. Initial results demonstrating H mode confinement, substantial beta ($\beta = 1.4\%$) with neutral beam heating and record plasma currents up to 2 MA were reported later that year [12]. DIII-D used the space within the Doublet III toroidal field coil($B_\phi = 2.2T$) for a large ($R = 1.66m, a =$

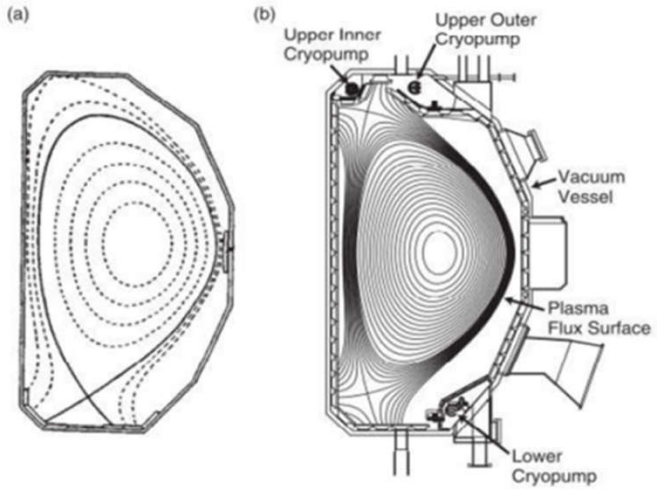

Figure 14: (a) A cross-section of the DIII-D vacuum vessel in 1986 with an MHD equilibrium superposed: a location between the ports is chosen. (b) Cross-section of the DIII-D vacuum vessel and typical ports in 2000 with MHD equilibrium superposed. Note no fundamental changes to the ports and their locations have occurred since construction.

$0.67m$) highly elongated ($\kappa \approx 2$) D shaped plasma chamber(figure 14).The plasma chamber and outer poloidal field coils were the major components replaced along with the internal armour, many diagnostics, the vacuum chamber interfaces of the auxiliary systems, and many aspects of the control and data interface system. Since then, the device has undergone a significant number of changes to evolve its scientific capability consistent with new understanding of the relevant physics and technologies. A comprehensive diagnostics set has evolved and effective heating systems have been developed and installed. The focus of the DIII-D research programme has been on improving our scientific understanding of the behaviour of high temperature plasmas and attaining high plasma performance. The DIII-D tokamak has achieved high beta ($\beta = 13\%$), high confinement and high performance, $n\tau T_i = 7 \times 1020 keV m^3 s$ (equivalent to $Q_{DT} = 0.32$) in a modest sized device. The stability of discharges has been compared with the results of MHD theory , and transport results have been carefully related to theory . The divertor configurations have been shown to be effective in managing the edge plasma and the plasma density, and in helium ash removal. The diverted plasma cross-section has become accepted for the design of later tokamaks (ASDEX Upgrade, JT-60U, ITER, KSTAR, TPX, FIRE, ARIES and the modification of JET). Most recently, the DIII-D programme has been in the forefront of understanding the science of reactor relevant plasmas. The DIII-D design was driven by the desire to achieve high plasma performance in a modest sized device while maintaining the flexibility in the configuration to allow the device to be modified in response to changing needs in the research programme. The design was optimized to allow the maximum useful plasma elongation and triangularity δ. Multiple close fitting plasma shaping coils were used to provide precise plasma shaping and control for a wide range of plasma cross-sectional shapes. A low aspect ratio, $R/a = 2.5$, was chosen to allow higher plasma currents within a given value of the safety factor q. High temperature baking (up to 400C) and high vacuum techniques

were implemented to allow rapid recovery of vacuum and wall conditions after periods of in-vessel work, both initially and after subsequent contamination, and to reduce impurities. Water cooling integral with the vessel walls allows in-vessel armour and other components to be cooled by thermal contact with the walls. Finally, excellent access was provided for auxiliary systems and diagnostics. The tokamak operates in a pulsed mode, with 10 s long discharges (6 s discharge flat-tops) 12 min or more apart. Most of the components are inertially cooled. The conductors of the major coils are water cooled copper. The coil systems were designed to support D shaped plasmas with up to 5 MA current ($q \approx 2.6at2.1T$) and divertor plasmas up to 3.5 MA ($q \approx 2at2.1T$). The lack of continued improvement in plasma performance with current below safety factors of q = 3, decisions to use part of the vessel aperture for divertor hardware and design limitations of the divertor hardware have resulted in the de facto current limit of the present machine being 3.0 MA for limiter and divertor discharges. The DIII-D tokamak has evolved in the intervening years in its role as a versatile research device. The vacuum vessel interior has been completely sheathed with graphite tiles and a series of three divertor baffles has been added. In situ cryogenic pumps have been added in the top and bottom of the plasma chamber (figure 2(b)). The coil power systems have been upgraded for longer pulse duration and improved performance, a nuclear radiation shielding enclosure added, extensive plasma chamber wall conditioning developed and a state of the art digital plasma control system has evolved. The upgraded neutral beam heating systems provide 16 MW of deuterium power into the plasma for 5.0 s, and up to 6 MW (source power) of ICRF and 4 MW (source power) of ECRF have been added. The addition of a radiation shield over the machine hall allows operation with deuterium fuel. A set of some 60 diagnostics provides temporal and spatial data for a wide range of plasma parameters[5]. DIII-D is the tokamak where the experimental data comes from. Here there are some parameters which summarize the characteristics of DIII-D and ITER.

Parameter	ITER	DIII-D
$Q_p = P_{fus}/P_{aux}$	10	0.01
P_{lcsf}/P_{L-H}	1.6	1
R(m)	6.2	1.85
a(m)	2.0	0.58
B(T)	5.3	1.91
I(MA)	15.0	2
T(Kev)	11.2	6.3
H_H(enhancement of H-mode)	1.0	0.88
$\tau_e(s)$	3.7	0.08
β	2.6%	2.9%
q_{95}	3.0	3.86
κ	1.8	1.86
δ	0.4	0.374
$n(m^{-3} \times 10^20)$	0.91	0.4

Table 2: ITER and DIII-D main parameters

CHAPTER II

TOKAMAKS COMPONENT

One of the major concerns in fusion reactor design is that of controlling the power reaching the solid surfaces around the plasma. ITER is designed to produce 500MW of fusion power that sums up with the necessary 50MW of external heating power, leading to 550MW of total power input in the machine. The major part of it, carried by fusion neutrons will escape the magnetic cage and get deposited in the reactor's blanket. The remaining 150MW (100MW of fusion power carried by α particles and 50MW of external heating) have to be exhausted in steady state operation. About 50MW will be spread over the first wall due to various radiation processes. In magnetic confinement devices the plasma is confined within closed magnetic flux surfaces, normally generated by a combination of fields due to external conductors and by currents flowing in the plasma. Such a fields can only be generated within a restricted volume and therefore a boundary determined by the last closed flux surface (LCFS). However closed magnetic surface may be interrupted by a solid surface which then determines the position of the last closed flux surface. Such a sold surface is called limiter. Alternatively the closed surface may determined entirely by the magnetic fields so that outside the LCFS, the plasma flows towards and eventually interacts with a solid surface. This is the basic geometry of a divertor. The essential difference between the two is that with a limiter the LCFS is in contact with a solid surface, while with a divertor the solid surface is removed some distance from LCFS. The ITER project encompass the divertor design. In this section we are going to describe two components of Tokamaks: the toroidal field coils (TF coils) which generate the toroidal magnetic field and the divertor.

2.1 Tokamak Magnets system

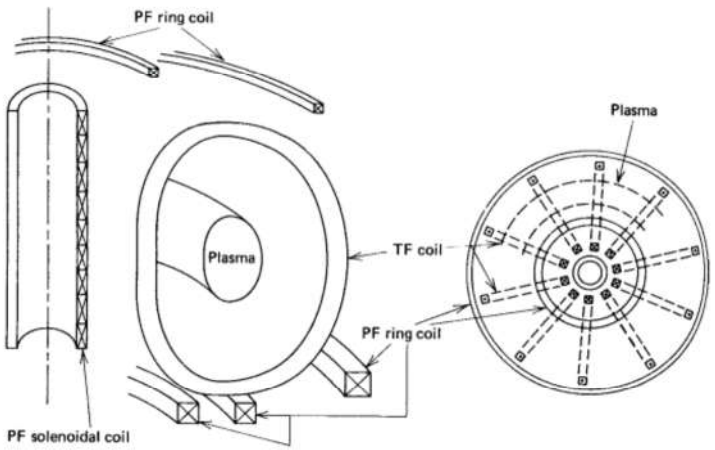

Figure 15: Tokamak magnet system configuration: elevation view and plan view

The plasma is confined and shaped by a combination of magnetic fields from three main origins: toroidal field coils, poloidal fields coils and plasma currents. For instance ITER is aiming at steady-state operation, and therefore all the coils are superconducting: copper coils would require too large electric power to be acceptable and this will be trues as well as for a future reactor like DEMO. A representative configuration is figure (15). The nested magnetic surfaces are able to confine a plasma pressure equivalent to a few atmospheres, with a density 10^6 times smaller than in the atmosphere ($n = 10^20/m^3, T \approx 10keV$)

2.1.1 Ideal Torus

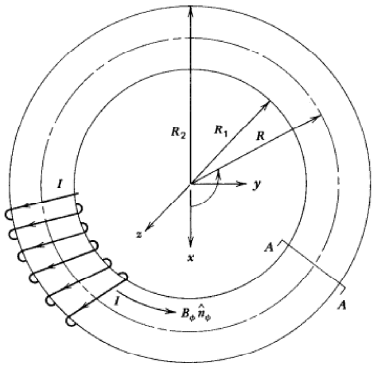

Figure 16: Ideal torus

Consider an ideal thin-shell torus wound with N turns, each carrying current I, to form a continuous form a continuous sheath. Using Ampere's law integrated around the loop at radius R relative to the major(z) axis of the torus leads to

$$\begin{aligned} \mu_0 NI = 2\pi R B_\phi(R) \qquad & R_1 < R < R_2, z = 0 \\ 0 = 2\pi R B_\phi(R) \quad & R < R_1, R > R_2, z = 0 \end{aligned} \tag{1}$$

from which the axial toroidal magnetic field within torus can be written.

$$\boldsymbol{B}_\phi(r) = \frac{\mu_0 NI}{2\pi R}\hat{n}_\phi \qquad R_1 < R < R_2 \tag{2}$$

Since the B_ϕ vanishes immediately outside the torus but has a finite value immediately inside the torus, its average value within the conducting sheath that forms torus wall

can be approximated as one-half the value immediately inside the torus. Then the differential force acting on a unit length of conductor is given by the Lorentz Law, using one-half of $\boldsymbol{B}_\phi(r)$.

$$d\boldsymbol{F} = \frac{1}{2} I\boldsymbol{l} \times \boldsymbol{B}_\phi = \frac{\mu_0 N I^2}{4\pi R} d\boldsymbol{l} \times \hat{n}_\phi \tag{3}$$

Denoting the value of R at the center of torus by $\overline{R}$, R can be written

$$R = \overline{R}\left(1 + \frac{r}{\overline{R}}\cos\theta\right) \equiv \overline{R}(1 + \epsilon\cos\theta) \tag{4}$$

Using the expression in the force relation yields an expression for the differential force per unit length acting on each turn,

$$d\boldsymbol{F} = \frac{\mu_0 N I^2 d\boldsymbol{l} \times \hat{n}_\phi}{4\pi\overline{R}(1 + \epsilon\cos\theta)} = \frac{\mu_0 N I^2 dl}{4\pi\overline{R}(1 + \epsilon\cos\theta)}\hat{n}_r \tag{5}$$

The differential force is everywhere outwardly normal to the surface of the torus (the direction $\hat{n}_R$) and varies in magnitude as $(1+\epsilon\cos\theta)^{-1}$. This force can be decomposed into R and z components. Thus there is a net inward (toward the major axis of the torus) force on each of the N turns, obtained by integrating around the turn.

$$\begin{aligned} \boldsymbol{F}_R = \oint \boldsymbol{F}_R = \frac{\mu_0 N I^2}{4\pi R_0}\int_0^{2\pi} \frac{r\cos\theta d\theta}{1 + \epsilon\cos\theta}\hat{n}_R = \\ = -\frac{\mu_0 N I^2}{2}\left[1 - \frac{1}{1-\epsilon^2}^{\frac{1}{2}}\right]\hat{n}_R \end{aligned} \tag{6}$$

This force must be balanced by some external support structure. The net axial (z-directed) force integrated over a turn is zero, so that no external support is required . However, the axial force does produce an internal tensile force in the conductor. This internal tensile force may be estimated by considering the axial force over half of the turn to be reacted internally by the tensile forces $T_1 + T_2$. Using the axial component

of $d\boldsymbol{F}$[4]:

$$T_1 + T_2 = \frac{\mu_0 N I^2}{4\pi R_0} \int_0^{2\pi} \frac{r \sin\theta d\theta}{1 + \epsilon \cos\theta} = \\ = \frac{\mu_0 N I^2}{4\pi} \ln\left(\frac{1+\epsilon}{1-\epsilon}\right) \tag{7}$$

2.1.2 Toroidal field coil

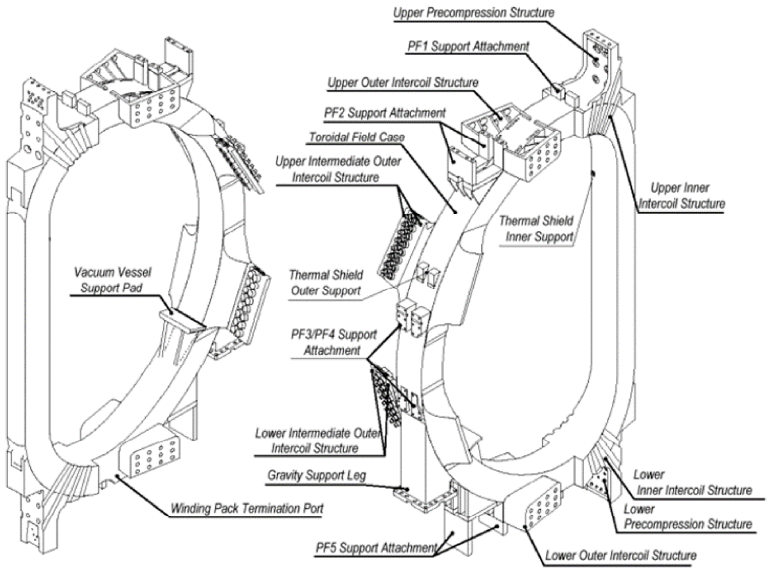

Figure 17: Toroidal field coil structure

The principal function of the TF coils is to provide a toroidal field to stabilize the plasma. This function is performed by a toroidal array of coils. For instance the ITER toroidal magnetic field value on the plasma axis is 5.3T, which leads to a maximum field on the conductor $\leq$12T. Because of this large value, Nb3Sn is used as superconducting material, cooled at 4.5K by a flow of supercritical helium at $\sim$ 0.6 MPa. The total magnetic energy in the toroidal field is around 40 GJ, the confinement of which leads to significant forces on each coil restrained by a thick steel case to resist circumferential tension ($\approx$ 100 MN) and by constructing a vault with the inboard legs

of all 18 coils (the large centripetal forces are due to the 1/R variation of the toroidal field). The compressive stress levels inside this vault are large, and therefore the side surfaces of each coil should match one another as perfectly as possible.The coils are connected together (figure 17) by bolted structures, and by two compression rings made of unidirectional glass fibres, that provide an initial inward radial force on each coil (2 x 30 MN).This very robust assembly is provided mainly to resist the toroidal forces induced by interaction of the TF coil current with the transverse poloidal field from plasma and poloidal field coils. These forces produce a distribution of torque around the TF coil proportional to the magnetic flux crossing unit length (the net torque is thus 0). These local forces are pulsed, and therefore mechanical fatigue is a concern for the highly stressed structural steel of the coils. These forces, due to the highly shaped plasma, are largest across the inboard coil legs (in particular at their lower curved region) where they are resisted by the friction between coil sides (under high compression) and by specific keys. The magnet system for ITER consists of 18 toroidal field (TF) coils, a central solenoid (CS), six poloidal field (PF) coils and 18 correction coils (CCs). The TF coil cases, which enclose the TF coil winding packs, form the main structural component of the magnet system. The TF coil inboard legs are wedged all along their side walls in operation, with friction playing an important role in supporting the out-of-plane magnetic forces. In the curved regions above and below the inboard leg, the out-of-plane loads are supported by four upper and four lower poloidal shear keys arranged normal to the coil centreline. In these regions, the coils are linked by means of two upper and two lower pre-compression rings which provide a radial centripetal force and improve the operation of the shear keys. In the outboard region, the out-of-plane support is provided by four sets of outer intercoil structures (OISs) integrated with the TF coil cases and positioned around the perimeter within the constraints provided by the access ducts to the vacuum vessel. The OISs are structures acting as shear panels in combination with the TF

coil cases. There is low voltage electrical insulation between TF coils in the inboard leg wedged region and between the OIS connecting elements in order to avoid the circulation of eddy currents. The TF magnet is subjected to two main force systems. The in-plane loads are generated by the interaction of the current in the TF coils with the toroidal field. The out-of-plane loads are generated by the interaction of the current in the TF coils with the poloidal field. The TF coil cases are the main structural component of the magnet system and they provide support against the TF coil in-plane as well as out-of-plane loads. The PF coils, CS and vacuum vessel are attached to the TF coil cases through supports which are rigid in the vertical and toroidal directions but flexible in the radial direction. In this way, the TF coil cases connect all the PF coils and the CS with the vacuum vessel, and balance all the electromagnetic forces within the magnet assembly. This arrangement results in a compact design without load transmission to structures external to the TF coil cases.

Number of TF coils	18
Magnetic energy in TF coils(GJ)	≈ 41
Maximum field in TF coils(T)	11.8
Vertical force per half TF coil (MN)	205
Centring force per TF coil(MN)	403
TF electrical discharge time constant(s)	11
CS peak field (T)	13.5
Total weight of magnet system(t)	10130

Table 3: Overall magnet system parameters for ITER

2.1.3 Superconductivity

At the field 8-12T required for a fusion reactor, the resistive power dissipation of normal conductor will be on the order of 100MW. That makes hard to get a positive power balance for the reactor. Therefore the use of superconductors in fusion magnets is desirable in order to work off a huge dissipative power loss associated to

a normal conductors.[4] Therefore it is expected to adopt the superconducting magnetic filed coils for fusion reactor like ITER. These coils will be required to provide the high magnetic inductions required for low β confinement, the long durations required to allow a burning plasma to reach a steady state equilibrium with respect to plasma-wall interactions and to test large total fluences of heat or neutrons on the first wall and divertor. It is a remarkable characteristic of some metals that when they are cooled to sufficiently low temperature, they lose all electrical resistance. This is called the superconducting state and for a particular material is determined by three parameters: the magnetic induction B, the temperature T_m, and the current density flowing through the superconducting material, j. As shown is figure(18) for a given superconducting material there exists a surface in the 3D space B, temperature of the material, current densities below which the material is in a superconducting state and above a normal conductor. For each material there is a critical magnetic induction B_{max}, a critical temperature max T_{max}, and a critical current density j_{max}. Near the plane j = 0 the critical magnetic induction is approximately parabolic with temperature. Hence there is a trade off between the critical magnetic induction and critical temperature, under that the material is considered as superconducting. There are two categories of superconducting material: "Type I superconducting" and "Type II superconducting". The first categories are not useful for superconducting since their critical magnetic field are far below the magnetic field it takes for fusion reactor. The second categories satisfies some of the requirement for the fusion energy. NbTi belongs to this category. It is an alloy for which there exists a rather substantial basi of experience with large magnets, it is ductile material which make easier the usage for magnet conductor. The only limitation is that it has a small superconducting regions which limitis the field to 8-10T. The issue of this material are overcome by Nb_3Sn since it has a larger superconducting region. Unfortunately it is brittle and there is

not a wider experience with it. However the recent development of a cable-type conductor configuration incorporating steel promises to get over this concern and Nb_3Sn has been tested in large magnets. [7] Superconducting wires, composed of many su-

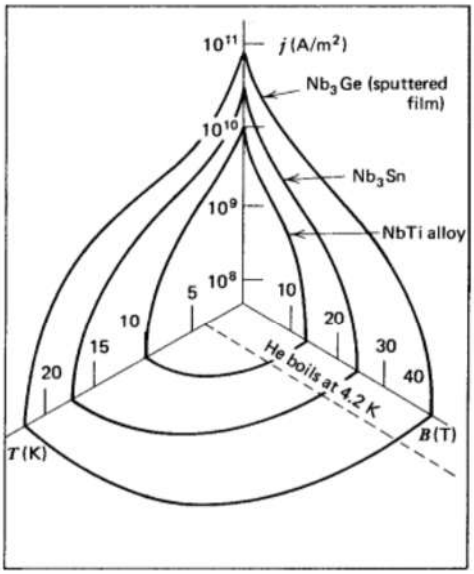

Figure 18: Superconducting regions in phase space

perconducting filaments, are embedded in a copper matrix, which in turn is wrapped in stainless steel and then wrapped with a spiral of tapelike electrical insulator to form the basic cable,see figure 19.The amount of superconducting is determined from the amount of current to be carried and from the upper limit on the current density. The purpose of copper is to provide stabilization of the superconducting state against

unanticipated heating, and the purpose of the steel is to provide structural support to counteract the Lorentz ($\boldsymbol{I} \times \boldsymbol{B}$) forces that act on the conductor. Several cables may be combined within the steel box to form a tape, with room left for liquid helium coolant. These tapes are built up within some structural system which is surrounded by thermal insulation and finally an outer case One of the major objectives of superconducting coil design is to prevent the superconducting material from reverting to the normal state, a process called as quench. Assume that a small length L of this superconducting wire has gone normal, and that it is cylindrically symmetric. The volume of normally conducting material V_c is given $V_c = \pi r^2 L$ where r is the radius of the wire. The heat energy evolved in this region is $Q_c = V_c \rho j^2 [W]$, where ρ is the electrical resistivity of the normally conducting wire and j the current density in the wire. The normally conduct volume V_c is bounded by two transition surfaces. The stability of these transition surfaces will depend upon the balance of ohmic heating power generated in the normally conducting material (Q_c) and the amount of heat transferred through the surface of the wire to the cooling medium surrounding it, usually liquid helium. The upper limit on heat transfer from the normally conducting wire to the liquid helium is the onset of film boiling. This limit Φ_{NB} is approximately equal to $0.5 W/cm^2$ for maximum heat transfer to liquid helium. When the temperature of the surface increases too greatly, the heat transfer will shift into film boiling regime, in which a film of helium vapor surround the conductor. This vapor film conducts far less heat away from the superconducting material than can be carried just below the limit Φ_{NB}. The maximum amount of heat that can be removed from the surface of the superconductor is given by $Q_{NB} = 2\pi r L \Phi_{NB} [W]$. As long as the total heat can be transferred to the liquid helium is greater thanthe limit given by the previous equation, the transition boundaries will move toward each other, and the entire wire will become superconducting when they coalesce. This occurs when $Q_c = \pi r^2 L \rho j^2 \leq Q_{NB}$ or $\Phi \geq (r \rho j^2)/2$. If the last condition is not satisfied, however,

the ohmic heat generated in the normal portion of the conductor volume will exceed the capability of the liquid helium to transfer heat away from the surface. Film boiling will then occur, and the transition boundaries will propagate into the superconducting material until the entire coil is normal and the stored magnetic energy has dissipated as ohmic losses. Three form of superconducting material are possible: cryogenic stabilization, adiabatic stabilization, dynamic stabilization.[7]

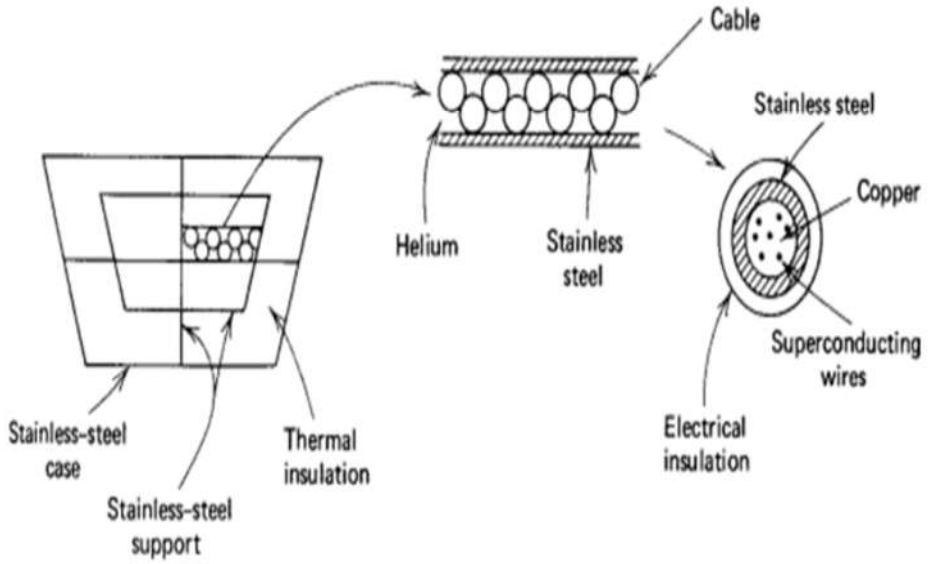

Figure 19: Superconducting conductor configuration

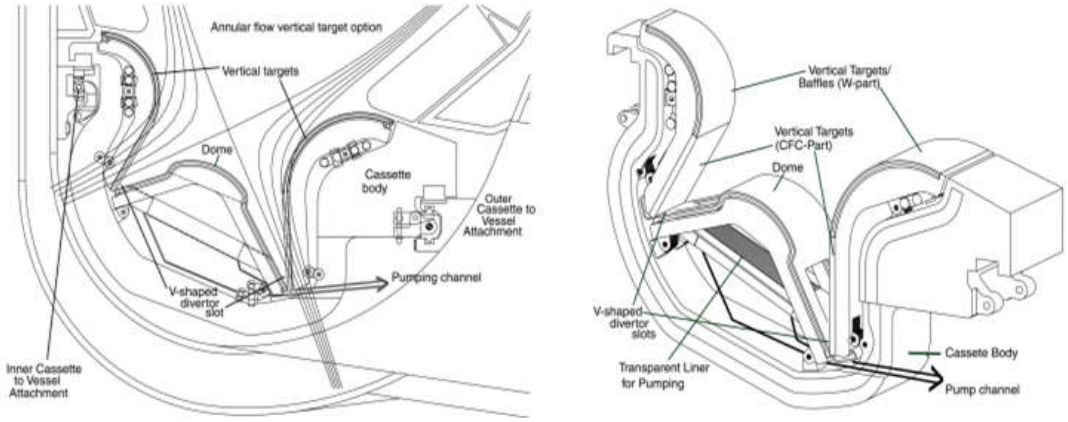

Figure 20: Left: Cross-section through the Divertor this shows the V-shaped strike zones and the pumping path as well as the attachment to the toroidal rails. Right: Divertor Cassette showing the large openings in the dome Support also shown is the transparent liner allowing pumping access from the private flux region.

2.2 Divertor & Power exhausted

In early Tokamak experiments, the plasma aperture was determined by a bar or a limiter, protruding from the chamber wall. Plasma ions and electrons following the field lines around the torus were transported radially outward until they reached a field line which passed within a gyroradius of the limiter, at which point they impacted the limiter and recycling as neutral atoms and molecules. In this time manner the region occupied by plasma or the plasma aperture was determined and the region between the tip of the limiter and the chamber wall proper was filled with a neutral gas.

The original motivation for the divertor was to remove the site of recycling and impurity production some distance from the plasma by diverting the magnetic field lines to guide particles escaping the main plasma into a separate chamber. Thus affording an opportunity to control the flow of recycling and impurity back into the plasma.

The divertor of any reactor class machine must be designed to:

- exhaust the fusion alpha and auxiliary heating power with acceptable loads on the plasma facing components;
- exhaust the helium (He) ash and keep the central He concentration below 10%;
- control the plasma density and fusion power;
- fuel the plasma;
- ensure an impurity level in the plasma that is low enough to avoid degradation of the plasma performance;
- ensure that the neutral density near the main plasma and X-point is sufficiently low that the confinement is not degraded.

Since the magnetic confinement is not perfect there are fluxes of charged particles: ions, electrons, $\alpha-$particles from fusion reaction, ions from NBI (neutral beam injection), impurity atoms due to the previous wall-eroded. The predominant effect of impurities upon a plasma is radiation cooling. The impurity ion interact with the plasma electrons via several mechanisms to reduce the electron energy and produce electromagnetic radiation which escapes from the plasma. There three contributes to radiative power loss:

- bremsstrahlung
- line radiation: collisional excitation of an orbital electron in a partially ionized impurity atom by a plasma electron,
- recombination free plasma electron will recombine with partially ionized impurity atoms to form an ion in a charge state lower by 1.

Most of all are recycled from the walls as "cool" neutral atoms, and some of these undergo charge-exchange neutrals incident upon the surface. Sputtering is a process where the an energetic particle transfer its energy to the lattice atoms, if this energy is higher than the surface binding energy of atom, that atom will be thrown away the surface. There are some surface materials,notably carbon, the incident hydrogen isotope apparently combines chemically with the surface material to form a compound with reduced surface binding energy. This chemical effect enhance the sputtering yield (atom ejected per incident particle) by more than of factor two. There is also an self-sputtering effect due to the atoms generated from the loss particles in the plasma. This atoms reenter in the plasma, become ionized, afterwards they are going to hit the surface as energetic ions.

The radiative power loss from a plasma depends strongly upon the impurity concentration and atomic number Z and in a rather complicated manner upon the electron temperature. At very low plasma electron temperature increasing T_e increases

the ionization state, hence the atomic radiation. At higher plasma temperatures the ion becomes fully stripped and the atomic radiation decreases with T_e. Finally with the ion is fully ionized, there is only bremsstrahlung.

This loss power give rise to a cooling down of the plasma edge without effective the plasma center, because in the cause of Z medium impurity (stainless steel) which become entirely ionized at the central plasma. Impurity control refers to those techniques that are employed to maintain the plasma purity within acceptable limits by preventing wall-eroded atoms from entering the plasma and/or by exhausting wall-eroded or fusion product ions from the plasma. The original motivation for the divertor was to remove the site of recycling and impurity production some distance from the plasma by diverting the magnetic field lines to guide particles escaping the main plasma into a separate chamber. Thus affording an opportunity to control the flow of recycling and impurity back into the plasma.

A fraction of the particles reflected from the divertor collector plate are pumped out a vacuum duct and the remainder remain in the divertor chamber as a cold partially ionized gas which serves to insulate the collector plate from the plasma by cooling the particle fluxes from the plasma as they pass through. Impurity atoms eroded from the collector plate are impeded from returning in the plasma chamber by high density gas and by the divertor action itself once they become ionized. Experiment has demonstrated conclusively that the impurity content of a plasma can be significantly reduced by means of divertors. For reason not well understood the magnetic configuration associated with the divertor also leads to improved energy confinement, altogether independent of the effect on the plasma purity. The principal disadvantage of the divertor is that require magnetic coil systems are complicated and expensive when extrapolated to a reactor.

The figure 21 shows the different configuration of the limiter compared at the divertor one. A divertor configuration is produced by locating other coils so as to

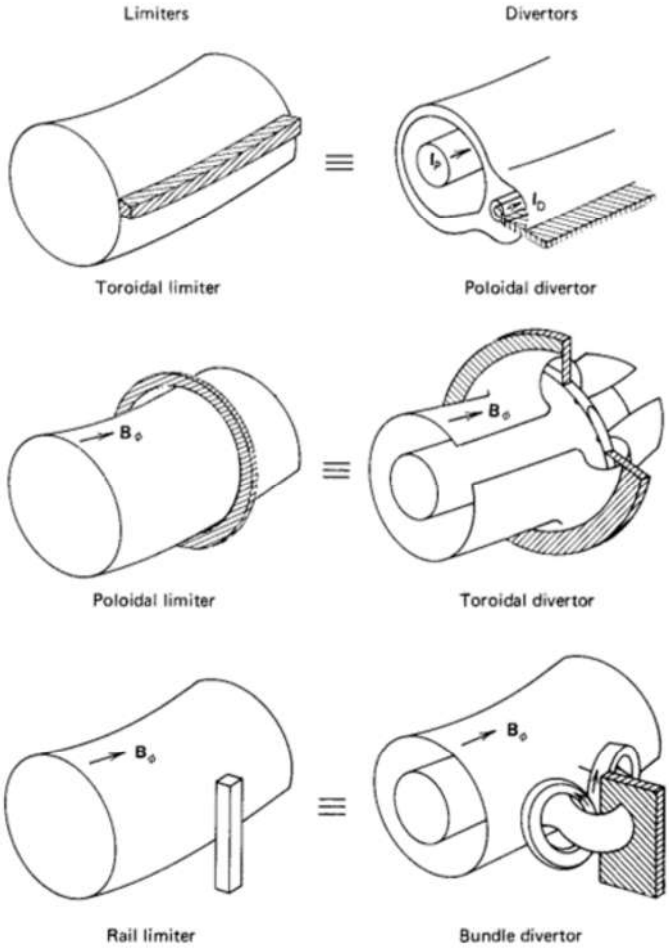

Figure 21: Various limiter and divertor configuration

divert the outermost magnetic field lines out of the main plasma chamber into a separate chamber where they intersect a material divertor target. Because it is easier to divert the poloidal field due to the plasma current than the larger toroidal field, the poloidal divertor is usual choice. A poloidal divertor is formed by nearby coils carrying current in the same direction as the plasma current so as to form a null, or X-point, in the net poloidal field of the plasma current plus that of the of the divertor coils.

The magnetic fields line passing through the X-point create the last closed flux surface(LCSF),know also as separtrix. All the field line interior to the separatrix remain within the confinement volume and the particles on them are confined, but particles that cross the separatrix are swept along field line to the divertor target in a separate chamber, see figure 22

The picture points out some of the divertor nomenclature that will be used. The plasma "core" region is well inside, and the plasma edge region is just inside the separatrix. Particles crossing the separatrix radially outward into the scrape-off layer (SOL) are swept along field lines past the X-point into the divertor region, where eventually hit the the target plate. Here the recycle as neutral atoms and molecules and produce sputtered impurity target plate surface atoms. The SOL and the divertor regions have a relatively high plasma density flowing towards the target plate. This density is highest at or near the separatrix and decrease rapidly towards the chamber wall. The baffle structure partially closes the entrance to the divertor region for the purpose of inhibiting the flow of neutral atoms and impurities back into the main plasma chamber. The magnetic field structure in the private flux region below the X-point is isolated from the magnetic field structure in the both the core plasma and the divertor region. LSN (lower single null), USN (upper single null), DN (upper and lower) are common configuration.

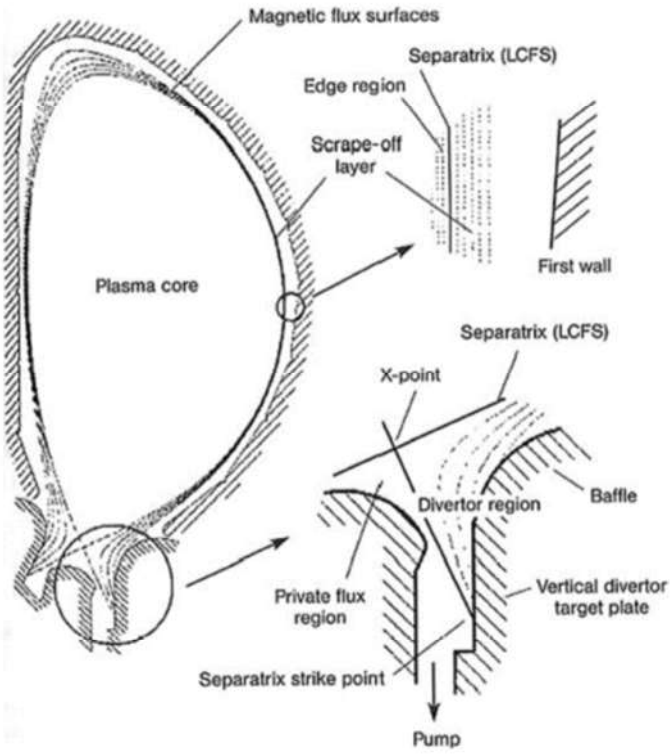

Figure 22: A single-null poloidal divertor configuration

The magnetic field configuration shows closed nested magnetic surfaces with increasing internal volumes from the plasma magnetic axis until a separatrix occurs, outside of which magnetic surface are open. The particles travel along largely toroidal field lines which slowly rotate poloidally around these surfaces, but they can diffuse outwards due to collisions. The particles diffusing out of the plasma through separatrix flow along fields line until they hit a target. Thus the plasma contact with the wall is located at a large distance along field lines. Along these field lines, the power flow is very high and if it were not for the possibility to induce power losses, the power density on the target (even taking into account its inclined position and the flux expansion due to a smaller poloidal field B_θ) would be too large for the capability of heat removal and the surface material temperature. This power should remain below $10MW/m^2$ on average, because this represents the upper limit that the available material can handle. With no power losses, the temperature gradient along the field lines remains small, the pressure constant and the plasma temperature at the target very high: this is so-called "attached" plasma divertor operation. Alternatively , if the plasma density is large enough at the sepratrix the possibility of radiation losses from impurities and from ionization of a large neutral density built in front of the target, provides a new more favorable condition, the so called "detached " plasma. Towards the divertor target, the pressure along field lines decreases, the plasma density increases significantly and the plasma temperature at the temperature at the target becomes very low (a few eV): the power crossing the separatrix becomes distributed by radiation (and charge exchange neutrals) onto the much larger surface of the divertor side walls, and the power density to the divertor target can remain inside reasonable limits.

CHAPTER III

ION ORBIT LOSS

This section represents the milestone of the thesis: Ion Orbit loss theory (IOL). The theory developed by Dr Stacey and al. is carving out an important rule in scientific community. Ion orbit loss (IOL) is somewhat an underestimate effect which it turns out to be relevant in many cases regarding the plasma physic edge. Relevance of the theory can be found in the references. For instance the collisionless loss of energetic ion on orbits through the X-region which carried them into the divertor seems to have been first suggested [8] and confirmed by Monte Carlo analysis of measured particle and heat fluxes in JET[9]. Collisional loss of ions on banana orbits near the boundary was the explored as a cause for the H-mode transition, [10][11] and direct loss of ions on banana orbits that crossed the separatrix was discussed in [12][13] A theory was developed [14][15][16] for L-H transition based on the bifurcation of the poloidal flow velocity due to the effect of ion orbit loss on viscosity, and later the experimental observation of large rotation velocities in MAST were explained in terms of the torques produced by return currents, compensating the ion orbit loss of energetic beam ions [17][18]. Recently the intrinsic rotation observed in DIII-D in the absence of an external torque has been explained by ion orbit loss of thermalized ions[19][20][21][22][23][24]

3.1 Plasma edge

The area of plasma we are going to focus on is the plasma edge. This is a region extending inward from the LCFS for a few centimeters where there are many evidences that the phenomena taking place in this relatively thin region play a major role in determining the overall performance characteristics of the confined plasma.These

processes involve an interplay of the transport and MHD stability phenomena that are dominant in the core plasma and the atomic physics and radiation phenomena that are relevant in the divertor. In a mathematical sense, the edge plasma conditions determine the boundary limit for the core plasma solutions, and in a physical sense the particles and energy that are transported out of the confined plasma region must pass through the plasma edge before they enter the unconfined scrape-off layer and divertor region. One of the most interesting and important phenomena associated with the edge plasma is the formation of steep edge density and temperature gradients when the non radiative power through the LCFS in a tokamak exceed a certain empirical threshold value : $P_{LH} = (2.84/A_i)\overline{n}_{20}{}^{0.58} B_\phi^{0.82} Ra^{0.81}[MW]$ where $\overline{n}_{20}{}^{0.58}[10^{20}m^{-3}]$ is the plasma line-average electron density and B_ϕ is the toroidal magnetic field. The formation of these steep edge gradients, referred to as an edge transport barrier or edge pedestal, is accompanied by a significant increase in energy confinement time for confined plasma.The plasma makes a transition from a low confinement mode (L-mode) to a high confinement mode (H-mode). The sharp edge gradients is sometimes observed subsequently to deteriorate, invariably with an accompanying reduction in energy confinement, and if the non radiative power crossing the LCFS drops below about $1/2P_{LH}$ the sharp edge gradients disappear and the energy confinement returns to the L-mode value.The steep gradients occur over a region of 1cm to 2 cm inside the LCSF. The location at which the steep edge gradient changes abruptly to a more gradual gradient that extends inward into the core plasma is referred as the "pedestal" location. Since its initial discovery in the asymmetric divertor experiment ASDEX, the H-mode has now been observed in all tokamak that have operated with auxiliary heating. The H-mode edge pedestal transport barrier is not yet fully understood and a lot of research effort is put on this topic. [2]

3.1.1 Plasma Fluid Theory

The properties of a plasma can be completely determined by solving Boltzman equation

$$\frac{\partial f_\sigma}{\partial t} + \boldsymbol{v} \cdot \nabla f_\sigma + \frac{e_\sigma}{m_\sigma}(\boldsymbol{E} + \boldsymbol{v} \times \boldsymbol{B}) \cdot \nabla_v f_\sigma \equiv C_\sigma + S_\sigma. \tag{8}$$

for each species and then computing the appropriate quantities from the distribution function. Such a procedure is not practical, excepts in rare cases. A knowledge of macroscopic, or average, quantities suffices to describes many plasma phenomena. These quantities can be defined as averages over distribution function of the form:

$$A_\sigma \equiv \int f_\sigma(\boldsymbol{v}) A(\boldsymbol{v}) d^3v \tag{9}$$

The particle density of species σ

$$n_\sigma = \int f_\sigma(\boldsymbol{v}) d^3v \tag{10}$$

and the average velocity associated with the species σ is

$$\boldsymbol{v}_\sigma = \frac{\int f_\sigma(\boldsymbol{v}) \boldsymbol{v} d^3v}{n_\sigma} \tag{11}$$

By taking appropriate velocity moments of equation(8), equation are obtained which can be solved directly for the macroscopic quantities, thus considerably simplifying the computational task. The first four moment equation are obtained by multiplying

Boltzman equation by $z_n(\boldsymbol{v})$ and integrating over velocity, where

$$\begin{aligned} z_0 &= 1 \\ z_1 &= m\boldsymbol{v} \\ z_2 &= \frac{1}{2}m(\boldsymbol{v}\cdot\boldsymbol{v}) \\ z_3 &= \frac{1}{2}m(\boldsymbol{v}\cdot\boldsymbol{v})\boldsymbol{v} \end{aligned} \tag{12}$$

For our purpose we need just two equations: the continuity equation and the energy balance equation.

In order to simplify the formalism the plasma edge is represented by one-dimensional radial transport in slab geometry approximation. The first velocity moment is the particle density (n_i), and the first moment equation is the continuity for the ion species "i".

$$\frac{\partial(n_i v_{ri})}{\partial r} = \frac{\partial n_i}{\partial t} + n_e n_o \left\langle \sigma\upsilon \right\rangle_{ion} + S_{nb} \tag{13}$$

this includes the second velocity momentum v_{ri}, the average radial ion particle velocity in the form of the radial particle flux $\Gamma_i = n_i v_{ri}$. The second term on the right is the ionization of recycling neutrals, $\left\langle \sigma\upsilon \right\rangle_{ion}$, and the last term is the neutral beam source S_{nb}. The third velocity momentum, or energy balance, equations for the main ion:

$$\begin{aligned} \frac{\partial Q_i}{\partial r} \equiv & \frac{\partial}{\partial r}\left(q_i + \frac{3}{2}\Gamma_i T_i\right) = \\ & = -\frac{\partial}{\partial t}\left(\frac{3}{2}n_i T_i\right) + q_{nb,i} - q_{ie} - n_e n_0^c \left\langle \sigma\upsilon \right\rangle_{cx} \frac{3}{2}\left(T_i - T_o^c\right) \end{aligned} \tag{14}$$

determine the main ion total energy fluxes Q_i. The q_{nb} term represent neutral beam (or other) heating, q_{ie} is the ion to electron collisional energy transfer, and the last terms in the equation represent charge-exchange cooling of the ions, where "cx" stand for "charge exchange plus elastic scattering" and the subscript c denotes the cold (i.e. not previously collided in the plasma edge) neutral atom species that have penetrated

into the pedestal.

3.2 Ion Orbit Loss

Understanding the pedestal physics and develop predictive model for the edge pedestal is fundamental because it will effect the performance of future Tokamaks. Ion orbit loss effect could significantly modify the results of most ongoing work and edge physics experimental and prediction. There two different basic mechanisms for ion orbit loss: the standard IOL, described in the next section, and the "X-loss". This mechanism is an ion loss through the X-point in diverted plasmas associated with the fact that ions on orbits that pass near the X-point, where the poloidal magnetic field is very small, have a very small poloidal displacement in time and are essentially trapped in the poloidal vicinity of the X-point, where they are subject to vertical curvature and grad-B drifts which take them outward across the LCFS and eventually in the divertor. The poloidal motion of the electron is sufficient that they are not affected by this trapping mechanism, so there is effectively a radially outward ion current which builds up an inward-directed radial electric field. This radial electric field interacts with the toroidal magnetic field to produce $\boldsymbol{E} \times \boldsymbol{B}$ poloidal drift that de-traps the ions by allowing them to drift poloidally to field lines that are not trapped in the vicinity of the X-point. Thus the ion orbit loss rate is determined by the relative values of the vertical curvature, and the grad-B drift loss rate and the de-trapping $\boldsymbol{E} \times \boldsymbol{B}$ poloidal drift rate.

3.2.1 Modelling of standard Ion Orbit Loss

The simplest loss mechanism is the loss of ions on passing or banana trapped orbit that leave the plasma by drifting outward across the LCFS. Both thermalized plasma ions and fast ions can be lost in that way. This type of ion orbit loss is also call "standard ion orbit loss". The basic ion orbit calculation is set up to determine the minimum required energy for an ion located at a particular poloidal position θ_0 on an internal

flux surface ψ_0 with a direction cosine ζ_0 ($\zeta_0 < 0$ co-current and $\zeta_0 > 0$ counter-current) in order to be able to execute an orbit which will cross the separatrix at a given poloidal location θ_S, see figures 23 and 24.The fast ions loss involves a transport mechanisms. From now on we are going to study only the thermalized ions, they flow radially outward and they are able to access orbits which will carry them across the separatrix. We define the directional cosine, relative to the torodial magnetic field B_ϕ as $\zeta_0 > 0$ for the counter-current direction. The minimum ion energy for this kinetic loss of ion at a point launched from an internal flux surface ψ_0 across the separatrix at a point ψ_S can be calculated by the requirement for the conservation of canonical angular momentum, energy and magnetic momentum.Following Miyamoto and others [13], we are going to use the conservation of canonical toroidal momentum ,equation (15) , to write the orbit constraint for an ion introduced at a location "0" on a flux surface ϕ_0, with parallel velocity $v_{\|0}$, where $f_{\phi 0}$ is $\frac{B_{\phi 0}}{B_0}$ and $f_{\phi S}$ is $\frac{B_{\phi S}}{B_s}$. $B_{\phi 0}$ and $B_{\phi S}$ are the the toroidal magnetic field at initial location and on the separatrix, whereas B_0 and B_S are the total magnetic field at the initial location and on the LCSF. B_0 is equal to $\sqrt{B_{\phi 0}^2 + B_{\theta 0}^2}$ and B_S is equal to $\sqrt{B_{\phi S}^2 + B_{\theta S}^2}$. $B_{\theta 0}$ and $B_{\theta S}$ are the poloidal magnetic field at initial location and on separtrix. The R_S and R_0 are the major radius associated to the initial location and the exit location.

ψ_0 and ψ_S are the flux surface value at initial location and on the separatrix. To complete the equation system we need to use the equation for the conservation of energy (eq. 16) and of poloidal angular momentum (eq.17). Once again ϕ_0 and ϕ_S are the electric potential at initial location and on LCFS.

$$R_S m v_\| f_{\varphi s} + e\psi = R_0 m v_{\|0} f_{\varphi 0} + e\psi_0 \tag{15}$$

$$\frac{1}{2}m(v_{\|S}^2 + v_{\perp S}^2) + e\phi = const = \frac{1}{2}m(v_{\|0}^2 + v_{\perp 0}^2) + e\phi \equiv \frac{1}{2}m v_0^2 + e\phi_0 \tag{16}$$

$$\frac{m v_\perp^2}{2B_S} = const = \frac{m v_{\perp 0}^2}{2B_0} \tag{17}$$

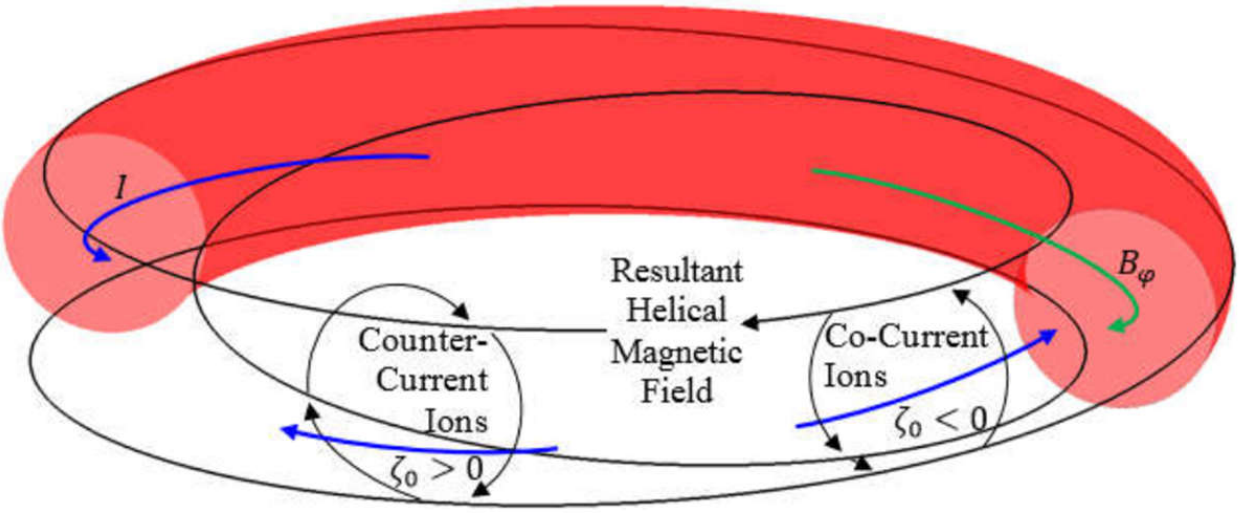

Figure 23: Toroidal ion direction shown with the resultant helical magnetic field also describing intra-flux surface poloidal motion directions.

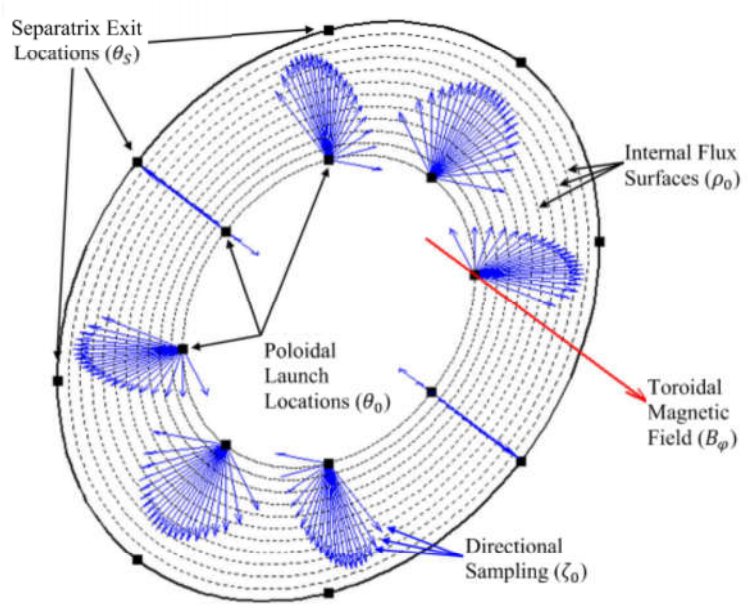

Figure 24: From the perspective of a poloidal cross section of the plasma at a fixed toroidal angle, φ, the poloidal launch and exit locations along with directions used for calculating minimum required energies for IOL to occur are shown

Combining the the equation (16) and (17) it is possible to get a relation between the initial velocity v_0 and $v_{\parallel S}$. To begin with, it is necessary multiply by two and divided by m and take on the other side $v_{\perp S}$, and afterwards collecting v_0

$$v_{\parallel S}^2 = v_0^2 - v_{\perp S}^2 + \frac{2e(\phi_0 - \phi_S)}{m}$$
$$v_{\parallel S}^2 = v_0^2 \left[1 - \frac{v_{\parallel S}^2}{v_0^2} + \frac{2e(\phi_0 - \phi_S)}{v_0^2 m}\right]$$

Splitting in the second term to the left v_0 in its component $v_{\parallel 0}$ and $v_{\perp 0}$. Collecting $v_{\perp 0}$ and using the equation (17), and ζ_0 as the cosine of the initial guiding center velocity relative to the toroidal magnetic field direction $\frac{v_{\parallel 0}}{v_0}$ we finally find the relation out:

$$v_\parallel = \pm v_0 \left[1 - \frac{B}{B_0}(1 - \zeta_0^2) + \frac{2e}{m v_0^2}(\phi_0 - \phi)\right]^{\frac{1}{2}} \tag{18}$$

Squaring both the equation (18) and (15) and remembering that $v_{\parallel 0} = \zeta_0 v_0$

$$v_\parallel^2 = v_0^2 \left[1 - \frac{B}{B_0}(1 - \zeta_0^2) + \frac{2e}{m v_0^2}(\phi_0 - \phi)\right]$$
$$v_\parallel^2 = \left(\frac{R_0 \zeta_0 f_{\phi_0} v_0}{R_s f_{\phi S}} + \frac{e(\psi_0 - \psi_s)}{R_s m f_{\phi S}}\right)$$

Using this two equations and sorting out the terms we get a quadratic equation in the initial ion velocity v_0

$$\begin{aligned} & v_0^2 \left[\left(\frac{R_0}{R_s}\frac{f_{\varphi 0}}{f_{\varphi S}}\zeta_0\right)^2 - 1 + (1 - \zeta_0^2)\frac{B_S}{B_0}\right] + \\ & + v_0 \left[\frac{2e(\psi_0 - \psi)}{R_S m f_{\varphi S}}\left(\frac{R_0}{R_S}\frac{f_{\varphi 0}}{f_{\varphi S}}\zeta_0\right)\right] + \\ & + \left[\left(\frac{e(\psi_0 - \psi_S)}{R_S m f_{\varphi s}}\right)^2 - \frac{2e(\phi_0 - \phi_S)}{m}\right] = 0 \end{aligned} \tag{19}$$

The equation (19) is quite general with respect to flux surface geometry representation of R, B and the flux surface ψ. By specifying an initial "0" location for an ion with

initial direction cosine ζ_0, and specifying a final location on flux surface ψ_S. The ion orbit loss equation can be solved for the minimum initial ion speed v_0 that is required in order for the ion orbit to reach the final location . Therefore it can be solved for the minimum ion energy necessary for an ion located on an internal flux surface to cross the LCSF at a given location or to strike the first wall at a given location.

3.2.2 Circular model

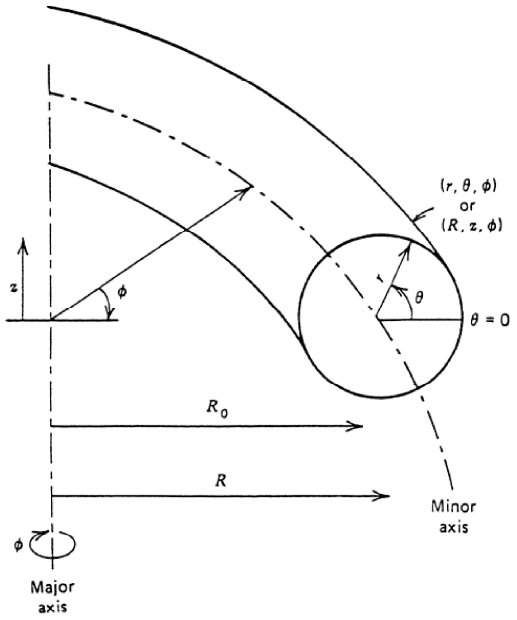

Figure 25: Toroidal (r, θ, ϕ) and cylindrical (R, z, ϕ) coordinates system

In order to use (19), with no lack of generality for our purpose, now we specify to

the circular flux surface geometry (figure (26)) described by:

$$\begin{aligned} R_0(r,\theta) &= \overline{R}h(r,\theta) \\ h_0(r,\theta) &= 1 + \left(\frac{r_0}{\overline{R}}\right) cos\theta_0 \\ R_S(r,\theta) &= \overline{R}h_S(r,\theta) \\ h_S(r,\theta) &= 1 + \left(\frac{r_S}{\overline{R}}\right) cos\theta_S \\ B_{\phi 0} &= \frac{B^0_\phi}{h_0} \\ B_{\phi S} &= \frac{B^0_\phi}{h_S} \end{aligned} \tag{20}$$

It is possible rewrite all this definition using the ϵ_0 and ϵ_S. By the second equation of Maxwell in toroidal coordinates

$$\nabla \cdot B = \frac{R}{r}\frac{\partial}{\partial\theta}\left[1 + \epsilon cos(\vartheta) B_\theta(r,\theta)\right] + \frac{\partial B_\phi(r,\theta)}{\partial\phi} = 0 \tag{21}$$

The last term vanishes because of axisymmetry and leading to

$$\begin{aligned} B_{\theta S} &= \frac{B^0_\theta}{h_S} \\ B_{\theta 0} &= \frac{B^0_\theta}{h_0} \end{aligned} \tag{22}$$

In a Tokamak, the poloidal field is related to the toroidal current density by Ampere's law. It is assumed a uniform current density j.

$$2\pi r B_\theta(r) = \int_0^r 2\pi x j_\phi(x) dx \tag{23}$$

From the equation (23) is obtained the B^0_θ. Introducing the vector potential A is possible to write Ampere's law

$$B_\theta = \nabla \times A_\varphi \tag{24}$$

and used it to write the flux surface as

$$\begin{aligned} \psi_S = R_S A_{\varphi S} &= \left(\frac{\mu_0 I}{2\pi a^2}\right) \overline{R} r_S^2 \\ \psi_0 = R_S A_{\varphi 0} &= \left(\frac{\mu_0 I}{2\pi a^2}\right) \overline{R} r_0^2 \end{aligned} \tag{25}$$

where I and a is the plasma minor radius. All the parameters necessary to model the edge experimental profiles come from DIII-[5] shot number 123302 at 2600ms. The model shot was in H-mode. The table 4 shows the main parameters for a DIII-D shot.

Parameters	Value
R	1.75m
a	0.885m
κ	1.84
I	1.50MA
B_ϕ^0	-1.98T
q_{95}	3.86m
P_{nb}	8.66MW
$\frac{n_C}{n_D}$	0.03

Table 4: Experimentals profiles DIII-D shot #123302

We assumed the plasma current flowing counter-clockwise direction looking down the tokamak, and the toroidal magnetic field is in the opposite direction. Thus the grad-B drifts are vertically downward in this model. The minor radius a was chosen to preserve the area of the elongated plasma. In this plasma model, the potential difference between some internal flux surface and the outermost last closed flux surface can be obtained from measurements of the local radial electric field by integrating to obtain the electrostatic potential. The diverted DIII-D plasma is approximated as an equivalent circular plasma enclosing the same magnetic flux at the corresponding radius. Most of the model parameters depend on the values on the flux surface, not on the geometric location of the flux surfaces. The Shafranov shift is neglected. The

final equation that is taken into account is:

$$\begin{aligned} &\upsilon_0^2 \left[\left(\frac{h_0}{h_S} \frac{f_{\varphi 0}}{f_{\varphi S}} \zeta_0 \right)^2 - 1 + (1 - \zeta_0^2) \frac{B_S}{B_0} \right] + \\ &+ \upsilon_0 \left[\frac{2e(\psi_0 - \psi)}{R_S m f_{\varphi S}} \left(\frac{h_0}{h_S} \frac{f_{\varphi 0}}{f_{\varphi S}} \zeta_0 \right) \right] + \\ &+ \left[\left(\frac{e(\psi_0 - \psi_S)}{R_S m f_{\varphi s}} \right)^2 - \frac{2e(\phi_0 - \phi_S)}{m} \right] = 0 \end{aligned} \tag{26}$$

If the equation 26 has a physical solution for a point on the LCSF ψ_S (or any other location) with normalized minor radius ρ_S,major radius R_S, poloidal angle θ_S, magnetic field B_S, then that ion can be lost from the confined plasma through that point. This is the equation we are going to solve in the GTEDGE code. This a background modeling and experimental data interpretation cod that will be described in the next chapter. The equation 26 is solved many times for each of 8 values of θ_S, 8 values of θ_0, 22 values of ζ_0 over $-1 \leq \zeta_0 < 1$ and 24 values of ρ_0 (see figure 26). Using experimental radial electric field, ion temperature (see figure 27) and a constant current density approximation for the flux surface (equation 25) the code is able to generate the minimum physically realistic value of energy:

$$E_{min}(\zeta_0, \rho_0, \theta_0, \theta_S) = \frac{1}{2} m \upsilon_0^2(\zeta_0, \rho_0, \theta_0, \theta_S) \tag{27}$$

as input for the IOL numerical computational strategy. When it is possible for an ion lost from a given locationθ_0 on an internal flux surface at radial location ρ_0 to be lost through more than one exit location θ_S we prorate the loss equally among all energetically possible loss locations. When it is not possible for an ion to be lost from location θ_0 we spiral the ion to the next nearest surface in the positive or negative direction in accordance with the sign of ζ_0, then check again if it can be lost. Ultimately we can notice that using equation(25) in equation(15) leads to an

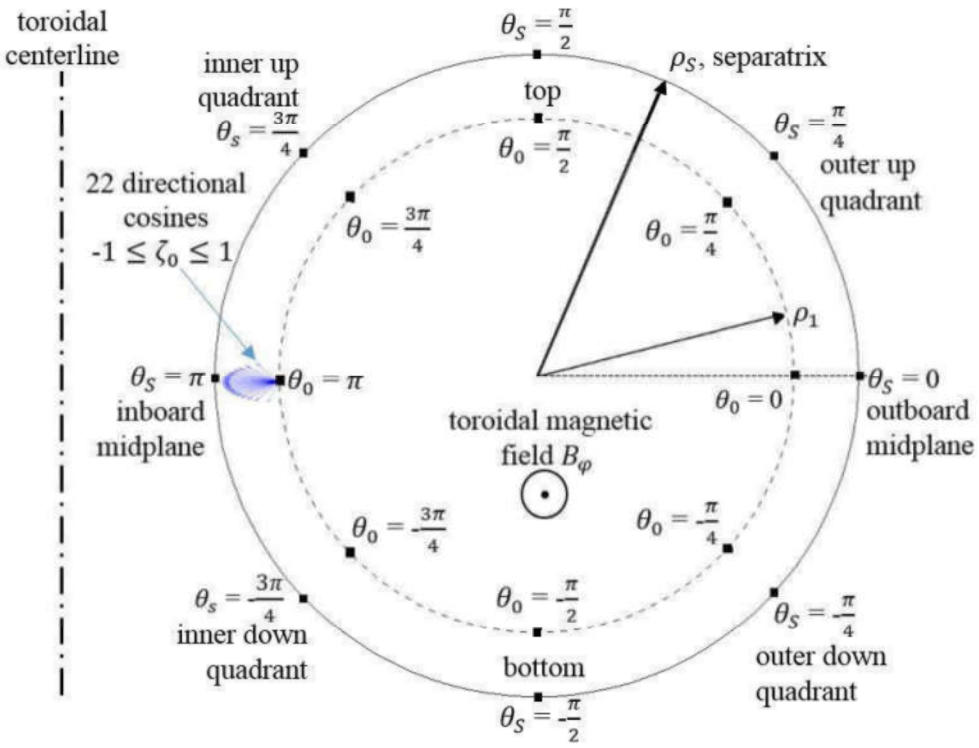

Figure 26: Location illustration for poloidal location θ_0 internal on the first flux surface ρ_1, poloidal locations on the separtix and θ_S, and a sample of the direction cosine ζ_0 with respect B_ϕ.

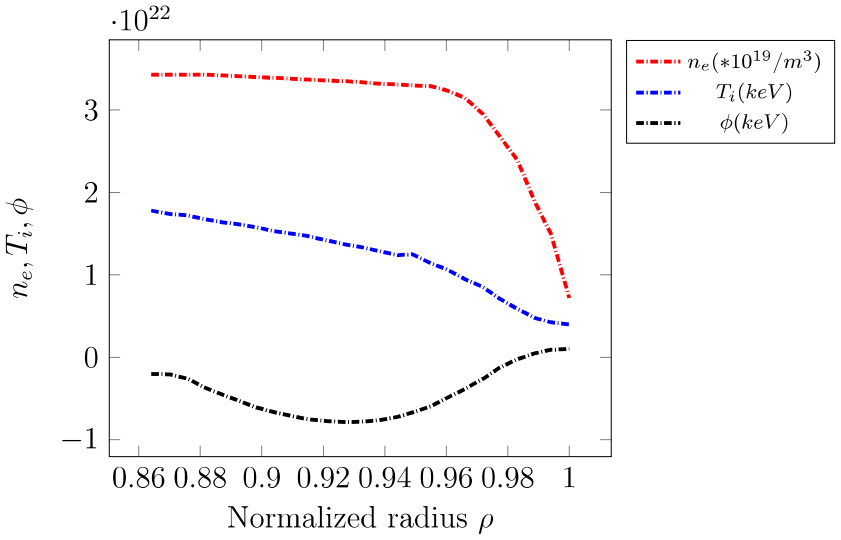

Figure 27: Edge experimental density,temperature, and electrostatic potential profiles for DIII-D H-mode shot #123302 at 2600ms

expression for the excursion from "0" flux surface:

$$(r_s^2 - r_0^2) = \frac{4\pi a^2 m}{e\mu_0 I}\left[h_s(r_s,\theta_s)\upsilon_0\zeta_0 - h_0(r_0,\theta_0)\upsilon_\parallel(r,\theta)\right] \tag{28}$$

The value of υ_0 obtained from equation(19) satisfies the equation(28) so any larger value of υ_0 would correspond to a larger displacement to a flux surface with r' r, requiring that the ion also cross flux surface r. Therefore, the value of υ_0 obtained from equation(19) is the minimum value for which the ion would cross the flux surface at rr_0. The minimum initial energy required for an ion with direction cosine ζ_0 located at poloidal positionθ_0 on flux surface "0" to be able to cross the LCFS at poloidal location θ_S. [25][23]

3.2.3 Loss definition

The results in figure(28) can be used to calculate a loss region in velocity space that increases with flux surface radius. The velocity loss region may be combined with an approximation of the particle distribution function in velocity space to allow us to calculate a particle loss rate. We assume that the ion velocity distribution function

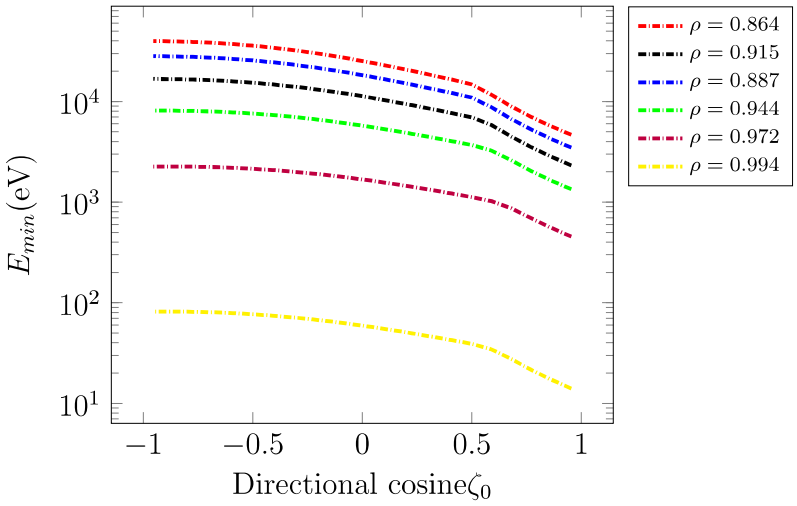

Figure 28: Lowest value of $E_{min}(\zeta_0, \rho_0)$ for any launch location θ_0 on several internal flux surface

is a Maxwellian at the local ion temperature chopped off above the local $E_{min}(\zeta_0, \rho)$. By using the directional cosine ζ_0 given by the azimuthal angle α, between the initial ion velocity,$\upsilon(\upsilon_0, \alpha)$, and the toroidal magnetic field $B_{\phi S}$, then the differntial volume element in spherical velocity space is

$$(\upsilon_0 d\alpha)(2\pi\upsilon_0 \sin(\alpha))d\upsilon_0 = 2\pi\upsilon_0^2 d\upsilon_0 d\zeta_0 \tag{29}$$

The number of ions lost within a given $d\alpha$ about a given α is the number within $d\alpha$ with a magnitude velocity of $\upsilon_0 \geq \upsilon_{0min}(\zeta 0)$. For ions in a velocity distribution given by $f(\upsilon_0)$, the number of ions within $d\alpha$ about a given $d\alpha$ which are lost are

$$dN_{loss}(\alpha) = 2\pi \sin(\alpha) \int_{\upsilon_{0min}(\alpha)}^{\infty} \upsilon_0^2 f(\upsilon_0) d\upsilon_0 d\alpha \tag{30}$$

The number of ions lost within $d\theta$ about a given angle θ is the number within $d\theta$ with $\upsilon \geq \upsilon_{min}(\zeta_0)$. If the ions are distributed in velocity as $f(\upsilon)$ then the number of ions

within $d\theta$ about a given θ which are lost is

$$\begin{aligned} dN_{loss}(\theta) &= 2\pi \int_{\upsilon_{min}(\theta)}^{\infty} \upsilon^2 f(\upsilon) d\upsilon d\theta \\ &= -2\pi \int_{\upsilon_{min}(\zeta_0)}^{\infty} \upsilon^2 f(\upsilon) d\upsilon d\zeta_0 \end{aligned} \tag{31}$$

At each poloidal θ_0 the minimum energy for which an ion with direction cosine $-1 \leq \zeta_0 \leq 1$ can escape across the last closed flux surface can be determined from equation (19). The total loss fraction of ions that escape across the LCSF is obtained by integrating the equation(31) over $-1 \leq \zeta_0 \leq 1$

$$N_{loss} = 2\pi \int_{-1}^{1} \left[\int_{\upsilon_{0min}(\zeta_0,\rho_0)}^{\infty} \upsilon_0^2 f(\upsilon_0) d\upsilon_0 \right] \zeta_0 \tag{32}$$

The total number of the ions on the flux surface before any loss is :

$$N_{tot} = 2\pi \int_{-1}^{1} d\zeta_0 \int_{0}^{\infty} \upsilon_0^2 f(\upsilon_0) d\upsilon_0 \tag{33}$$

leading to a definition of ion loss fraction:

$$F_{orb}(\rho_0) \equiv \frac{N_{loss}}{N_{tot}} = \frac{\int_{-1}^{1} \left[\int_{\upsilon_{0min}(\zeta_0,\rho_0)}^{\infty} \upsilon_0^2 f(\upsilon_0) d\upsilon_0 \right] d\zeta_0}{2 \int_{0}^{\infty} \upsilon_0^2 f(\upsilon_0) d\upsilon_0} \tag{34}$$

The effect of scattering are neglected because this mechanism is able to repopulate the loss region since the particles that undergo a scattering reaction has a non zero possibility to come back in the plasma. Further consideration on the scattering are made by [23] and [25]. So assuming no scattering between the directional bins, so each direction has a Maxwellian distribution at the local ion temperature with an upper cut-off energy corresponding to $\upsilon_{0min}(\zeta_0)$ which determines the loss fraction in that direction ζ_0,by equation 32. Thus using the Maxwellian distribution and integrating

over $-1 \leq \zeta_0 \leq 1$ we find that the loss fraction are

$$\begin{aligned} F_{orb}(\rho_0) &= \frac{\int_{-1}^{1} \int_{\epsilon_{\zeta_0,\rho_0}}^{\infty} \epsilon^{\frac{1}{2}} e^{-\epsilon} d\epsilon d\zeta_0}{2\int_0^{\infty} \epsilon^{\frac{1}{2}} e^{-\epsilon} d\epsilon} \\ &= \frac{\int_{-1}^{1} \Gamma(\frac{3}{2}, \epsilon_{min}(\zeta_0, \rho_0)) d\zeta_0}{2\Gamma(\frac{3}{2})} \end{aligned} \tag{35}$$

where $\epsilon_{min}$is the reduced energy corresponding to the minimum velocity for which ion orbit loss is possible.

$$\epsilon_{min}(\zeta_0, \rho_0) = \frac{m\upsilon_{0min}^2(\zeta_0, \rho_0)}{2\kappa T} \tag{36}$$

We make a few generalizations about the energy distribution as a function of direction and flux surface for the radially outward flowing ion flux as a result of IOL. Out to a certain radius (we assume this a t $\rho_{min} = 0.864 = \rho_1$, the minimum required energies $E_{min}(\zeta_0, \theta_S, \theta_0, \rho_0)$ for IOL to occur are so large that few ions can meet the energetic requirements regardless of their direction. Based on the relative difference between the ion poloidal motion and radial transport speeds we assume the ion pass through all poloidal loss location ($\theta_0 = 0, \pm\pi/4, \pm\pi/2, \pm 3\pi/4$ and π) many times in the time required to be transported radially across flux surface. So all ions in the radial range $\rho_{min} \leq \rho \leq \rho_{min}\Delta\rho_1$ with the energy in the range $E_{min}(\zeta_0, \theta_S, \theta_0, \rho_{min}) \geq E \geq E_{min}(\zeta_0, \theta_S, \theta_0, \rho_{min} + \Delta\rho_1)$. dependent upon their directional bin ζ_0 are lost (the fraction of such lossions is different for the different directional bins ζ_0). For the next radial range $\rho_{min} + \Delta\rho_1 \leq \rho \leq \rho_{min} + \Delta\rho_1 + \Delta\rho_2$ those ions in the directional bin ζ_0 with energy in the range $E_{min}(\zeta_0, \theta_S, \theta_0, \rho_{min} + \Delta\rho_1) \geq E \geq E_{min}(\zeta_0, \theta_S, \theta_0, \rho_{min} + \Delta\rho_1 + \Delta\rho_2)$ are lost. We continue this process for each directional bin ζ_0 from $(-1 \leq \zeta_0 \leq 1)$ and for each radius from $\rho_1 = 0.864$ out to $\rho = 1.0$. The energy distribution for the outward flowing ion flux, for ions of a given directional cosine ζ_0, is a continuously decreasing upper energy limit as the radius increases due to the effect of IOL. The ions with energy above the surface minimums

$E_{lowestmin}(\zeta_0, \rho_1 = 0.864)$ at the first flux surface we invenstigate ($\rho_1 = 0.864$) would all be lost. For the next flux surface ($\rho_2 = 0.870$) the energy distribution function would start already chopped off above the energy $E_{lowestmin}(\zeta_0, \rho_1 = 0.864)$ and the ions between this cut-off energy and $E_{lowestmin}(\zeta_0, \rho_1 = 0.870)$ would then be lost. This procedure followed for all the remaining flux surface for each of the directional cosine bins so that the energy distribution function, in each direction, would be chopped off at the energy $E_{lowestmin}(\zeta_0, \rho_{k-1})$ all the way out to $\rho = 1.0$. The ions not lost before reaching $\rho = 1.0$ are determined by integrating over the energy distribution function chopped off at $E_{lowestmin}(\zeta_0, \rho_{24})$ from the last flux surface. The minimum energy for IOL of ions with direction cosine ζ_0 as a function of flux surface position after these chopping steps are performed on the energy distribution function for each directional cosine on each flux surface is shown in figure 28. The counter-current ions have dramatically lower minimum energy requirements even at the first flux surface resulting in few non-lost ions, while the non-lost co-current ions have almost the same amount left on their seventeenth surface. Defining the same quantity for the ion energy through a similar derivation it is possible obtained an expression for the energy loss fraction:

$$E_{orb}(\rho_0) \equiv \frac{E_{loss}}{E_{tot}} = \frac{\int_{-1}^{1} \left[\int_{\upsilon_{0min}(\zeta_0,\rho_0)}^{\infty} \left(\frac{1}{2} m \upsilon_0^2\right) \upsilon_0^2 f(\upsilon_0) d\upsilon_0 \right] d\zeta_0}{\int_{-1}^{1} \left[\int_{0}^{\infty} \left(\frac{1}{2} m \upsilon_0^2\right) \upsilon_0^2 f(\upsilon_0) d\upsilon_0 \right] d\zeta_0} \tag{37}$$

And applying a Maxwellian velocity distribution:

$$\begin{aligned} E_{orb}(\rho_0) &= \frac{\int_{-1}^{1} \int_{\epsilon_{min}(\zeta_0,\rho_0)}^{\infty} \epsilon^{\frac{3}{2}} e^{-\epsilon} d\epsilon d\zeta_0}{2 \int_{0}^{\infty} \epsilon^{\frac{3}{2}} e^{-\epsilon} d\epsilon} \\ &= \frac{\int_{-1}^{1} \Gamma(\frac{5}{2}, \epsilon_{min}(\zeta_0, \rho_0)) d\zeta_0}{2\Gamma(\frac{5}{2})} \end{aligned} \tag{38}$$

In both expressions (35) and (38) are utilized the gamma function of order n, $\Gamma(n)$, and the incomplete gamma function of order n, $\Gamma(n, \epsilon_{min})$.

3.2.4 Calculation of the loss fraction

For evaluating the loss fraction the code begins from the innermost radius ($\rho = 0.864$) at which ion orbit loss is important, the ion distribution is treated as isotropic in direction and Maxwellian in energy. A solid angle sampling factor $f(\zeta_i)$ may be used to represent the fraction of the total solid angle contained within each directional cosine bin ζ_0(this remove the need for the factor of 2 in the total loss for ion and energy). Due to our uniform sampling of the directional cosine, the factor $f(\zeta_i)$ is a constant equal to 1/22 for each directional cosine bin. Working out with the ion loss fraction, with the gamma function, the solid angle factor $f(\zeta_i)$, and the minimum reduced energy ϵ, we find the definition for the differential loss fraction for all launch and exit location and directional cosine bins on the first flux surface (ρ_1) for ions, where $\epsilon = \frac{1/2mv_0^2}{KT_{ion}}$. The fractions that come out from this step are called "un-allocated" because they are not yet specified how ion and energy from a given location on an inner flux surface could exit at multiple location on the separatrix. Therefore the loss fraction need to be allocated among these chosen locations.

To calculate the full differential loss fractions for ions and energy it is necessary to understand where these various fluxes are permitted to go poloidally. We assume that the outward ion flux, from the first flux surface for which ion orbit loss is important $\rho_1 = 0.864$, is isotropically distributed in direction and uniform in poloidal distribution over the flux surface. The outward radial ion flux reaching each flux surface is evenly distributed among the eight octant centered on the eight poloidal launch location, θ_0=$\pi, \pm 3\pi/4, \pm\pi/2, \pm\pi/4$ and 0, so as an eighth of the ions go to each of the poloidal launch location within each direction for each flux surface. For example in figure 29 we took the ion in the Maxwellian energy distribution with the flux surface $\rho_1 = 0.864$ local ion temperature in the directional bin centered on ζ_0= 0.955 and placed a distribution of the same shape but at $1/8^{th}$ of the total flux magnitude at each of eight poloidal launch location θ_0=$\pi, \pm 3\pi/4, \pm\pi/2, \pm\pi/4$ and 0.

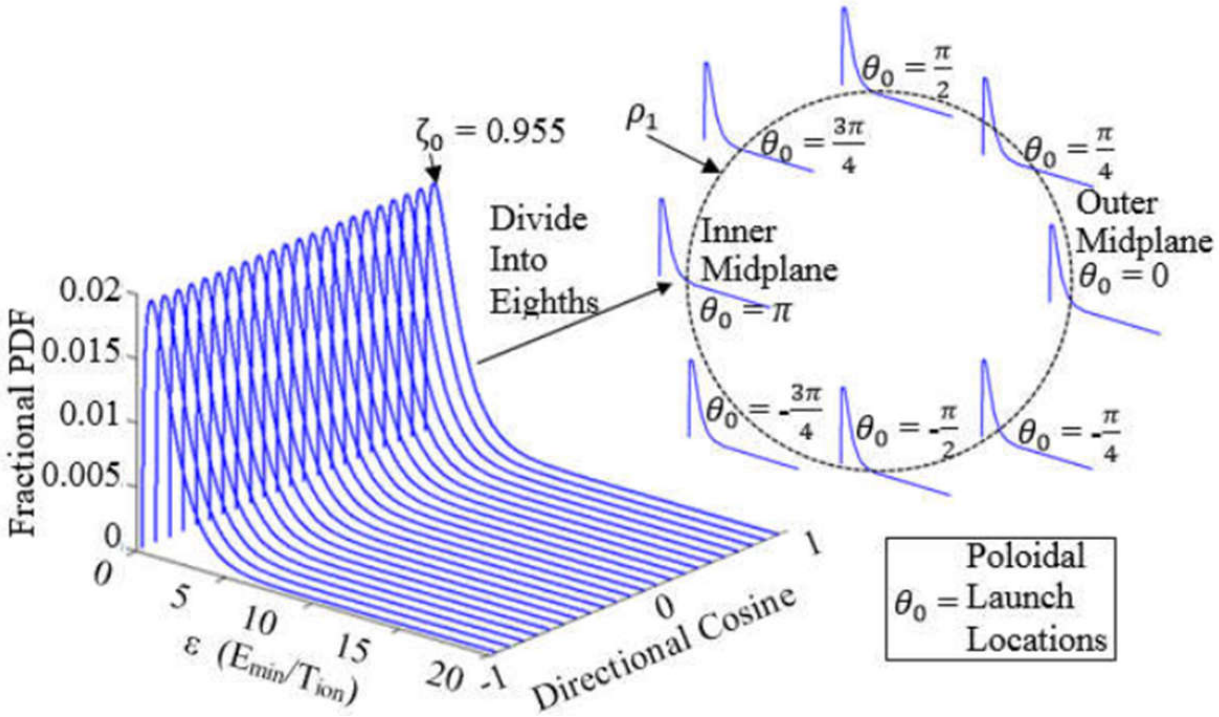

Figure 29: Initial even distribution of ions from $\zeta_0 = 0.955$ directional cosine bin on the first internal flux surface to the eight poloidal launch locations

This method does not involve particle tracking so we only know whether or not an ion has enough energy to reach a given exit location, not that it will go there without having first passed through another energetically allowed exit location. However, knowledge of the minimum required energy to reach exit location from each launch location, along with the assumed Maxwellian ion energy distribution function, may be used to develop an approximation in place of the calculation intensive particle following method. From figure 29 and using ϵ_{min} we can calculate the minimum energy an ion with directional cosine ζ_0= 0.955 must have at each of eight poloidal launch location (θ_0) in order to exit the separatrix at each of eight poloidal exit location (θ_S) on the separatrix. With the known minimum required energies $E_{min}(\zeta_0, \theta_S, \theta_0, \rho_0)$ it has been devised an algorithm for making the allocation over the poloidal exit locations θ_S on the separatrix (ρ_S). For instance the ions located at the poloidal launch position on the first flux surface $\rho_1 = 0.864$ at the inner midplane (θ_0=π) the corresponding minimum required energies to stream along an orbit out to various poloidal exit points on the separatrix can be found in the figure 31. This figure also shown as the minimum energy are placed on $\theta_S = 0$ and highest in $\theta_S = \pi$.

The relative number of ions which meet the energetic requirements demanded by equation 19 , in $\zeta_0 = 0.955$(counter-current),$\rho_1 = 0.864$,$\theta_0 = 0$ and θ_S from 0 to 2π.

The poloidal exit location on the outer midplane ($\theta_S = 0 = 2\pi$) has the lowest required minimum energy, resulting in the largest number of available ions which can meet this energetic requirement. The poloidal exit position on the inner midplane ($\theta_S = \pi$) results in the smallest number of available ions which meet this energetic requirements.

All of the ions contained in the energy range corresponding to an orbit exiting at inner midplane ,$\theta_S = \pi$,(magenta colored region in figure 30), on the sepratrix ρ_S also have enough energy to execute an orbit taking them to any of the other poloidal exit location $\theta_S = \pm 3\pi/4, \pm\pi/2, \pm\pi/4$ and 0, eight in total. The ions in the energy

range from $\theta_S = \pm 3\pi/4$ to $\theta_S = \pi$ (cyan colored region in figure 30) have enough energy to execute orbits exiting at $\theta_S = \pm 3\pi/4, \pm\pi/2, \pm\pi/4$ and 0, seven in total. We count the number of energetically allowable exit locations for each energy range until the last energy range between $\theta_S = 0$ and $\theta_S = \pm\pi/4$ (grey colored region in figure 30) which contains ions only having enough energy to make it to one location on the outer midplane $\theta_S = 0$.

It has been assumed that the ions from each launch location are distributed evenly among all the energetically allowed exit locations. The ions loss fraction from equation for the ions which have enough energy to exit at the poloidal location $\theta_S = \pi$ (magenta energy region in figure 30) is divided by the number of energetically allowable exit location and allocated evenly over all eight exit locations. The process is applied until the grey region. Here the ions are only lost to the poloidal exit location $\theta_S = 0$ as it is the only exit location on the sepratrix they have enough energy to execute an orbit to. The seven poloidal launch location $\theta_0 = \pm 3\pi/4, \pm\pi/2, \pm\pi/4$ and π are allocated over their poloidal exit the same method.

We calculate the unallocated loss fraction for each polodial exit location in equation, then the code sorts the minimum energy $E_{min}(\zeta_0, \theta_0, \theta_S, \rho_0)$ for each poloidal exit location to establish energy range bins. Next operation is to divide the un-allocated loss fraction by the number of energetically allowed exit locations and allocate them to the proper poloidal exit location θ_S. These allocation are summed for the total fraction of ions which it has been estimated at each poloidal exit location θ_S on the separatrix ρ_S from a given polodial launch location θ_0 in some inner flux surface ρ_0.

All of the ions which are physically capable of being lost to the poloidal exit locations on the separatrix from each poloidal launch location on an inner flux surface are assumed to be lost immediately. However, each poloidal exit locations has different minimum energies required to reach the various poloidal exit locations on the separatrix. Due to this difference the energy range, and number, for the non lost ions

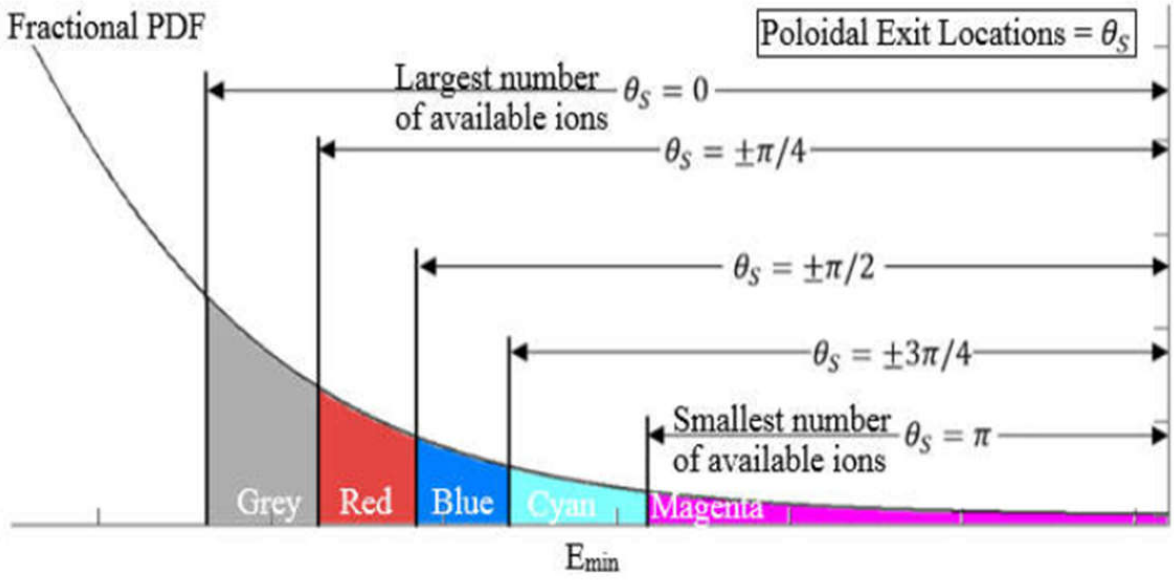

Figure 30: Allowable energy ranges (not to scale) for the ions which start their path in $\theta_0 = 0$ for all the polodial exit positions θ_S

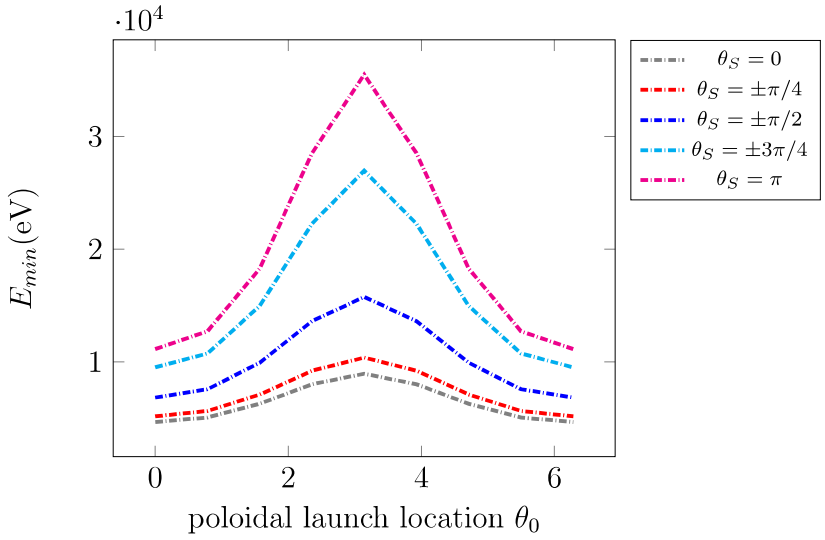

Figure 31: Lowest value of $E_{min}(\zeta_0, \rho_0)$ for any launch location θ_0 on several internal flux surface

will be different for each poloidal launch position (θ_0) in a given directional cosine. The $\theta_S = 0$ poloidal exit location has the lowest minimum required energy for each poloidal launch location so it may be used this minimum curve to set the upper limit of the expected energy of non lost ions at each poloidal launch position. Ions exist at these different poloidal launch locations which could be lost from other poloidal launch locations. The ions spiral about the flux surface many times before they move radially to the next flux surface, so they are able to reach the other poloidal launch locations where they can be lost. These ions also have a preferential poloidal spiral direction about the flux surface which is determined by the orientation of the ion guiding center velocity relative to the toroidal current I and magnetic field B_ϕ. Ions for this tokamak shot, moving in the co-current direction ($\zeta_0 < 0$) spiral poloidally about thier flux surface counter clockwise while ions moving in the counter-current direction ($\zeta_0 > 0$) spiral poloidally about the flux surface in the clock wise direction, see figure 23.

To account for this intra-flux surface poloidal ion motion we perform a secondary allocation over the polodial launch position θ_0. Using the energy curve from figure 31

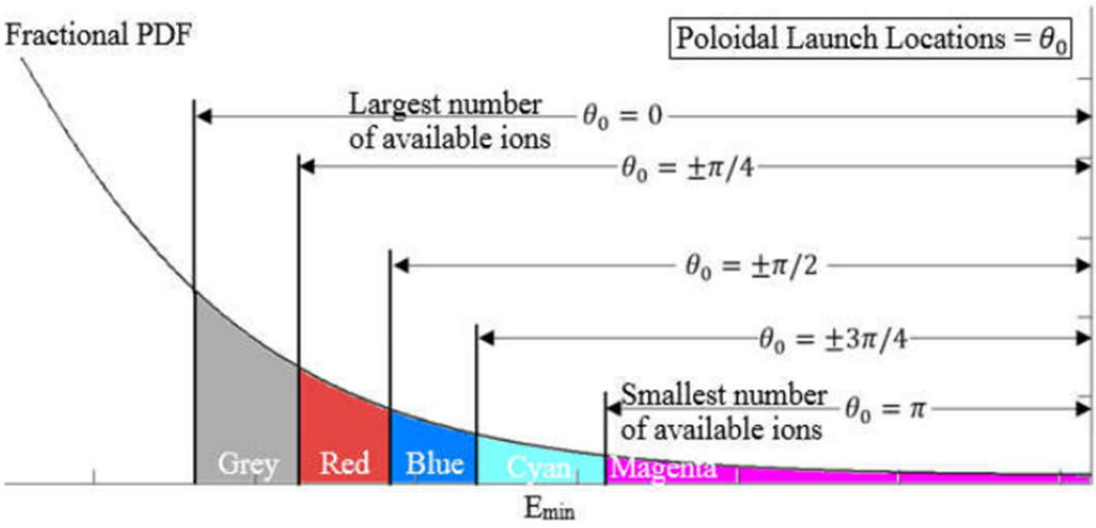

Figure 32: Allowable energy ranges (not to scale) for example poloidal launch position (θ_0) from the gray curve, figure 31

together with the given loss definition, we can find the loss fraction from each poloidal launch position. (figure 32) The ions at the inner midlplane ($\theta_0 = \pi$) are assumed to be immediately lost int he magenta region. These ions are solely lost from the poloidal launch location position $\theta_0 = \pi$ to the various poloidal exit positions θ_S on the separatrix and the loss fractions are allocated according to the method described above. Since we deal with ions in a directional cosine bin pointing int he counter-current direction $\zeta_0 > 0$ so the remaining non lost ions will move clockwise poloidally. The non lost ions at $\theta_0 = \pi$ (the grey through cyan energy ranges in figure 32) will spiral clockwise poloidally to the next position (figure 33). We continue the process until we reach $\theta_0 = 0$, the outboard midplane, where the grey energy region of ions will be lost and the corresponding remaining loss fraction is allocated accordingly. At the end of the allocation process all the non lost ions have energies below the surface minimum energy. The ions in the other directional cosine bins in the counter-current direction $1 > \zeta_0 > 0$ will also be allocated by this same method. For the ion in co-current directional bins $0 > \zeta_0 > -1$ both allocation process will be identical with only one exception. The ions will spiral in the poloidal counter clockwise direction when moving from a poloidal launch location with high overall minimum energy with respect to one with lower overall minimum energy. Once the allocation over poloidal exit θ_S and poloidal launch θ_0 locations is completed for each directional cosine ζ_0 on the first flux surface $\rho_1 = 0.864$ we generate the loss fractions for the next flux surface and allocate them accordingly. However each flux surface, beyond the first one we evaluate, has a truncated or "chopped" energy distribution due to the ions lost on the previous flux surface(s). All directional cosine bins within each flux surface beyond the first, ρ_k where $k > 1$, will contain energy distributions which only include those ions with energies below the surface minimum from the previous flux surface $E_{cut}(\zeta_0, \rho_{k-1})$ for the directional cosine bin. This "cutting energy" is similar to the minimum energy introduced before. So it can be used these overall minimums to

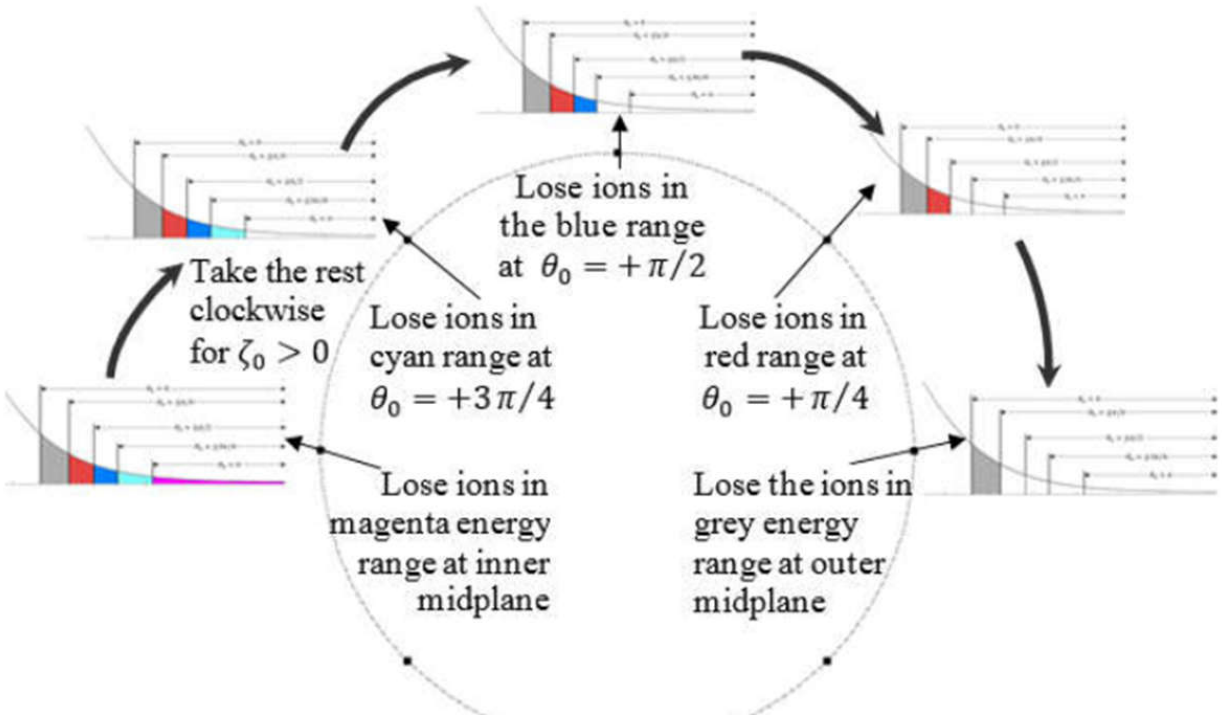

Figure 33: Poloidal launch location θ_0 allocation method for a positive directional cosine case ($\zeta_0 > 0$) starting at $\theta_0 = \pi$. The rotating distribution is taken directly from figure 32

truncate the energy distributions for ions where $\epsilon = 1/2(mv_0^2)/KT_{ion}$:

$$N_{loss} = \int_{\epsilon_{min}}^{\infty} \left(\frac{2kT}{m}\right)^{1/2} exp\left(-\epsilon\frac{2kT}{m}\right) d\epsilon - \int_{\epsilon_{cut}}^{\infty} \left(\epsilon\frac{2kT}{m}\right)^{1/2} exp\left(-\epsilon\frac{2kT}{m}\right) d\epsilon \tag{39}$$

$$E_{loss} = \int_{\epsilon_{min}}^{\infty} \left(\frac{2kT}{m}\right)^{3/2} exp\left(-\epsilon\frac{2kT}{m}\right) d\epsilon - \int_{\epsilon_{cut}}^{\infty} \left(\epsilon\frac{2kT}{m}\right)^{3/2} exp\left(-\epsilon\frac{2kT}{m}\right) d\epsilon \tag{40}$$

These loss number equations are used to derive the un-allocated loss fractions for all flux surfaces beyond the first by replacing the loss number equations in the derivation of equations 34 and 37. Now we have calculated the unallocated loss fractions for all flux surfaces ρ_k for $1 < k < 24$ over all directional cosine bins we allocated these loss fractions from all the poloidal launch location θ_0 over all the energetically allowable poloidal exit locations θ_S. Any remaining ions which do not meet the energetic requirement at their initial poloidal launch location θ_0 are taken nearby poloidal launch location $\theta_{0,\epsilon_{minlower}}$ with lower overall minimum reduced energy requirements $\epsilon_{min}(\zeta_0, \theta_S, \theta_{0,\epsilon_{minlower}}, \rho_0) < \epsilon_{min}(\zeta_0, \theta_S, \theta_0, \rho_0)$. The choice of nearby poloidal launch locations is determined solely by the particular directional cosine bin of the ions. For co current directed ions the poloidal spiral motion is counter clock-wise while the counter current directed ions the poloidal motion is clockwise. This allocation is continued until all the non lost ions in a given directional cosine bin are below the surface minimum energy.($E_{lowestmin}(\zeta_0, \rho_0)$). All the fully allocated loss fractions are stored in differential form over the diretional cosine ζ_0 bin to which they belong, the poloidal exit locations θ_S on the sepratrix they exit at, the poloidal launch location θ_0 they are launched from and the inner flux surface radius ρ_0 they were at when their orbit took them out to the separatrix to be lost. These allocated full differential loss fraction for ions and energy can be summed over the variable we need to get our

output plot.

Lastly,it is possible to take standard IOL into account in fluid calculation of the plasma edge, the natural effect will be reducing the particle and energy fluxes. This quantities are calculated by the fluid code by the appropriate loss function. The radial ion flux and energy flux can be calculated using the equations (13) and (14). Now we are able to define the effective radial particle, $\hat{\Gamma}_i(r)$, and energy fluxes, $\hat{Q}_i(r)$.

$$\begin{aligned} \hat{\Gamma}_i(r) &= \Gamma_i(r)[1 - F_{loss}(r)] \\ \hat{Q}_i(r) &= Q_i(r)[1 - E_{loss}(r)] \end{aligned} \tag{41}$$

The importance of IOL does not stand in changing the magnitude of ion flux or energy flux, but taking these effects into account it does change how these fluxes are distributed among conduction, convection, free-streaming. [23].

CHAPTER IV

GTEDGE

The primary computation tool utilized for this project is GTEDGE, which is an in-house Georgia Tech edge pedestal code developed by Dr. Stacey that employs fluid particle, momentum, and energy balance equations in conjunction with a two-dimensional neutral recycling model with kinetic corrections for both predictive and interpretive analysis of DIII-D plasmas. GTEDGE takes in experimental radial profiles for densities, temperatures and velocities performing calculations to determine the background plasma and boundary conditions for the edge pedestal. A pinch-diffusion edge pedestal model is used to interpret transport quantities like diffusion coefficients and heat diffusivities from the measured data. A particle and energy balance is first applied to the core plasma; then a two-dimensional neutral particle calculation using integral neutron transport theory is used to determine the net ion flux across the separatrix into the SOL. After calculating the inward and outward particle fluxes, the ion densities at the separatrix midplane and divertor plate are calculated using a two-point divertor model. With these necessary boundary conditions, both the transport of neutrals refueling the plasma edge and the ion density profile are simultaneously processed. Model parameters are then adjusted to predict the experimental plasma core line average density, energy confinement time and both central and edge pedestal temperatures. With the core and edge plasma modeled, quantities of interest such as radial particle flux, rotation velocities and heat conduction can be success for both the main and impurity ions, which are used to determine the radial electric field. These calculations are determined by conserving particles,

momentum and energy equations. Non-diffusive transport mechanisms such as electromagnetic particle pinch, ion orbit loss and x-transport are incorporated into fluid equations to calculate quantities like the radial particle flux and rotation velocities to interpret various theoretical predictions for the radial electric field. [26]

4.1 Subroutine "e0min.for"

The main aim of this subroutine is to solve the equation (26). The first part of this subroutine sets up the variables that we need for solving the equation and the result is working out a quadric equation:

$$\upsilon^2 [a] + \upsilon [b] + [c] \tag{42}$$

This part was modified in order to take into account the modification of toroidal magnetic field in certain location and electrostatic potential. Changing manually the value of "coeff1" and "coeff2", the value of magnetic field in three points can be modified. It has been explored also a strategy which changes 82 points (24×3). Fixing arbitrarily a distance for the shim coil, we will scale the increment of the magnetic field based on the distance from the coil and the maximum increment on the outboard midplane. Since the obtained results are almost equal to the three point changing, we decide to vary the field in only this three location. The "coeffE0" and "coeffED" occur to the modification of the electric potential on several initial flux surface, ψ_0 and on LCFS ψ_S respectively. Here it is the part of the code:

```
        xxI = (xmu0*plasmacur)/(2.0*xpi*(radminor**2))
      h0 = 1. + (rminor0/Rs0)*cos(theta0)
      hd = 1. + (rminorD/RsD)*cos(thetaD)

   bthetaDc = (xmu0*plasmacur) / (2.*xpi*rminorD)
 btheta0c = (xmu0*plasmacur) / (2.*xpi*rminor0)
```

```
          bthetaD=bthetaDc/hd
          btheta0=btheta0c/h0

               coefE0=1.0
               coefED=1.0

          delphi = (coefE0*ephi0) - (ephiD*coefED)

          coeff1=1.0
          coeff2=1.0

          xpot = 2.*(eq/xm)*delphi

             Bphi0=(-Btor)/h0
           Btot0=sqrt((btheta0**2)+(Bphi0**2))
           fphi0=Bphi0/Btot0
if ((cos(thetaD).eq.cos(0.0))
1             .OR. (cos(thetaD).eq.cos(2*xpi)))then

BphiD= (-1*Btor*coeff1)/(hd)
BtotD=sqrt((bthetaD**2)+(BphiD**2))
fphid= BphiD/BtotD


a = ((BtotD/Btot0)*(1.-(psi0**2)))+
1        (((h0/hd)*(fphi0/fphid)*psi0)**2)- 1.

          xflux= xxI*(eq/(xm*hd*fphiD))*
1                        ((rminor0**2)-(rminorD**2))
```

```
          bterm = xflux*(h0/hd)*psi0*(fphi0/fphid)

               c = ((xflux**2)/4.0) - xpot

         elseif((cos(thetaD).eq.cos(xpi/4))
     1          .OR. (cos(thetaD).eq.cos(1.75*xpi)))then

         BphiD= (-Btor*coeff2)/hd
         BtotD=sqrt((bthetaD**2)+(BphiD**2))
          fphid= (BphiD)/(BtotD)

         a = ((BtotD/Btot0)*(1.-(psi0**2)))+
     1          (((h0/hd)*(fphi0/fphid)
     2           *psi0)**2)- 1.

         xflux= xxI*(eq/(xm*hd*fphiD))*
     1          ((rminor0**2)-(rminorD**2))

         bterm =xflux*(h0/hd)
     1          *psi0*(fphi0/fphid)

           c = ((xflux**2)/4.0) - xpot

             else
                 BphiD= (-Btor)/hd
                 BtotD=sqrt((bthetaD**2)+(BphiD**2))
                 fphid= (BphiD/BtotD)
```

```
                a = ((BtotD/Btot0)*(1.-(psi0**2)))+
1                       (((h0/hd)*(fphi0/fphid)*psi0)**2)- 1.

                xflux= xxI*(eq/(xm*hd*fphiD))*
1                       ((rminor0**2)-(rminorD**2))

                bterm = xflux*(h0/hd)*psi0*(fphi0/fphid)

                c = ((xflux**2)/4.0) - xpot
          endif
```

Afterwards, the positive and negative solution of the quadratic equation are transfer to the solutions into energy (mass dependent). Here there is a part which makes sure that the code selected only the smallest positive solutions: because the definition of v_0 is $\sqrt{v_{\|0}^2 + v_\perp^2}$, it must be positive or else suffer a non-real solution which we are not willing to do this time. In the original E0min.for only the smallest energies were selected and stored in memory to check against later. The variable chosen to store this data "emin()" had only three dimensions as only one value was selected for the θ_s dimension. The ions would be lost on the orbit with the overall lowest energy requirement regardless of other orbits were also physically possible. Thus there is no need to store energy data over the various exit positions. However the new version of GTedge works with four variable because the loss fraction is allocated over the LCFS and it is accomplished by adding in a second storage variable for using four dimension instead of three. This variable is eminall(). The code section below is doing that:

```
c                        Both Positive - Continue -
          if(v0m(n,m).gt.0.0.and.v0p(n,m).gt.0.0)then
c                               v0m < v0p -> choose v0m
             if(v0m(n,m).lt.v0p(n,m))then
```

```
                                if(emin(npsi,n,nnn0).gt.xke0m(n,m))then
                                     emin(npsi,n,nnn0) = xke0m(n,m)
                                 L0(npsi,n,nnn0) = m
                    eminAll(npsi,n,nnn0,m)=xke0m(n,m)
                   else
                                 eminAll(npsi,n,nnn0,m)=xke0m(n,m)
                                endif
                             endif
c                                    v0m > v0p -> choose v0p
               if(v0m(n,m).gt.v0p(n,m))then
                                if(emin(npsi,n,nnn0).gt.xke0p(n,m))then
                                     emin(npsi,n,nnn0) = xke0p(n,m)
                                 L0(npsi,n,nnn0) = m
                                     eminAll(npsi,n,nnn0,m)=xke0p(n,m)
                                else
                                     eminAll(npsi,n,nnn0,m)=xke0p(n,m)
                                endif
                    endif
           endif
```

4.2 Subroutine "lossfraction.for"

Lossfraction.for is the heart of IOL calculation. This part of the code helps us to calculate and allocated the loss fraction in the right way. The first things is to define the reduced minum energy ϵ_{min}.This quantity is the one used in gamma function $\Gamma(n)$. Its dependent upon n_0 or ρ_0 is used to understand what flux surface is considered. In the code is call "etta()". Since Lossfraction.for is inside of loop that goes over ρ_0, most of the variables inside it do not have four dimensions. The matrix "etta" is an example. Afterwards in the code is introduced the minimum reduced energy

"minetta", the lowest reduced minimum energy. Important difference between the theory and the code is that the code works with the lowest reduced minimum energy "minetta", instead of the theory works with the lowest minimum energy which would be E_{min}.

```
if(Etta(npsi,n,m).lt.minEtta(npsi,roh))then
   minEtta(npsi,roh) = Etta(npsi,n,m)
endif
```

Reminding that "lossfrac.for" subroutine is inside of a do loop over the 24 flux surface, the first internal loop is over the directional cosine bins or npsi, the next one is over the poloidal launch location (θ_0 or n) and the final one is over poloidal exit locations(θ_S or m). Nevertheless all these loops, it could be seen that minEtta() is dimension two over npsi and roh. This makes clear that "minEtta" is the minimum reduced energy for each direction cosine within each flux surface over both launch and exit locations. These overall minimums are useful when comparing against minimums in different flux surfaces, (figure (28)), and they are helpful to keep track of the ions which have already been lost when we start solving over flux surfaces.

4.2.1 Un-allocated loss fraction

Before the sorting section is introduced the gamma functions used to calculate our Maxwellian approximation of the ion energy distribution functions. The complete gamma functions are pre-computed in code to save time during the loops. For everything else the incomplete gamma functions are adopted. The first part of this routine, using the equation(34)(35)(37)(38) for getting the fraction of ions which are escaping that is due to IOL. From a computational point of view is easy doing it because it's possible to move from one equation to another only changing the arguments of Γ function. Not dealing with the momentum, this thesis doesn't take it into account from now on.

```
          if(Etta(npsi,n,m).lt.20.0)then
                  flrone(npsi,n,m,k) = ((bigG(k)
1                                      -GAMI(Aeh(k),Etta(npsi,n,m)))
2                                        /bigG(k))/22.0
          if(flrone(npsi,n,m,k).lt.0.0.or.
1                         flrone(npsi,n,m,k).gt.1.0)then
                          flrone(npsi,n,m,k) = 0.0
          endif
                                    else
                                            flrone(npsi,n,m,k) = 0.0
           endif
                  else
```

The 1/22 in the code is a construct used to bin the ions into specific directional bins. Adding the resulting fractions over the 22 directions will give rise to the expected totals. The "bigG()" is a variable used to store the values for the full gamma function so it is not recomputed every loop. The variable "flrone()" being less than zero or greater than one is due to the known issues with the built-in gamma functions. It is used as a temporary storage place for the unallocated fractions prior to sorting and allocation into "delf()" where the full differential fractions for all three areas of interest are stored. Afterwards in the code it is calculated the loss fraction for flux surface 2 to 24.

```
                  else
if(Etta(npsi,n,m).lt.minEtta(npsi,roh-1))then
                  flrone(npsi,n,m,k) = ((GAMI(Aeh(k),minEtta(npsi,roh-1))
     1                                   -GAMI(Aeh(k),Etta(npsi,n,m)))
     2                                   /bigG(k))/22.0
                  if(flrone(npsi,n,m,k).lt.0.0.or.
1                                 flrone(npsi,n,m,k).gt.1.0)then
```

```
                        flrone(npsi,n,m,k) = 0.0
                endif
        else
                flrone(npsi,n,m,k) = 0.0
        endif
endif
```

where the incomplete gamma function with the ϵ_{min} is used in place of the full gamma function from the previous flux surface (note the roh-1). Based upon our previous discussion of "minEtta()", it formed the lowest possible energetic value which can be lost on a given surface for ions of a given direction. During the loss calculation from the next surface (no scattering was assumed), it is no useful to count ions in the distribution which were lost on the previous surface. This is easily done by using an incomplete gamma function in place of the full gamma function and plugging in the minEtta() from the previous flux surface (thus the roh-1).

4.2.2 Allocation over θ_S

Before chopping and allocating the fraction, the code must first sort the un-allocated fractions coming out of the gamma function equations ("flrone()"). We have sorting of the fractions over the poloidal exit location θ_S, the poloidal launch location θ_0 and finally θ_S and θ_0 together.There are two reasons for all these sorts. First, it helps to simplify the code. Instead of having to do a bunch of comparisons multiple times during the allocation process we can step through a list of values knowing that they are already in order. Second, fractions of various values which all came out of a Maxwellian distribution are the important stuff. This is important because due to equations, the fractions are all cumulative. While this does not lend itself to a differential approach, values were sorted according to size and then it was use the subtraction to find the contribution magnitude available from each launch point to

each exit point that was not already lost from, or to, elsewhere. Once all of these sorts arecompleted, we move on to the first stage of the allocations.

```
c                Allocations & Ajustment Section
do 2000 npsi = 1,22
octet(1:64) = rohit1st(1:64,npsi)/8.0
do 2001 itit = 1,8
        n = order1nst(itit,npsi)
        do 2013 m = 8,2,-1
        chopM(m) = (octet(actord1st((n
1               +(order1mst(n,m,npsi)-1)*8),npsi))
     2          -octet(actord1st((n+(order1mst(n,m-1,npsi)-1)
     3          *8),npsi)))/(mb(m)*1.0)
2013                            continue
        chopM(1) = octet(actord1st((n
1                       +(order1mst(n,1,npsi)-1)*8),npsi))/8.0
          do 2011 m = 1,8
                sortM(m) = 0.0
                mqm = m
                do 2012 mrm = 1,mqm
                        sortM(m) = sortM(m) + chopM(mrm)
2012                                    continue
2011                            continue
        do 2010 m = 1,8
          delf(n,order1mst(n,m,npsi),npsi,roh,k) =
1       delf(n,order1mst(n,m,npsi),npsi,roh,k)+sortM(m)
2010                            continue
```

The first do loop over "npsi" corresponds to the splitting of the loss fractions over

the 22 directional cosines. The "octet()", which is filled in by taking an even 8th of the magnitude of "rohit1st()" (that is a sorted version of flrone() which was created in the last sorting routine), is the second step where the loss fractions are evenly distributed over the 8 poloidal launch locations. Next it is necessary to step through these 8 poloidal launch locations (that is "n" in the code). Utilizing "order1nst()", it pulls the correct indicies for n out of octet(). order1nst() is a sorted list of "n" by the largest "m" (thats sorted θ_0 by largest θ_S). This is necessary because it is apparent that each "n" may have different requirements for loss to each exit location. And since all of the loss fractions is stored together in one large sorted variable "rohit1st()", "order1nst()" shows where each "n" is at inside of "octet()". The next part is a relatively simple chopping mechanism. Until now the code just generates the unallocated loss fractions and afterwards they are stored in the large sorted variable octet(). Once octet is available, the fractional pieces were selected from a launch location which could go to each of the eight exit points. Each point is the amount that can be lost to each θ_S that is not also lost to lower energy location. If these were summed up, they offer the amount that can be lost from θ_0 but, searching for the differential loss fraction, the code subtracts the value selected and do the allowed division. All this means that each of these fractions is permitted to go to a certain number of poloidal exit locations which is based upon the energy requirements for each. And as it so happens that corresponds directly to how large the fraction is, the larger the fraction the fewer location it is allowed to go. Since the code is dealing with a circle, the number of location where the particle can go out will be always an odd number, except for the case when the particle con go out to the $\theta_s = \pi$ that is the worst case and therefore the fraction loss are allowed to be loss in all exit locations. All of these values are then recorded into the variable "chopM()". So the fraction will be divided by 1,3,5,7,8 according to their energy. This numbers are stored in an array "mb", at the beginning of the subroutine, as integer numbers from 1 to 8. It is

used also if the result is a even number because the code has to divide the fraction in chop fraction by then (that does not a physical meaning), this does not effect the calculation because due to the symmetry of the problem there are some chopped pieces that are 0 and this system takes care of it in this way. These chopped pieces were reassemble into a fully allocated variable "sortM()". The allocation process works by placing each chopped piece into "sortM()" by the number of times it was divided during the chopping process. As the name implies the "sortM()" variable also has the allocated values in the correct location corresponding to the θ_S. The final step is simply to put the fully allocated fractions into the variable storing all of the fractions into, "delf()". Since we are working with fully differential fractions, the values from "sortM()" are literally added to "delf()" at the location specified. Which, means if there is already a value in that location it gets larger after "sortM()" is added in. The reason of this will become apparent in the next section dealing with allocation over θ_0.

4.2.3 Allocation over θ_0

The next allocation section starts off by reviewing the the allocation of the loss fraction from a single launch position (n=θ_0) over all possible exit locations (m=θ_S) and points out is not yet considered the other launch location θ_0. The logic is the same used in the previous part. The code is exactly equal at the one above for all eight launch locations. None of the launch locations have the same values of fractions going to the exit positions, but this is largely ignored because of the chopping the code does to break up the fractions making these distinctions moot. What is significant is the difference in the "upper bounds" of the launch locations. The label "upper bound" could be confusing since fundamentally launch locations are presented with different minimum energy requirements. It is clear from of the discussion above that the locations with lower energy requirements being able to lose more ions and thus

having a higher loss fraction. So the locations with the greatest "upper bounds" also have the lowest minimum energy requirements.To sum up with, there is a non-negligible difference in the fraction of ions lost from each launch location. Assumed no poloidal ion rotation inside of flux surfaces, calculations are stopped here and it is needed only to add a few things to the code to ensure it keeps track of these different levels for the next surface. However, since it was assumed there is a poloidal rotation mechanism, it is necessary to account for this in the code. In doing so, it has to take the non lost fractions and move them to the next nearest locations and see if they can be lost there. Afterwards it allocates these fractions in the same way it has been described in a previous section just at a different launch location. This is continued until the allotment (that is "octet()") in the code to each launch location is fully exhausted, or lost.

```
if(topedge.lt.64)then
c2009                                          continue
         do 2008 nm = (topedge+1),64
c                          The restwill be sent CW or CCW
            octetNcwORccw(nm) = (octet(nm)
1                                              - octet(topedge))
2008                                           continue


         if(npsi.gt.11)then
c                        Clockwise loop
                  nsn = cw(n)
         elseif(npsi.lt.12)then
c        Counter Clockwise loop
                  nsn = ccw(n)
         endif
```

```
         stayloop = 1
do while (stayloop.gt.0)
         do 2007 m = 8,2,-1
                  chopM(m) = (octetNcwORccw(actord1st((nsn
1                                 +(order1mst(nsn,m,npsi)-1)*8),npsi))
     2                            -octetNcwORccw(actord1st((nsn
     3                            +(order1mst(nsn,m-1,npsi)
     4                               -1)*8),npsi)))/(mb(m)*1.0)
2007                      continue
                  chopM(1) = octetNcwORccw(actord1st((nsn
1                         +(order1mst(nsn,1,npsi)-1)*8),npsi))/8.0

        do 2005 m = 1,8
                  sortM(m) = 0.0
                  mqm = m
         do 2006 mrm = 1,mqm
                  sortM(m) = sortM(m) + chopM(mrm)
2006                                  continue
2005                                     continue
                  do 2004 m = 1,8
                         delf(nsn,order1mst(nsn,m,npsi),
1                                 npsi,roh,k) = delf(nsn,order1mst(nsn,
     2                                    m,npsi),npsi,roh,k)+sortM(m)
2004                              continue
                  if(nsn.eq.order1nst(8,npsi))then
                         stayloop = 0
                  else
                  topedge = actord1st((nsn
1                         +(order1mst(nsn,8,npsi)-1)*8),npsi)
```

```
                        if(topedge.lt.64)then
                                slice = octetNcwORccw(topedge)
                do 2003 nm = 1,topedge
                        octetNcwORccw(nm) = 0
2003                            continue
                do 2002 nm = (topedge+1),64
                        octetNcwORccw(nm) =
1                                       (octetNcwORccw(nm)
2                                                       - slice)
2002                    continue
                        endif
                        if(npsi.gt.11)then
                                nsn = cw(nsn)
                        elseif(npsi.lt.12)then
                                nsn = ccw(nsn)
                        endif
                endif
        enddo
c                       End of CW or CCW loop
                  endif
2001                    continue
c                       End of n loop
2000            continue
c               End of npsi loop
c               End of Allocations Section
s
```

It starts by creating the "topedge" variable which is the "upper bound" index pulled out using the "actord1st()" variable which comes from the earlier sorting section.

This "upper bound" is the upper bound for the current θ_0. Since the aim is to get a result beyond the current upper bound the code subtracts all the remaining values in "octet()" by the upper bound in "topedge" to store the truncated fractions in "octetNcwORccw()". It has exploited the word "truncated" since the code has already taken care of the fractions up to the upper bound, therefore the next step is to remove that amount from total left fraction before checking the remaining values at the next launch location θ_0. The variable "octetNcwORccw()" either send the remaining fractions after truncation clock-wise or counter clock-wise depending on the sign of ζ_0. Assuming ζ_0 values greater than 11 clock-wise and those less than 11 counter clock-wise. This was originally handled by two separate loops but using an indexing vaiable "nsn" (given by "ccw()" or "cw()") that changes based on the value of ζ_0 both loops can be done with a single string of code. The "stayloop" variable was initialize with a value of 1 which is like a "flag" that it allows to come out the do loop. The next section is almost the same described during the allocation over θ_S, chops them, sort them and allocates in "delf()" in the same way. It is not equal because the long string which develops the proper index for sorting (which occurs during the assignment of values into "chopM()") has a few slightly different terms but still operates in fundamentally the same manner. Right after three conditions were used to choose whether or not to exit the do while loop. The first condition checks to see if we are currently at the poloidal launch location θ_0 with the minimum energy (that is the one with the highest upper bound in fraction values). It does this by checking "nsn" against "order1nst()". If that does not trip the code next updates the "topedge" variable with the new upper bound for the current launch location. After there is a check to make sure that its not at the end of the "octetNcwORccw()" variable. This is done by ensuring "topedge" has a value less than 64. If that does not trip the code use slice to record the value of the upper bound and then truncate "octetNcwORccw()" again by this new value. Lastly, "nsn" was updated with either

"cw" or "ccw", and if any of these checks fail, "stayloop" was loaded with a new value and exit out of the do while loop. All these operation allow finally to get the differential loss fraction stored in "delf()", that is also the variable combined with used "eminAll" to obtain the results.

Name	What is it?	Variable Name	Type	Range
ρ_0	radial flux surface position	n0, roh, nnn0, others	integer	24
ζ_0	directional cosine	npsi	integer	22
θ_0	Poloidal launch position	n, itit	integer	8
θ_S	Poloidal exit position	m	integer	8

Table 5: Indexes used in the code

Matrix name	What is it?	Dimension
emin()	Lowest minimum required energies for IOL	$npsi = \zeta_0, n = \theta_0, n0 = \rho_0$
eminAll()	All minimum required energies for IOL	$npsi = \zeta_0, n = \theta_0, n0 = \rho_0, m = \theta_S$
etta()	All reduced minimum required energies for IOL	$npsi = \zeta_0, n = \theta_0, m = \theta_S$
big()	Pre computed full gamma function	$k : 1 = ions, 2 = mom. 3 = eng$
flrone()	Un-allocated loss fraction	$npsi = \zeta_0, n = \theta_0, m = \theta_S$
delf()	Fully differential loss fraction	$npsi = \zeta_0, n = \theta_0, n0 = \rho_0, m = \theta_S, k$
rohit1st()	Sorted n and m values from flrone() for a given npsi and rho	length: $n * m$ sorted
octet	1/8 magnitude of rohit1st()	length: $n * m$ sorted
order1nst	Generates indices for n	$npsi = \zeta_0, n = \theta_0,$
chopM()	Chopped fractional magnitudes	$m = \theta_S$
sortM()	Allocated fraction	$m = \theta_S$
topedge	index for octetNcwORccw specifying upper bound of current of θ_0	$[n/a]$
actord1st	Index variable from the sorting section	length: $n * m$ sorted
octetNcwORccw	Truncated version of octet used during $n = \theta_0$	length: $n * m$ sorted
nsn	Specifies which θ_0 location based upon rotation from cw or ccw	$[n/a]$
cw	Provide clock-wise indexing selection	$n = \theta_0$ 8,1,2,3,4,5,6,7
ccw	Provide counter clock-wise indexing selection	$n = \theta_0$ 2,3,4,5,6,7,8,1
stayloop	Loop flag	[n/a]
slice	Hold the value of the upper bound used in the truncation of octetNcwORccw	$[n/a]$

Table 6: Main variables used in the code

CHAPTER V

CHANGING FLUXES VIA IOL

The previous results of ion orbit loss showed that the particle and energy loss are peaked on the outboard midplane. This fact is due to the minimum energy for a particle being loss has its minimum value right on the outboard midplane. Thus the heat load on this side is higher than the inboard midplane. This cause serious problem to the integrity and lifetime of the divertor. For getting rid of this inconvenient it has been solved the ion orbit loss equation 19 by means of GTEDGE, changing some terms in the coefficients (a,b,c) of the quadratic equation as the toroidal magnetic field on last closed surface and electrostatic potential on the whole flux surface taken into account. In doing so we want to ascertain if there is any chance to redirect and reduce the particle and energy loss from outboard midplane and to the inboard midplane. Hence the result we would like to reach is to get a more uniform heat load distribution over the divertor in order to improve the its performance and consequently the efficiency of the whole system. The model presented in this previous chapters can calculate whether or not an ion with a given energy and direction cosine located at a given location (ρ_0, θ_0) on an inner flux surface can reach a location (ρ_S, θ_S) at a different radial and poloidal location. Previously we have chosen ρ_S to be on the LCFS and have used a factor $0 \leq R_{loss}^{ios} \leq 1$ to represent the probability that an ion from the interior reaching a point on the LCFS will leave the plasma and not return.First of all it is possible to make other choices for (ρ_S, θ_S) (e.g. the location of a limiter or divertor entrance) and moreover calculation of the possibility that a particle that crosses the LCFS follows that orbit and returns into the plasma has done as result to set the R_{loss}^{ios} up to 0.5. For this reason the cumulative distribution loss fraction are

not normalized to 1, but to 0.5.

5.1 Effect due to the change of B_ϕ

The analysis started looking at the toroidal magnetic field. The figure 34 shows how is the trend of the toroidal magnetic field in a Tokamak poloidal section, it has a maximum on the inboard midplane and a minimum on the outboard midplane. On the account of asymmetric distribution of the toroidal magnetic field and according to the equation 19, it could be stated that a particle leaves the plasma with less struggle on the outboard midplane due to here the required energy for going out has its minimum value. So the question is how strong is the influence that this toroidal magnetic field has on the particle in the IOL theory? We care about the answer because the high difference of escape energy between inboard and outboard gives rise to a higher particle (and energy) flux on the outboard midplane, which brings about a higher heat load on this side of the divertor. Moreover for an outward flowing plasma and a decreasing ion temperature the minimum energy decreases with radius and the lost ion are replenished by outward flowing inward surface with higher escape energy.

Looking at equation 19, it seems to be interesting exploring what happen at the particle and energy fluxes when we modify the toroidal magnetic field on the separatrix. Besides our first aim of redistributing the particle flux,increasing the toroidal magnetic field has also the effect to improve the confinement parameter, as β.The changing of magnetic field could be done using a new set of coils, called shim coils.This coils have essentially the same physic and engineering issues of the toroidal field coils, previously described. A representative picture is shown in the figure 35 where the gray coils are the toroidal field coils, they also represent the skeleton of our Tokamak, while the light blue coils are the shim coils. The direction of the current in the shim coils is set in the way that the toroidal magnetic field created is going to sum with the toroidal magnetic field generated from the TF coil. For starters we assumed

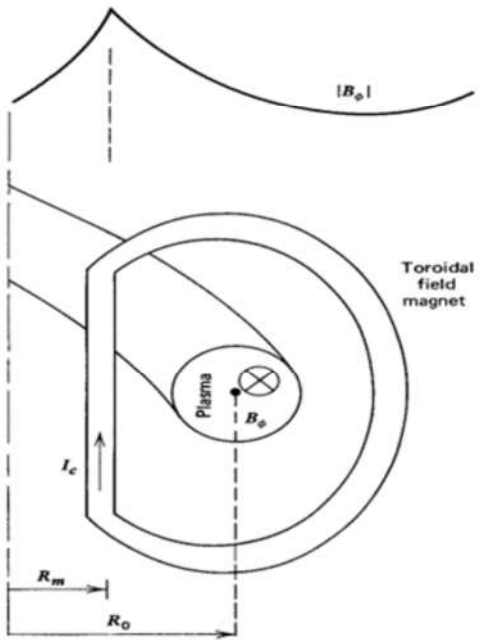

Figure 34: Toroidal configuration

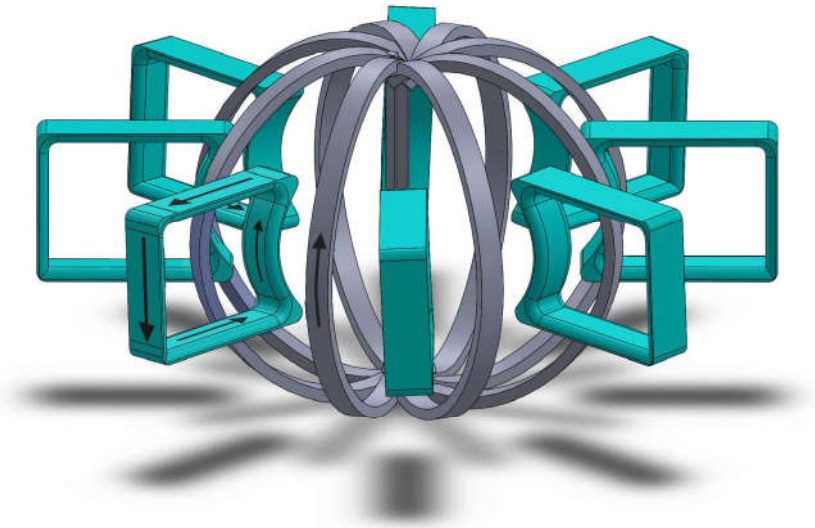

Figure 35: Toroidal field coil and shim coil

for hypothesis that the most significant change are just in three points over LCSF where $\theta_S = 0, \pm\pi/4$. During the analysis we have performed also a better calculation. Picturing the coil "stuck" on the LCSF we assumed to modify all the inner region that starts from the initial three points. The B_ϕ has been modified based on its distance from the LCSF. In this case the points modified are $24 \times 3 = 72$. Since the number involved are small, the second strategy doesn't give a significant improvement of our results, thus we decided to work with our first hypothesis. Two cases are taken into account: one with a 30% boost of $B_{\phi S}$ that can be reached with a bit effort and as borderline value the double of $B_{\phi S}$. Using a higher value of B_ϕ would not have had any sense because we will lose some of the peculiar characteristic of a Tokamak reactor. The result of our changing on the minimum energy $E_{min}(\zeta_0, \rho_0)$ are shown in the figures 36 and 37. Only three flux surface are taken into account:$\rho = 0.864$ (the first flux surface), $\rho = 0.972$, $\rho = 0.994$ (the one before the separatix). We notice that the minimum energy has his lower value for the counter-currents ions ($0 < \zeta_0$¡1). The effect of changing is higher for the inner flux surface. On the whole changing the magnetic field cause a weak increasing of the minimum energy that is higher on the inner flux surface especially for ion with ζ_0 around 0. Clearly the modification is higher when the $B_{\phi S}$ double its value.

Figures 38, 39,40, 41 show the cumulative loss fraction of ions and energy in the two cases analyzed. We can point out that we have a higher decreasing of the loss over the normalized radius when the $B_{\phi S}$ raises. This is an overstatement, because this increment is practically unobtainable and it will turn the machine is something that it could be defined as "non-Tokamak".

The most important plot concerns about the poloidal distribution of the cumulative particle and energy loss fraction across the separatrix. Figures 42,43,44,45 show the results for the two cases in a semilog-y scale. As we claimed before the original distributions are strongly peaked about the outboard midplane. Our purpose was to

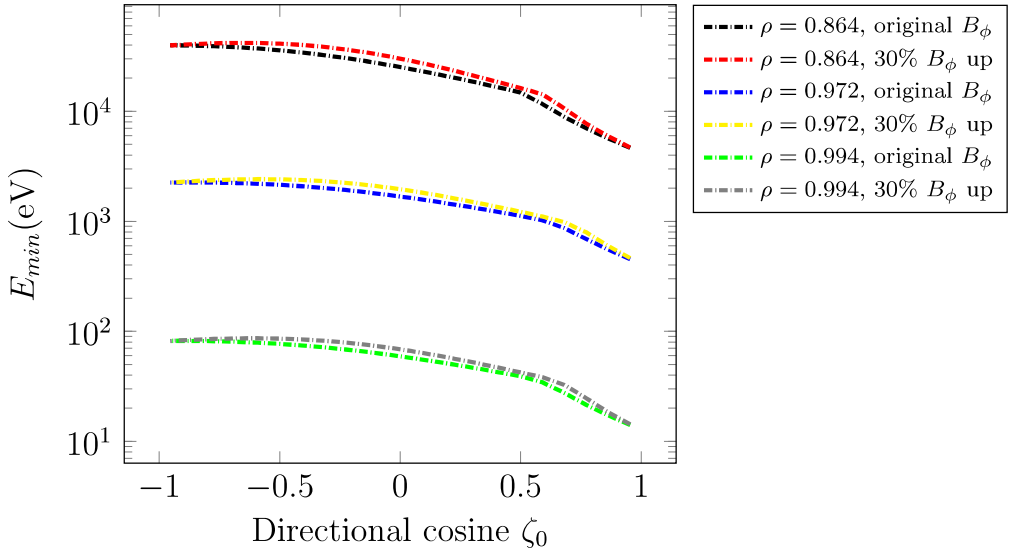

Figure 36: Lowest value of $E_{min}(\zeta_0, \rho_0)$ for any launch location θ_0 on several internal flux surface

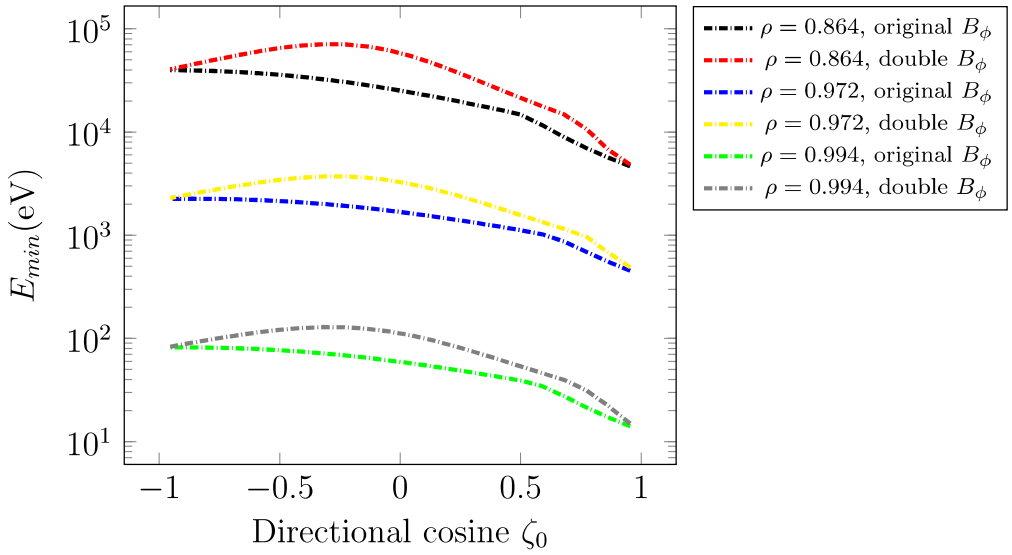

Figure 37: Lowest value of $E_{min}(\zeta_0, \rho_0)$ for any launch location θ_0 on several internal flux surface

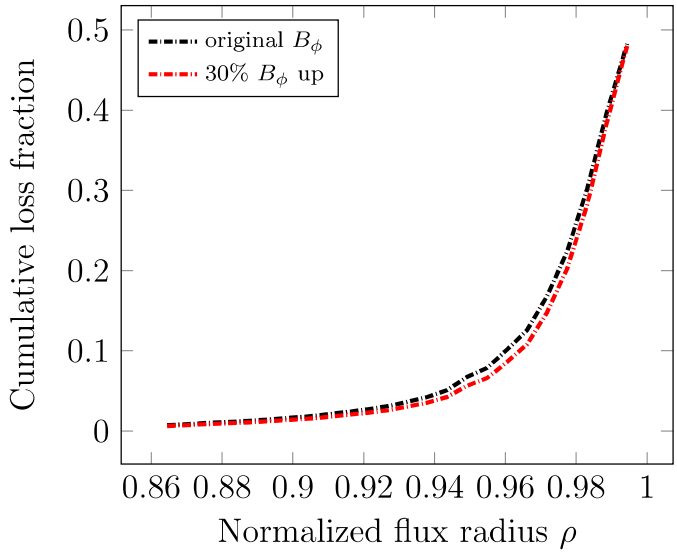

Figure 38: Cumulative IOL ion loss fraction at different radial flux locations

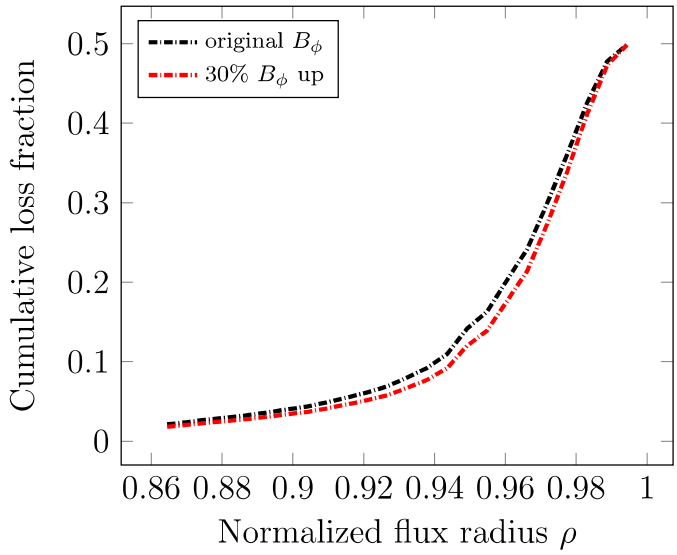

Figure 39: Cumulative IOL energy loss fraction at different radial flux locations

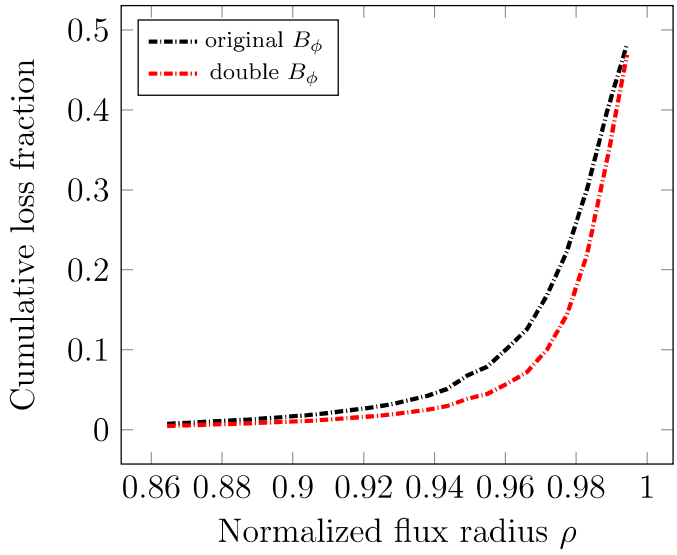

Figure 40: Cumulative IOL ion loss fraction at different radial flux locations

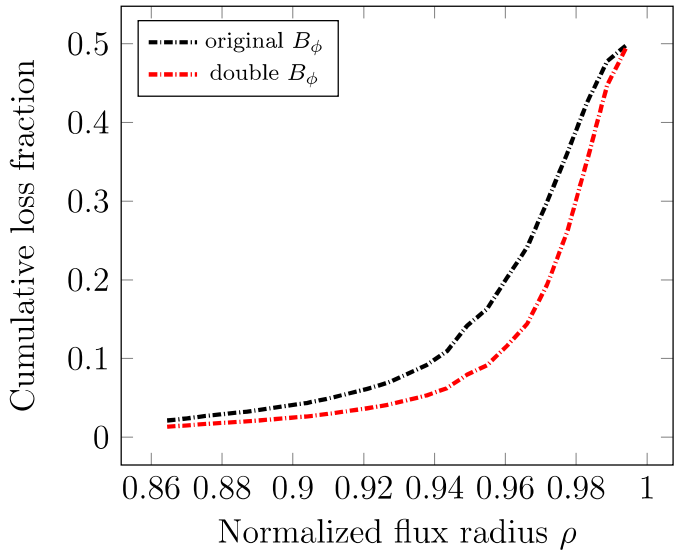

Figure 41: Cumulative IOL energy loss fraction at different radial flux locations

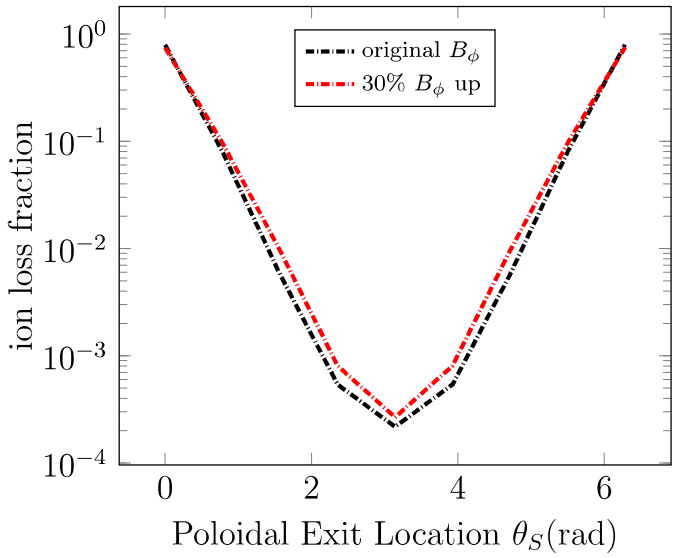

Figure 42: IOL ion loss fraction poloidal distribution over LCSF

find a way to make flatter this distribution. After the 30% boost of $B_{\phi S}$ there only a small improvement. In the first case even though the loss fraction decreasing in the $\theta_S = 0$, they raise around the nearest exit locations. That does not satisfy our goal. The situation gets slightly better when we double the toroidal magnetic field.

5.2 Effect due to the change electric potential ϕ

Since the outcome of toroidal magnetic field are not exciting, we started over to look at equation 19 and asking what will be another term that could introduce a significantly in our fluxes. The second choice that we consider worthwhile to evaluate is the changing due to the electrostatic potential ϕ. The way of how this is feasible is described in reference [27]. We are going to analyze what are the effect on the IOL assuming that is possible to modify the electrostatic potential. The ϕ was boosted by 30% in order to increase the well between the inner flux surface and LCFS. As the previous case the figure 46 the minimum energy over the directional cosine bin shows a small improvement for counter current particle when the particle is close to the separatrix. Figures 47 and 48 shows how change the loss fraction over the poloidal

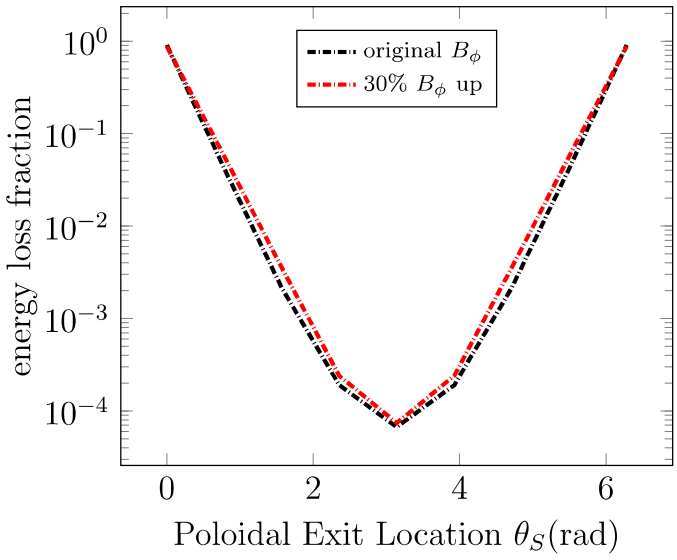

Figure 43: IOL energy loss fraction poloidal distribution over LCSF

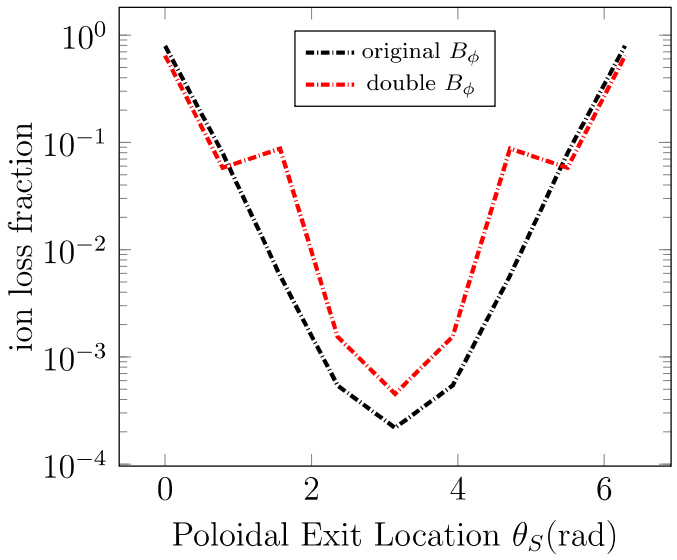

Figure 44: IOL ion loss fraction poloidal distribution over LCSF

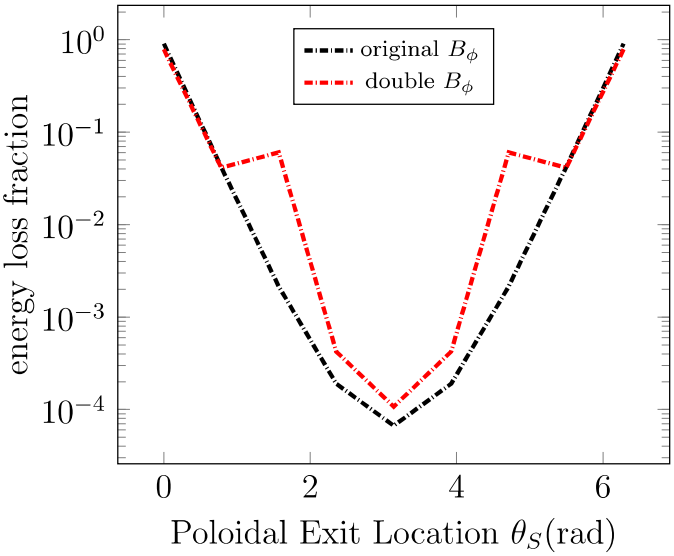

Figure 45: IOL energy loss fraction poloidal distribution over LCSF

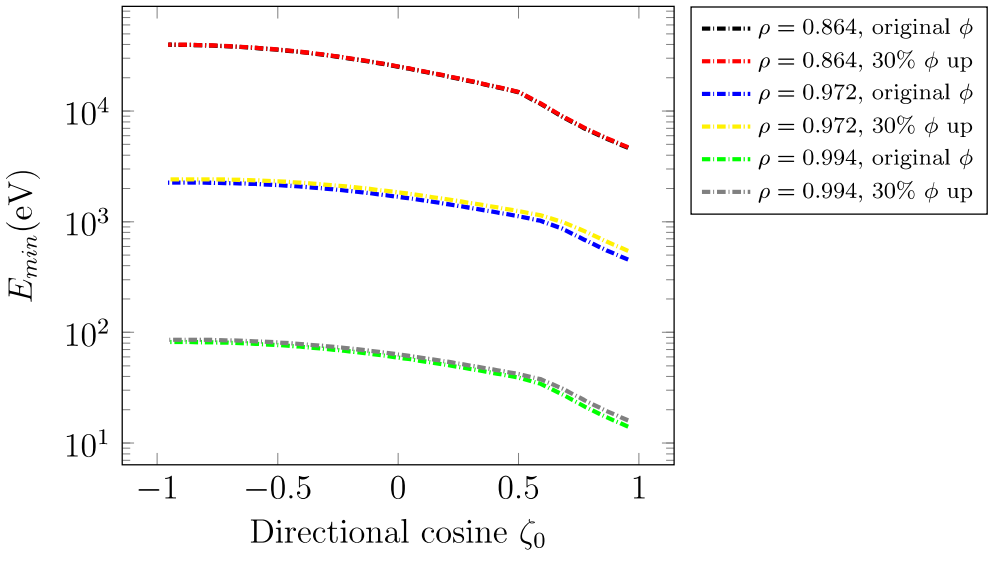

Figure 46: Lowest value of $E_{min}(\zeta_0, \rho_0)$ for any launch location θ_0 on several internal flux surface

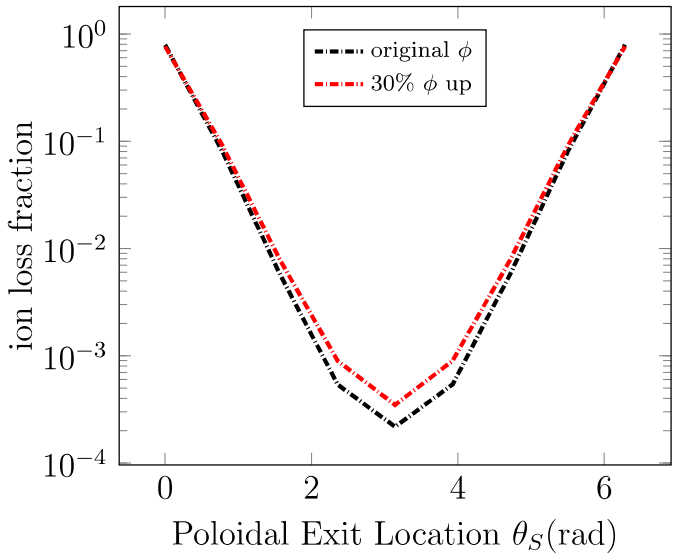

Figure 47: IOL ion loss fraction poloidal distribution over LCSF

exit angle, whereas figures 49 and 51 shows how the loss fraction change over the several flux surfaces

5.3 Conclusion

The modification of two important components of the ion orbit loss equation gives to us a non positive results. The effort it will be take to build new coils it is not worth to try and the boost of electric potential does not improve our results in the way we would have hoped. The gain calculated is really small and the cost will be surely too high. It is important to underline that the effect of the interaction between electric and magnetic field are neglected. So at the end of the analysis we asked ourself if magnetic field and the electrostatic potential that are critical parameters not only for IOL, but for general description of the plasma are not able to influence the equation, what are the the terms of the equation which can dramatically change the situation? To answer at this question, the table 7 are going to help us. Below we reminds the

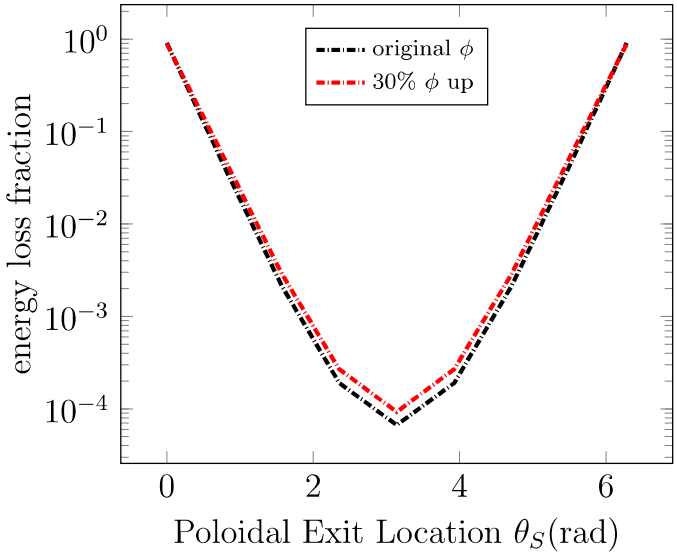

Figure 48: IOL energy loss fraction poloidal distribution over LCSF

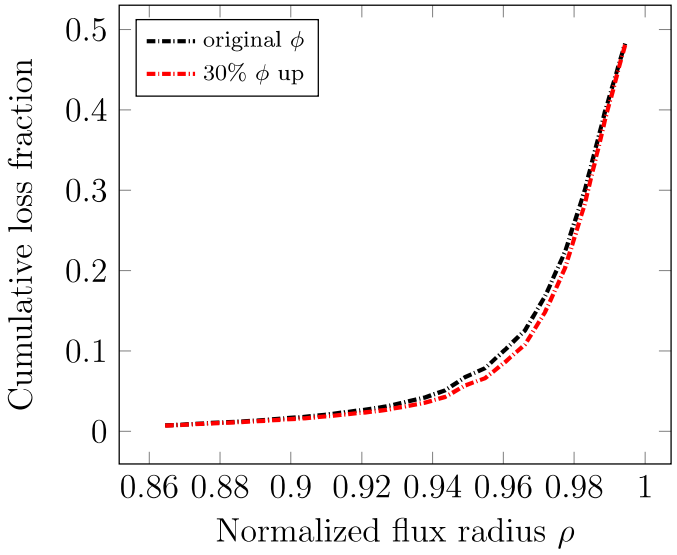

Figure 49: Cumulative IOL ion loss fraction at different radial flux locations

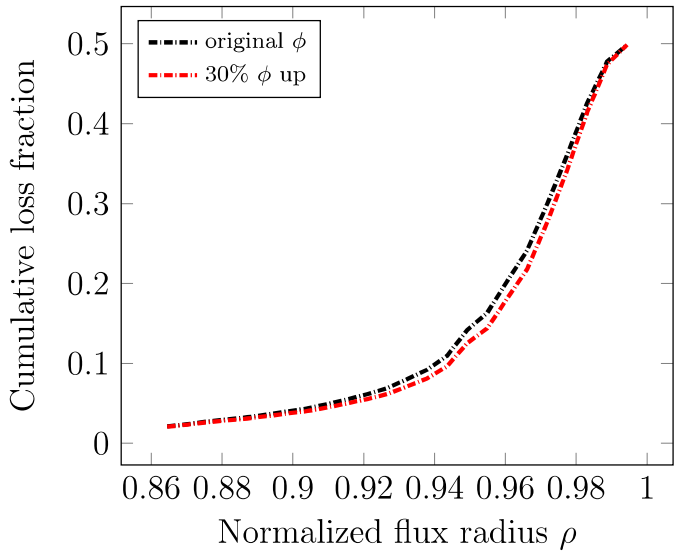

Figure 50: Cumulative IOL energy loss fraction at different radial flux locations

definition of the coefficients:

$$
\begin{aligned}
a &= \left[\left(\frac{R_0}{R_s}\frac{f_{\varphi 0}}{f_{\varphi S}}\zeta_0\right)^2 - 1 + (1-\zeta_0^2)\frac{B_S}{B_0}\right] \\
b &= \left[\frac{2e(\psi_0-\psi)}{R_S m f_{\varphi S}}\left(\frac{R_0}{R_S}\frac{f_{\varphi 0}}{f_{\varphi S}}\zeta_0\right)\right] \\
c &= \left[\left(\frac{e(\psi_0-\psi_S)}{R_S m f_{\varphi s}}\right)^2 - \frac{2e(\phi_0-\phi_S)}{m}\right]
\end{aligned}
$$

The first thing that jumps out is that the coefficient of the quadratic term is many orders of magnitude smaller than the other two. The first term is the one governed by the magnetic field. This explain why the changing of $B_{\phi S}$ does not effect the distribution. The electrostatic potential is many order of magnitude higher, as we can see from c term. Even though our analysis does not a give a dramatical improvement of our problem. So for answering our question the only quantity can make a significant change is the flux surface ψ. So taking into account the Shafranov shift and using the Miller model could give us a better results and another way to investigate the problem.

The table 10 compared the loss fraction on the inboard and outboard midplane in

	$\theta_0 = 0$		$\theta_0 = \pi$	
$B_{\phi S}$ and ϕ	$\theta_s = 0$	$\theta_s = \pi$	$\theta_s = 0$	$\theta_s = \pi$
a	-10.3512e-003	2.0393e+000	-664.2517e-003	28.2512e-003
b	-24.2105e+003	-226.4292e+003	-8.2248e+003	-76.9222e+003
c	106.8265e+009	711.6521e+009	106.8265e+009	711.6521e+009
30% $B_{\phi S}$ up				
a	278.4317e-003	2.0393e+000	-566.1414e-003	28.2512e-003
b	-23.9292e+003	-226.4292e+003	-8.1292e+003	-76.9222e+003
c	105.9851e+009	711.6521e+009	105.9851e+009	711.6521e+009
double $B_{\phi S}$				
a	956.0364e-003	2.0393e+000	-335.9420e-003	28.2512e-003
b	-23.6938e+003	-226.4292e+003	-8.0492e+003	-76.9222e+003
c	105.2809e+009	711.6521e+009	105.2809e+009	711.6521e+009
30% ϕ up				
a	-10.3512e-003	2.0393e+000	-664.2517e-003	28.2512e-003
b	-24.2105e+003	-226.4292e+003	-8.2248e+003	-76.9222e+003
c	117.1508e+009	721.9763e+009	117.1508e+009	721.9763e+009

Table 7: Evaluate the coefficient of quadratic equation at $\zeta = 0.0455$, $\rho = 0.972$ when $B_{\phi S}$ and ϕ change

θ_S	B_ϕ	30%B_ϕ	double B_ϕ	30%ϕ
0	0.7938	0.7474	0.6437	0.7638
$\pi/4$	0.0795	0.0960	0.0579	0.0904
$\pi/2$	0.0057	0.0096	0.0873	0.0078
$3\pi/4$	0.0005	0.0008	0.0015	0.0009
π	0.0002	0.0003	0.0005	0.0003
$5\pi/4$	0.0005	0.0008	0.0015	0.0009
$3\pi/2$	0.0057	0.0096	0.0873	0.0078
$7\pi4$	0.0795	0.0960	0.0579	0.0904

Table 8: Ion Loss Fraction on the eight exit location in the four different cases

θ_S	orginal B_ϕ	30%B_ϕ	double B_ϕ	30%ϕ
0	0.8670	0.8265	0.7287	0.8408
$\pi/4$	0.0585	0.0753	0.0500	0.0695
$\pi/2$	0.0032	0.0057	0.0748	0.0046
$3\pi/4$	0.0003	0.0004	0.0008	0.0004
π	0.0001	0.0001	0.0002	0.0002
$5\pi/4$	0.0003	0.0004	0.0008	0.0004
$3\pi/2$	0.0032	0.0057	0.0748	0.0046
$7\pi/4$	0.0585	0.0753	0.0500	0.0695

Table 9: Energy Loss Fraction on the eight exit location in four different cases

the cases analyzed, instead of the tables 8 and 9 gives us an idea of the loss around the poloidal section of the plasma. Even if there is an increment of loss on the inboard midplane, there are still a couple order of magnitude of difference between the the side of the plasma, that points out how this is not the right path.

	original B_ϕ	30%$B_\phi up$	double B_ϕ	30%ϕ up
$floss_{inb}$	7.0231e-003	11.4373e-003	90.8381e-003	9.9578e-003
$floss_{outb}$	958.4912e-003	948.9379e-003	846.8540e-003	952.4486e-003

Table 10: Loss fraction on the inboard and outboard midplane

Finally the figure 51 shows how changes the minimum energy on the first flux surface, which was the one most influenced by the changing of $B_{\phi S}$. This figure shows how small are the differences compared by all the cases studied.

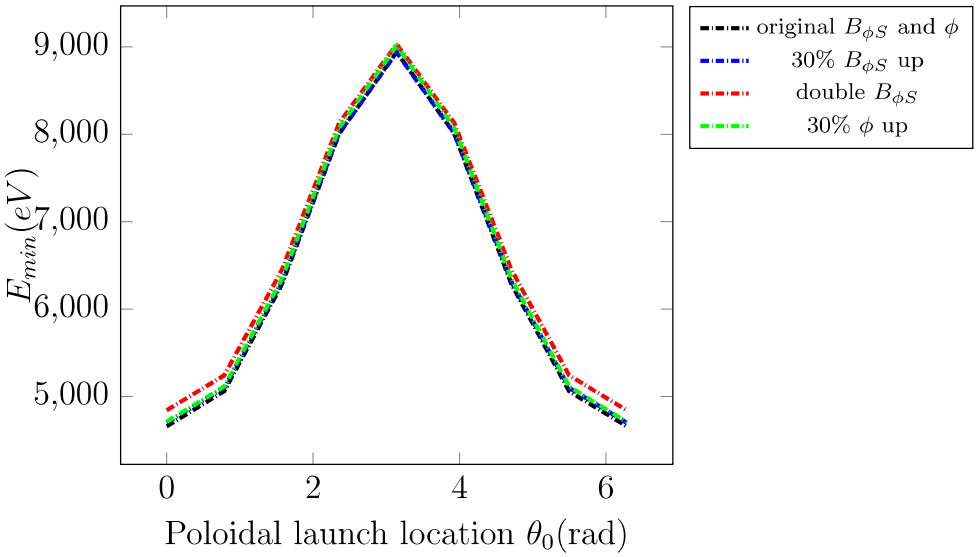

Figure 51: $E_{min}(\zeta_0 = 0.955, \rho_0 = 0.864, \theta_0, \theta_S = 0)$ for counter-current($\zeta_0 = 0.955$) ions launched at θ_0 on $\rho_0 = 0.864$ to be lost at θ_S on the LCSF at $\rho = 1.0$

REFERENCES

[1] Jeffrey P Freidberg. *Plasma physics and fusion energy.* Cambridge university press, 2008.

[2] Weston M Stacey. *Fusion Plasma Physics.* John Wiley & Sons, 2012.

[3] John Wesson and David J Campbell. *Tokamaks*, volume 149. Oxford University Press, 2011.

[4] Weston M Stacey. *Fusion: an introduction to the physics and technology of magnetic confinement fusion.* John Wiley & Sons, 2010.

[5] James L Luxon. A design retrospective of the diii-d tokamak. *Nuclear Fusion*, 42(5):614, 2002.

[6] MW Maisel, T Ohkawa, KH Burrell, RL Freeman, FJ Helton, TH Jensen, RJ La Haye, DO Overskei, R Prater, JM Rawls, et al. The fusion power research programme at ga technologies inc. *Nuclear fusion*, 25(9):1113, 1985.

[7] J Reece Roth. *Introduction to fusion energy.* Classworks, 1986.

[8] FL Hinton and MS Chu. Neoclassical ion transport through the separatrix in divertor tokamaks. *Nuclear fusion*, 25(3):345, 1985.

[9] MA Kovanen, R Reichle, E Lazzaro, DDR Summers, and TS Taylor. Modelling of the observed particle and heat fluxes in the x-point region in jet. *Nuclear fusion*, 32(5):863, 1992.

[10] S-I Itoh and Kimitaka Itoh. Model of the h-mode in tokamaks. *Nuclear fusion*, 29(6):1031, 1989.

[11] Ker-Chung Shaing and EC Crume Jr. Bifurcation theory of poloidal rotation in tokamaks: A model for l-h transition. *Physical Review Letters*, 63(21):2369, 1989.

[12] AV Chankin and GM McCracken. Loss ion orbits at the tokamak edge. *Nuclear fusion*, 33(10):1459, 1993.

[13] Kenro Miyamoto. Direct ion orbit loss near the plasma edge of a divertor tokamak in the presence of a radial electric field. *Nuclear fusion*, 36(7):927, 1996.

[14] Ker-Chung Shaing, EC Crume Jr, and WA Houlberg. Bifurcation of poloidal rotation and suppression of turbulent fluctuations: A model for the l-h transition in tokamaks. *Physics of Fluids B: Plasma Physics (1989-1993)*, 2(6):1492–1498, 1990.

[15] Ker-Chung Shaing and RD Hazeltine. Effects of orbit squeezing on ion transport in the banana regime in tokamaks. *Physics of Fluids B: Plasma Physics (1989-1993)*, 4(8):2547–2551, 1992.

[16] Ker-Chung Shaing. Radial electric field and plasma confinement in the vicinity of a magnetic island. *Physics of Plasmas (1994-present)*, 9(8):3470–3475, 2002.

[17] P Helander, RJ Akers, and L-G Eriksson. On neutral-beam injection counter to the plasma current. *Physics of Plasmas (1994-present)*, 12(11):112503, 2005.

[18] KG McClements and A Thyagaraja. Collective electric field effects on the confinement of fast ions in tokamaks. *Physics of Plasmas (1994-present)*, 13(4):042503, 2006.

[19] JS Degrassie, JE Rice, KH Burrell, RJ Groebner, and WM Solomon. Intrinsic rotation in diii-da). *Physics of plasmas*, 14(5):6115, 2007.

[20] RJ Groebner, KH Burrell, WM Solomon, et al. Intrinsic toroidal velocity near the edge of diii-d h-mode plasmas. *Nuclear Fusion*, 49(8):085020, 2009.

[21] SH Müller, JA Boedo, et al. Plasma flow due to a loss-cone distribution centred around the outboard edge in diii-d. *Nuclear Fusion*, 52(1):013010, 2011.

[22] Weston M Stacey and Brian A Grierson. Interpretation of rotation and momentum transport in the diii-d edge plasma and comparison with neoclassical theory. *Nuclear Fusion*, 54(7):073021, 2014.

[23] Weston M Stacey. The effect of ion orbit loss and x-loss on the interpretation of ion energy and particle transport in the diii-d edge plasma. *Physics of Plasmas (1994-present)*, 18(10):102504, 2011.

[24] WM Stacey. Extensions of ion orbit loss theory. *Phys. Plasmas*, 21:014502, 2014.

[25] Weston M Stacey and Matthew T Schumann. The distribution of ion orbit loss fluxes of ions and energy from the plasma edge across the last closed flux surface into the scrape-off layer. *Physics of Plasmas (1994-present)*, 22(4):042504, 2015.

[26] Theresa Wilks. Calculation of radial electric field in the diii-d tokamak edge plasma., 2016.

[27] Weston M Stacey. Effect on the divertor and scrape-off layer plasma properties of the distribution of power and particle influxes from the core. *Physics of Plasmas (1994-present)*, 16(3):032506, 2009.

[28] Matt Schuman. The effect of ion orbit loss on the distribution of ion, energy and momentum from the edge plasma into the scrape off layer in tokamaks., 2015.

[29] Weston Monroe Stacey. A coupled plasma-neutrals model for divertor simulations. *Physics of Plasmas (1994-present)*, 5(4):1015–1026, 1998.

[30] WM Stacey, JA Boedo, TE Evans, BA Grierson, and RJ Groebner. Intrinsic rotation produced by ion orbit loss and x-loss. *Physics of Plasmas (1994-present)*, 19(11):112503, 2012.

[31] Weston Monroe Stacey. Modelling the neutral density in the edge of the diii-d plasma. *Nuclear fusion*, 40(5):965, 2000.

[32] WM Stacey and TM Wilks. Inclusion of ion orbit loss and intrinsic rotation in plasma fluid rotation theory. *Physics of Plasmas (1994-present)*, 23(1):012508, 2016.

[33] Weston M Stacey, Richard J Groebner, and TE Evans. Non-diffusive transport in the tokamak edge pedestal. *Nuclear Fusion*, 52(11):114020, 2012.

[34] Weston M Stacey and Cheonho Bae. Representation of the plasma fluid equations in miller equilibrium analytical flux surface geometry. *Physics of Plasmas (1994-present)*, 16(8):082501, 2009.

[35] Amanda E Hubbard. Physics and scaling of the h-mode pedestal. *Plasma Physics and Controlled Fusion*, 42(5A):A15, 2000.

[36] JD Callen, RJ Groebner, TH Osborne, JM Canik, Larry W Owen, AY Pankin, T Rafiq, TD Rognlien, and WM Stacey. Analysis of pedestal plasma transport. *Nuclear Fusion*, 50(6):064004, 2010.

[37] KH Burrell. Effects of e× b velocity shear and magnetic shear on turbulence and transport in magnetic confinement devices. *Physics of Plasmas (1994-present)*, 4(5):1499–1518, 1997.

[38] Weston M Stacey. Comparison of theoretical and experimental heat diffusivities in the diii-d edge plasma. *Physics of Plasmas (1994-present)*, 15(5):052503, 2008.